STRUCTURAL BEHAVIOR

OF SIMPLY SUPPORTED FERROCEMENT-

ALUMINUM COMPOSITE BEAMS

A THESIS
SUBMITTED TO THE COLLEGE OF ENGINEERING
OF THE UNIVERSITY OF BASRAH IN PARTIAL
FULFILLMENT OF THE REQUIREMENTS FOR
THE DEGREE OF DOCTOR OF PHILOSOPHY
IN CIVIL ENGINEERING (STRUCTURES)

BY
SA'AD FAHAD RESAN
(M.Sc. 2006)

February 2012

بِسْمِ اللهِ الرَّحْمنِ الرَّحِيمِ

اللَّهُ نُورُ السَّمَاوَاتِ وَالْأَرْضِ مَثَلُ نُورِهِ

كَمِشْكَاةٍ فِيهَا مِصْبَاحٌ الْمِصْبَاحُ فِي زُجَاجَةٍ الزُّجَاجَةُ

كَأَنَّهَا كَوْكَبٌ دُرِّيٌّ يُوقَدُ مِن شَجَرَةٍ مُّبَارَكَةٍ زَيْتُونِةٍ لَّا شَرْقِيَّةٍ وَلَا غَرْبِيَّةٍ

يَكَادُ زَيْتُهَا يُضِيءُ وَلَوْ لَمْ تَمْسَسْهُ نَارٌ نُّورٌ عَلَى نُورٍ يَهْدِي

اللَّهُ لِنُورِهِ مَن يَشَاءُ وَيَضْرِبُ اللَّهُ الْأَمْثَالَ لِلنَّاسِ

وَاللَّهُ بِكُلِّ شَيْءٍ عَلِيمٌ ۝

صدق الله العلي العظيم

سورة النور (35)

To

My Parents

My Brothers My Sisters

My Wife

And My Lovely Kids

Fatima, Zynab, Mohammed, and Hassan

With Love

And Appreciation

CERTIFICATION

I certify that the thesis titled **(Structural Behavior of Simply Supported Ferrocement - Aluminum Composite Beams)** which is being submitted by *Sa'ad Fahad Resan* is prepared under my supervision at the University of Basrah in partial fulfillment of the requirements for the Degree of Doctor of Philosophy in Civil Engineering (Structures).

Signature:
Prof. Dr. Nabeel Abdulrazzaq Jasim
Date: / / 2012

In view of the available recommendations, I forward this thesis for discussion by examining committee.

Signature:
Dr. Ahmad M. Al-Kadhimi
Head of the Civil Engineering Department
Date: / / 2012

EXAMINING COMMITTEE'S REPORT

We certify that we, the examining committee, have read the thesis titled **(Structural Behavior of Simply Supported Ferrocement - Aluminum Composite Beams) which is being submitted by (Sa'ad Fahad Resan),** and examined the student in its content and in what is connected with it, and that in our opinion, it meets the standard of a thesis for the degree of Doctor of Philosophy in Civil Engineering (Structures).

Signature:
Name: **Dr. Nabeel Abdulrazzaq Jasim**
(Professor)
(supervisor)

Signature:
Name: **Dr. Nameer A. Alwash**
(Professor)
(Member)

Signature:
Name: **Dr. Ammar Yaser Ali**
(Professor)
(Member)

Signature:
Name: **Dr. Haithem H. Muteb**
(Professor)
(Member)

Signature:
Name: **Dr. Mustafa B. Dawood**
(Assist. Professor)
(Member)

Signature:
Name: **Dr. Anis A. Mohamad Ali**
(Professor)
(Chairman)

Approval of the College of Engineering:

Signature:
Name: Prof. Dr. Nabeel Abdulrazzaq Jasim
Dean, College of Engineering

AKNOWLEDGMENT

First and always first, Thanks are to the almighty God for many blessings, past, present and future.

The author is most grateful and highly indebted to his supervisor Prof. Dr. Nabeel Abdulrazzaq Jassim, Dean of the College of Engineering for the considerable assistance offered continually during the various stages of this work.

Thanks are due to Dr. Ahmed M. Al-Kadhimi, head of the Civil Engineering Department and Mr. Na'ma Yousif for their continued support.

Special thanks are presented to the staff of the Construction Materials Laboratory in the Department of Civil Engineering and Library staff for providing all available facilities necessary for conducting this investigation.

Many thanks and appreciation is due to Dr. Mohammed Salih, Mr. Abd ulkhaliq Jaafer, Mr. Abbass Oda, Mr. Saddam Khalaf , Mr. Muthana Shaker and Mr. Ahmed Naema for their help, real support and encouragement in conducting experimental work.

Special thanks are presented to Mr. Amer Sa'addon, Mr. Qassim Nasser, Mr. Basher Abdulrida, Mr. Riadh Toma, Mr. Hassan Najim, Mr. Ali Falih, Mr. Ali Qassim for their assistance throughout the experimental work.

Finally, great deal of thanks is dedicated to my family for their continued encouragement and patience.

Sa'ad Fahad Resan

2012

Abstract

The present study is aiming to investigate the structural behavior of simply supported composite beams, in which a ferrocement slab is connected together with aluminum beam by adhesive epoxy layer. Structural Aluminum Alloy sections (Box and I – section) produced by Jordanian aluminum industry has been used in this investigation. Sikadur 31 thixotropic epoxy resin adhesive is used as shear connector layer, which is a solvent-free, thixotropic, two component adhesive and repair mortar, based on a combination of epoxy resins and specially selected high strength fillers. It complies with ASTM C 881-78.

The study consists of two parts, the first part is the experimental work in which three push-out specimens and ten composite beams, designed to fail in bending, were tested in additional to four aluminum beams and two ferrocement slabs. A series of tests was conducted to investigate the effects of the dimensions of the aluminum section on the structural behavior and strength of composite ferrocement aluminum beams. The composite beams specimens were subjected to one point loading. The load - deflection, load - slip and load - uplift relationships were presented. Tests revealed that the proposed beams (ferrocement aluminum composite beams) have a good loading capacity relative to their weight. The strength increase ratio ranged between 1.57 to 2.69. The composite system of ferrocement and aluminum beams is efficient in eliminating local buckling of aluminum beams. It was observed that using epoxy provides adequate bond between the two components. Measurements also showed that the connection could be considered to be perfect as the slip remains very small during the test.

In the second part of the study, the tested beams were analyzed using nonlinear three dimensional finite element models. The constitutive models of the nonlinear material behavior for ferrocement matrix, aluminum, and steel wire mesh are used to take into account the nonlinear stress-strain relationships.

ANSYS version 11.0 program code used to analyze the three dimensional model. Ferrocement modeled by using the 8-noded isoparametric brick elements (SOLID65), while the aluminum beam modeled as isoparametric brick elements (SOLID45) with 8-nodes. Different models with different interface element types were used to simulate the adhesive epoxy layer. Model COMPIN14 spring element gave closer results to experimental ones, the ratio is 1.03, as well as less solution iterations and so less solution time. The wire mesh reinforcement was modeled as a volume ratio distributed within the ferrocement brick elements. The adopted finite element models were found to predict the ultimate strength, deflections, strains, and slip distribution, in a reasonable agreement with the test results.

Also, the capacity resistance of studied sections was determined using plastic analysis principles. The plastic analysis results depicted that the ultimate strength capacity of ferrocement aluminum composite beams can be estimated by using conventional equilibrium procedures and the constitutive laws prescribed by Euro codes and standard tests for the materials.

CONTENTS

Subject	Page
Acknowledgment	I
Abstract	II
Contents	IV
Notation	VIII
List of Abbreviations	X
List of tables	XI
List of figures	XII
List of plates	XVII
Chapter One: Introduction	
1.1 General	1
1.2 Aluminum	3
1.2.1 Aluminum Applications	5
1.3 Ferrocement	6
1.3.1 Ferrocement Applications	8
1.4 Why Using Ferrocement and Aluminum in Composite beam	9
1.5 Adhesive bonded connections	10
1.6 Objective of Study	10
1.7 Thesis Layouts	11
Chapter Tow: Review of Literature	
2.1 General	12
2.2 Aluminum Beams	12
2.3 Ferrocement Members	20
2.4 Composite Beams	26
2.4.1 Aluminum in Composite Beams	31

Subject	Page
2.5 Concluding Remarks	33
Chapter Three: Experimental Program	
3.1 Introduction	34
3.2 Aluminum	36
3.2.1 Mechanical Properties	39
3.2.2 Aluminum Alloy Chemical Analysis	43
3.3 Ferrocement	43
3.3.1 Cement	44
3.3.2 Fine Aggregate (Sand)	46
3.3.3 Water	46
3.3.4 Steel Wire Mesh	46
3.3.5 Direct Tensile Tests of Ferrocement Elements	48
3.3.6 Cement Mortar	51
3.3.6.1 Mix Design	51
3.3.6.2 Mixing, Casting and Curing	54
3.3.6.3 Compressive Strength of Mortar	54
3.3.6.4 Flexural Strength of Mortar	55
3.4 Epoxy Resin	57
3.5 Push - Out Test	57
3.5.1 Test Specimens	57
3.5.2 Test Procedure	58
3.6 Beam Specimens	61
3.6.1 Fabrication of the Specimens	61
3.7 Instrumentation	64
3.8 Test Procedure	65
Chapter Four: Mathematical Modeling	
4.1 General	66

Subject	Page
4.2 Finite Element Formulation	66
4.2.1 Basic Finite Element Relationships	66
4.2.2 Strain-Displacement Matrix	69
4.2.3 Element Stiffness Matrix	71
4.3 Material Constitutive Relationships	71
4.3.1 Ferrocement Mortar	72
4.3.1.1 Ferrocement Stress Strain relationship	72
4.3.1.2 Failure Criteria	73
4.3.2 Steel Wire Mesh	76
4.3.3 Aluminum Beam	77
4.3.4 Epoxy Layer	80
4.4 Material Modeling of Composite Beam	81
4.4.1 Representation of Ferrocement Slab	82
4.4.2 Representation of Wire Mesh	83
4.4.3 Representation of Aluminum Beam	86
4.4.4 Representation of Epoxy Layer	86
4.5 General Procedure for Nonlinear Solution	89
4.5.1 Incremental Method	89
4.5.2 Newton-Raphson Iterative Method	91
4.5.3 Step-Iterative Method (Mixed Procedure)	92
4.6 Convergence Criteria	93
Chapter Five: Results and Discussion	
5.1 General	95
5.2 Experimental Results	95
5.2.1 Ferrocement Flexural Tests	95
5.2.2 Aluminum Beam Flexural Tests	98
5.2.3 Push - Out Tests	99

Subject	Page
5.2.4 Ferrocement Aluminum Composite Beams	109
5.2.4.1 Failure modes	109
5.2.4.2 Deflection distribution	121
5.2.4.3 End slip	135
5.2.4.4 Midspan uplift	142
5.2.4.5 Strain distribution	149
5.3 Finite Element Analysis	156
5.3.1 Finite Element Discretization	156
5.3.2 Finite Element Model	157
5.3.3 Loads and Boundary Conditions	159
5.3.4 Adhesive Epoxy Layer Modeling	162
5.3.5 Ultimate Load	164
5.3.6 Deflection	164
5.3.7 End Slip	165
5.3.8 Strain	165
5.4 Plastic Analysis	189
Chapter Six: Conclusions and Recommendations	
6.1 Introduction	192
6.2 Conclusions	192
6.3 Recommendations for Future Work	194
References	195
Appendix A	203
Appendix B	206
Abstract in Arabic	

Notation

Symbol	Definition
A_a	net cross section area of aluminum beam
Al	chemical symbol of aluminum
{a}	nodal displacement vector
$\{a\}_e$	column vector of nodal displacements
$\{a^*\}_e$	arbitrary virtual nodal displacement
B	ferrocement slab width
[B]	strain-nodal displacement matrix
b	aluminum flange width
b_{eff}	effective breadth of the slab
D	aluminum section depth
[D]	constitutive matrix
d_{exp}	experimental ultimate deflection
d_{th}	theoretical ultimate deflection
{d}	displacement vector
d	ferrocement slab depth
E	modulus of elasticity
e	2.7182818
F	function of principal stress state
{f}	total external force vector
$\{f\}_e$	nodal force vector
$f_{0.1}$	stress at 0.1% offset strain
$f_{0.2}$	stress at 0.2% offset strain
f_t	minimum tensile strength (or ultimate stress)
f_y	yield strength of steel wire mesh
f_{ul}	ultimate strength of steel wire mesh
f_u	ultimate strength of ferrocement element
$f_{c'}$	compressive strength of ferrocement matrix
f_r	flexural strength of ferrocement matrix
f_{cb}	ultimate biaxial compressive strength
f_1	ultimate compressive strength for a state of biaxial compression
f_2	ultimate compressive strength for a state of uniaxial compression
f_p	limit of proportionality for aluminum
I_a	moment of inertia of aluminum section
[J]	Jacobian matrix
$\lvert J \rvert$	determinate of the Jacobian matrix
$[K]_e$	element stiffness matrix
[K]	overall stiffness matrix
$[K_t]$	tangent stiffness matrix

Symbol	Definition
$[Kt]_0$	initial tangent stiffness
[L]	matrix of differential operator
L	beam length
Mg	chemical symbol of manganese
[N]	matrix of shape functions
Ni	shape functions
N	hardening exponent
P_{cr}	cracking load
P_{ul}	ultimate load
P_{exp}	experimental ultimate load
P_{th}	theoretical ultimate load
P	total applied load
Q	load on one connector
R_f	compression force of ferrocement slab.
R_a	tensile force in aluminum section
R_{ref}	reference values
$\{R^j\}$	applied external loads
$\{R^i\}$	internal resisting loads
$\{R^u\}_i$	unbalanced forces at any stage
$\|\{R\}\|$	out of balance convergence
{R}	residual vector
Si	chemical symbol of silicon
s	end slip
s, t, and r	local coordinates
S	failure surface
T_n	normal traction at interface
T_t	shear traction at interface
t	aluminum section thickness
u, v, and w	displacement components
u_1, u_2,and u_3	nodeless variables for extra shape functions
$\{U\}_e$	displacement vector at any point within the element
W_{ext}	external work
W_{int}	internal work
xi, yi and zi	global coordinates of node i
α	a correction factor depending upon limit state
β	slenderness parameter (b/t)
ε	strain
$\{\varepsilon\}_e$	strain vector
ε_{cu}	ultimate concrete crushing strain
ε_t	fracture elongation of aluminum
$\{\sigma\}_e$	stress vector

Symbol	Definition
σ_h^a	ambient hydrostatic stress state
σ_1, σ_2, and σ_3	principal stresses
$\varphi(\delta)$	surface potential
σ_{max}	maximum normal traction at the interface
$\bar{\delta}_n$	normal separation across the interface where the maximum normal attraction attained
$\bar{\delta}_t$	shear separation across the interface where the maximum shear attraction attained
γ	specific weight
α	coefficient of thermal expansion
δ	extrapolated slip at ultimate load
Δv	deflection increment due to slip
ε_R	tolerance

List of Abbreviations

Symbol	Definition
ACI	American Concrete Institute
Ansys	Analysis system (Finite element program)
ASTM	American Society of Testing and Material
BNAIL	Big nail
B.S	British standard
CFRP	Carbon fiber reinforced polymer
DOF	Degree of freedom
ETF	End two flange
Fj	Ferrocement panel
FEA	Finite Element Analysis
FRP	Fiber reinforced polymer
HAZ	Heat Affected Zone
ITF	Interior two flange
MOR	Modulus of rupture
Si	Aluminum section
SiFj	Ferrocement-aluminum composite beam
w/c	Water- cement ratio

List of tables

Title	Page
Table (3-1) Details of aluminum sections	35
Table (3-2) Details of ferrocement – aluminum composite beams	35
Table (3-3) Mechanical Properties of Aluminum Alloy	40
Table (3-4) Main ingredients of structural aluminum alloy	43
Table (3-5) Physical properties of ordinary Portland cement	44
Table (3-6) Chemical composition of cement	45
Table (3-7) Sieve analysis of sand	46
Table (3-8) Properties of wire mesh	49
Table (3-9) Ferrocement tensile strength	52
Table (3-10) Properties of trial mixes	55
Table (3-11) Compressive and Flexure Strengths of Mortar	55
Table (3-12) Mechanical strengths of Sikadur 31 Epoxy Resin	57
Table (3-13) details of push out test specimens	58
Table (4-1) Details of used interface models	80
Table (5-1) Experimental results of tested ferrocement segments	96
Table (5-2) Experimental results of tested aluminum beams	100
Table (5-3) Ultimate values of load and slip in push-out test	106
Table (5-4) Failure modes for the tested beam specimens	110
Table (5-5) Experimental results of tested composite beams	126
Table (5-6) Experimental comparison of tested aluminum and composite beams	127
Table (5-7) End-slip of tested composite beams	136
Table (5-8) End-slip effect upon deflection for composite beams	137
Table (5-9) Midspan uplift of tested composite beams	144
Table (5-10) Midspan strains of tested composite beams	150
Table (5-11) Convergence of results	157
Table (5-12) Adhesive epoxy layer representation	162
Table (5-13) Ultimate and service loads of tested beams	166
Table (5-14) Deflections of tested beams	167
Table (5-15) End-slip of composite beams	168
Table (5-16) Comparison of experimental and theoretical strain for tested beams	169
Table (5-17) Comparison of plastic analysis results with experimental and FEA results for composite sections	191
Table (A1) Wrought alloy designation system and characteristics	204

List of figures

Title	Page
Figure (1-1) Composite action effect	2
Figure (1-2) Stress-strain curves of AlMgSi alloy and Fe360 steel	7
Figure (1-3) Comparison of strength ratio for aluminum alloy and steel	7
Figure (2-1) Load applications specified in EC9 Code Part 1.1. (a) ITF, (b) ETF	18
Figure (2-2) The stress distribution in aluminum / hybrid beam	33
Figure (3-1) Typical ferrocement aluminum composite beam	36
Figure (3-2) Aluminum sections used in the study	38
Figure (3-3) Geometrical details of aluminum tensile coupons	40
Figure (5-4) Typical stress - strain relationship for aluminum alloy	41
Figure (3-5) Stress –Strain relationship for aluminum alloy,a1	41
Figure (3-6) Stress –Strain relationship for aluminum alloy,b_1	41
Figure (3-7) Details of steel wire mesh	47
Figure (3-8) Details of wire mesh tensile coupons	48
Figure (3-9) Typical stress-strain relationship for wire mesh	49
Figure (3-10) Stress –Strain relationship for wire mesh, w_1	49
Figure (3-11) Details of ferrocement elements tensile coupons	51
Figure (3-12) Typical stress-strain relationship for ferrocement element	52
Figure (3-13) Stress –Strain relationship for ferrocement element, t_1	52
Figure (3-14) Details of precast ferrocement segments	54
Figure (3-15) Details of push out specimen	59
Figure (3-16) Details of typical used mould	61
Figure (3-17) Instrumentation of beams	65
Figure (4-1) Idealized uniaxial stress-strain curve for ferrocement matrix	74
Figure (4-2) Adopted uniaxial stress-strain curve for ferrocement matrix (ANSYS 11.0)	74
Figure (4-3) Failure surface in principal stress space with nearly biaxial stress states	76
Figure (4-4) Idealized uniaxial stress-strain curve for steel wire mesh	78
Figure (4-5) Adopted uniaxial stress-strain curve for steel wire mesh (ANSYS 11.0)	78
Figure (4-6) Piecewise form of Rambert-Osgood curve	79
Figure (4-7) Adopted uniaxial stress-strain curve for aluminum alloy, box section (ANSYS 11.0)	79
Figure (4-8) SOLID65-3D Reinforced concrete element	84
Figure (4-9) Local and global coordinates of SOLID65 element	84
Figure (4-10) Models for reinforcement in reinforcement concrete ;(a) discrete, (b) embedded and (c) smeard	85
Figure (4-11) Reinforcement orientation for distributed model	85
Figure (4-12) SOLID 45 3-D Structural Solid element	86

Title	Page
Figure (4-13) COMPIN14-Spring element	90
Figure (4-14) COMBIN39 nonlinear spring element	90
Figure (4-15) INTER205 3-D Cohesive Zone element	90
Figure (4-16) SOLSH190 3-D Structural Solid Shell element	91
Figure (4-17) Scheme of the solution procedure in a non-linear problem	94
Figure (5-1) Variation of mid-span deflection with load for ferrocement panels – Experimental work	97
Figure (5-2) Variation of mid-span deflection with load for aluminum beams – Experimental work	101
Figure (5-3) Strain distribution at mid-span for aluminum beam (S1) under ultimate load and intermediate load value in the linear stage -Experimental work	102
Figure (5-4) Strain distribution at mid-span for aluminum beam (S2) under ultimate load and intermediate load value in the linear stage - Experimental work	102
Figure (5-5) Strain distribution at mid-span for aluminum beam (S3) under ultimate load and intermediate load value in the linear stage - Experimental work	103
Figure (5-6) Strain distribution at mid-span for aluminum beam (S4) under ultimate load and intermediate load value in the linear stage - Experimental work	103
Figure (5-7) Load–slip relationships for push out tests – Experimental work	107
Figure (5-8) Load–slip relationships for push out tests, P2	108
Figure (5-9) Load–slip relationships for push out tests, P3	108
Figure (5-10) Load–uplift relationships for push out tests	109
Figure (5-11) Variation of mid-span deflection with load for different conditions between the components of composite beams – Experimental work	127
Figure (5-12) Variation of mid-span deflection with load for composite beams with 1.2 m length – Experimental work	128
Figure (5-13) Variation of mid-span deflection with load for composite beams with 2.4 m length – Experimental work	128
Figure (5-14) The effect of aluminum beam depth on variation of mid-span deflection with load for composite beams with 1.2 m length – Experimental work	129
Figure (5-15) The effect of aluminum beam depth on variation of mid-span deflection with load for composite beams with 2.4 m length – Experimental work	129
Figure (5-16) The effect of aluminum beam wall thickness on variation of mid-span deflection with load for composite beams with 1.2 m length – Experimental work	130
Figure (5-17) The effect of aluminum beam wall thickness on variation of mid-span deflection with load for composite beams with 2.4 m length – Experimental work	130
Figure (5-18) The effect of aluminum beam shape on variation of mid-span deflection with load for composite beams with 1.2 m length – Experimental work	131
Figure (5-19) The effect of aluminum beam shape on variation of mid-span deflection with load for composite beams with 2.4 m length – Experimental work	131
Figure (5-20) Comparison of load-mid span deflection relationships of composite section with its components for S1-F1.2 – Experimental work	132

Title	page
Figure (5-21) Comparison of load-mid span deflection relationships of composite section with its components for S1F1.2# – Experimental work	132
Figure (5-22) Comparison of load-mid span deflection relationships of composite section with its components for S1F1.2 – Experimental work	133
Figure (5-23) Comparison of load-mid span deflection relationships of composite section with its components for S2F1.2 – Experimental work	133
Figure (5-24) Comparison of load-mid span deflection relationships of composite section with its components for S3F1.2 – Experimental work	134
Figure (5-25) Comparison of load-mid span deflection relationships of composite section with its components for S4F1.2 – Experimental work	134
Figure (5-26) Variation of end slip with load for different conditions between the components of composite beam – Experimental work	137
Figure (5-27) Variation of end slip with load for composite beams with 1.2 m length – Experimental work	138
Figure (5-28) Variation of end slip with load for composite beams with 2.4 m length – Experimental work	138
Figure (5-29) The effect of aluminum beam depth on variation of end slip with load for composite beams with 1.2 m length – Experimental work	139
Figure (5-30) The effect of aluminum beam depth on variation of end slip with load for composite beams with 1.2 m length – Experimental work	139
Figure (5-31) The effect of aluminum beam thickness on variation of end slip with load for composite beams with 1.2 m length – Experimental work	140
Figure (5-32) The effect of aluminum beam thickness on variation of end slip with load for composite beams with 2.4 m length – Experimental work	140
Figure (5-33) The effect of aluminum beam shape on variation of end slip with load for composite beams with 1.2 m length – Experimental work	141
Figure (5-34) The effect of aluminum beam shape on variation of end slip with load for composite beams with 2.4 m length – Experimental work	141
Figure (5-35) Variation of central uplift with load for different conditions between the components of composite beam – Experimental work	144
Figure (5-36) Variation of central uplift with load for composite beams with 1.2 m length – Experimental work	145
Figure (5-37) Variation of central uplift with load for composite beams with 2.4 m length – Experimental work	145
Figure (5-38) The effect of aluminum beam depth on variation of central uplift with load for composite beams with 1.2 m length – Experimental work	146
Figure (5-39) The effect of aluminum beam depth on variation of central uplift with load for composite beams with 2.4 m length – Experimental work	146
Figure (5-40) The effect of aluminum beam thickness on variation of central uplift with load for composite beams with 1.2 m length – Experimental work	147
Figure (5-41) The effect of aluminum beam thickness on variation of central uplift with load for composite beams with 2.4 m length – Experimental work	147

Title	Page
Figure (5-42) The effect of aluminum beam shape on variation of central uplift with load for composite beams with 1.2 m length – Experimental work	148
Figure (5-43) The effect of aluminum beam shape on variation of central uplift with load for composite beams with 2.4 m length – Experimental work	148
Figure (5-44) Strain distribution at mid-span for S1-F1.2 under ultimate load and intermediate load value in the linear stage - Experimental work	151
Figure (5-45) Strain distribution at mid-span for S1F1.2# under ultimate load and intermediate load value in the linear stage - Experimental work	151
Figure (5-46) Strain distribution at mid-span for S1F1.2 composite beams under ultimate load and intermediate load value in the linear stage - Experimental work	152
Figure (5-47) Strain distribution at mid-span for S2F1.2 composite beams under ultimate load and intermediate load value in the linear stage - Experimental work	152
Figure (5-48) Strain distribution at mid-span for S3F1.2 composite beams under ultimate load and intermediate load value in the linear stage - Experimental work	153
Figure (5-49) Strain distribution at mid-span for S4F1.2 composite beams under ultimate load and intermediate load value in the linear stage - Experimental work	153
Figure (5-50) Strain distribution at mid-span for S1F2.4 composite beams under ultimate load and intermediate load value in the linear stage - Experimental work	154
Figure (5-51) Strain distribution at mid-span for S2F2.4 composite beams under ultimate load and intermediate load value in the linear stage - Experimental work	154
Figure (5-52) Strain distribution at mid-span for S3F2.4 composite beams under ultimate load and intermediate load value in the linear stage - Experimental work	155
Figure (5-53) Strain distribution at mid-span for S4F2.4 composite beams under ultimate load and intermediate load value in the linear stage - Experimental work	155
Figure (5-54) Results from convergence study: (a) mid-span deflection, (b) compressive strain, and (c) tensile strain	158
Figure (5-55) Discretization of the half span length of the composite beam	160
Figure (5-56) Distribution of applied loads	161
Figure (5-57) Boundary condition for symmetrical plane	161
Figure (5-58) Boundary condition for supports	161
Figure (5-59) Variation of mid span deflection with load for different adhesive epoxy layer models	163
Figure (5-60) Variation of end slip with load for different adhesive epoxy layer models	163
Figure (5-61) Variation of mid-span deflection with load for ferrocement specimen (F1.2)	170
Figure (5-62) Variation of mid-span deflection with load for ferrocement specimen (F2.4)	170
Figure (5-63) Variation of mid-span deflection with load for aluminum beam (S1)	171
Figure (5-64) Variation of mid-span deflection with load for aluminum beam (S2)	171
Figure (5-65) Variation of mid-span deflection with load for aluminum beam (S3)	172
Figure (5-66) Variation of mid-span deflection with load for aluminum beam (S4)	172
Figure (5-67) Variation of mid-span deflection with load for composite beam without adhesive epoxy layer (S1-F1.2)	173
Figure (5-68) Variation of mid-span deflection with load for composite beam (S1F1.2#)	173

Title	page
Figure (5-69) Variation of mid-span deflection with load for composite beam (S1F1.2)	174
Figure (5-70) Variation of mid-span deflection with load for composite beam (S1F2.4)	174
Figure (5-71) Variation of mid-span deflection with load for composite beam (S2F1.2)	175
Figure (5-72) Variation of mid-span deflection with load for composite beam (S2F2.4)	175
Figure (5-73) Variation of mid-span deflection with load for composite beam (S3F1.2)	176
Figure (5-74) Variation of mid-span deflection with load for composite beam (S3F2.4)	176
Figure (5-75) Variation of mid-span deflection with load for composite beam (S4F1.2)	177
Figure (5-76) Variation of mid-span deflection with load for composite beam (S4F2.4)	177
Figure (5-77) Variation of end slip with load for composite beam (S1-F1.2)	178
Figure (5-78) Variation of end slip with load for composite beam (S1F1.2#)	178
Figure (5-79) Variation of end slip with load for composite beam (S1F1.2)	179
Figure (5-80) Variation of end slip with load for composite beam (S1F2.4)	179
Figure (5-81) Variation of end slip with load for composite beam (S2F1.2)	180
Figure (5-82) Variation of end slip with load for composite beam (S2F2.4)	180
Figure (5-83) Variation of end slip with load for composite beam (S3F1.2)	181
Figure (5-84) Variation of end slip with load for composite beam (S3F2.4)	181
Figure (5-85) Variation of end slip with load for composite beam (S4F1.2)	182
Figure (5-86) Variation of end slip with load for composite beam (S4F2.4)	182
Figure (5-87) Variation of strain distribution with load at midspan for aluminum beam(S1)	183
Figure (5-88) Variation of strain distribution with load at midspan for aluminum beam(S2)	183
Figure (5-89) Variation of strain distribution with load at midspan for aluminum beam(S3)	183
Figure (5-90) Variation of strain distribution with load at midspan for aluminum beam(S4)	183
Figure (5-91) Variation of strain distribution with load at midspan for composite beam (S1F1.2)	184
Figure (5-92) Variation of strain distribution with load at midspan for composite beam (S1F2.4)	184
Figure (5-93) Variation of strain distribution with load at midspan for composite beam (S2F1.2	184
Figure (5-94) Variation of strain distribution with load at midspan for composite beam (S2F2.4	184
Figure (5-95) Variation of strain distribution with load at midspan for composite beam (S3F1.2)	185
Figure (5-96) Variation of strain distribution with load at midspan for composite beam (S3F2.4	185
Figure (5-97) Variation of strain distribution with load at midspan for composite beam (S4F1.2	185
Figure (5-98) Variation of strain distribution with load at midspan for composite beam (S4F2.4	185
Figure (5-99) Deformed shapes and contour plots under intermediate load at linear stage and ultimate loads for longitudinal strain distribution of ferrocement slab (F1.2)	186
Figure (5-100) Deformed shapes and contour plots under intermediate load at linear stage and ultimate loads for longitudinal strain distribution of aluminum beam (S2)	187

Title	Page
Figure (5-101) Deformed shapes and contour plots under intermediate load at linear stage and ultimate loads for longitudinal strain distribution of composite beam (S2F1.2)	188

List of plates

Title	Page
Plate (1-1) Installation of an aluminum deck on aluminum beams	8
Plate (1-2) Two story house units under construction in Baghdad	9
Plate (3-1) Aluminum sections used in the study	38
Plate (3-2) Aluminum alloy tensile coupons before test	42
Plate (3-3) Aluminum alloy tensile coupons after test	42
Plate (3-4) Test arrangement for aluminum alloy tensile coupons	42
Plate (3-5) Fabrication details of wire mesh tensile coupons specimens	50
Plate (3-6) Wire mesh tensile coupons	50
Plate (3-7) Failure mode of wire mesh	50
Plate (3-8) Test arrangement for wire mesh tensile coupons	50
Plate (3-9) Fabrication of ferrocement tensile coupons specimens	53
Plate (3-10) Ferrocement tensile coupons	53
Plate (3-11) Failure mode	53
Plate (3-12) Test arrangement for ferrocement tensile coupons	53
Plate (3-13) Compressive and flexure specimens	56
Plate (3-14) Test arrangement for compressive specimens	56
Plate (3-15) Test arrangement for flexure specimens	56
Plate (3-16) Push out specimens' elements	60
Plate (3-17) Push out specimen	60
Plate (3-18) Push out test arrangement	60
Plate (3-19) Ferrocement mould	62
Plate (3-20) Sikadur 31 components mixing	63
Plate (3-21) Ferrocement aluminum adhesion	64
Plate (3-22) Testing setup	65
Plate (5-1) Various views for ferrocement panel F1.2 after failure	97
Plate (5-2) Various views for ferrocement panel F2.4 after failure	98
Plate (5-3) Aluminum beams after failure	101
Plate (5-4) Failure of push – out specimen (P1)	106
Plate (5-5) Failure of push – out specimen (P2)	106
Plate (5-6) Failure of push – out specimen (P3)	107
Plate (5-7) Various views of S1-F1.2 after failure	111
Plate (5-8) Various views of S1F1.2# after failure	112
Plate (5-9) Various views of S1F1.2 after failure	113

Title	Page
Plate (5-10) Various views of S2F1.2 after failure	114
Plate (5-11) Various views of S3F1.2 after failure	115
Plate (5-12) Various views of S4F1.2 after failure	116
Plate (5-13) Various views of S1F2.4 after failure	117
Plate (5-14) Various views of S2F2.4 after failure	118
Plate (5-15) Various views of S3F2.4 after failure	119
Plate (5-16) Various views of S4F2.4 after failure	120

CHAPTER ONE

INTRODUCTION

1.1 General

In civil engineering construction, different materials can be arranged in an optimum geometric configuration, with the aim that only the desirable property of each material will be utilized by virtue of its designated position. The structure is then known as a composite structure. Composite structures combine two or more materials in a unit structure to provide tangible benefits and a versatile solution to suite different applications. A composite system reduces the unnecessary and unwanted material properties, such as weight and cost, without sacrificing required capacity. A structure can be considered composite only so far as the various components are connected to act as a single unit. The structural performance depends on the extent to which composite action can be achieved. Composite structures, in general, have a higher stiffness and a higher load bearing capacity when compared with their non-composite counterparts. Hence the composite sections have got smaller section depth.

In conventional composite construction, concrete slabs rest over steel beams and are supported by them. Under load these two components act indecently and a relative slip and uplift occur at the interface if there is no connection between them.With the help of a deliberate and appropriate connection provided between the beam and the slab, [1] the slip and uplift can be eliminated and their action is similar to that of monolithic Tee beam.

The connection either at discrete points along the beam or continuously which is an alternative solution to eliminates concentrated stresses and the risk of fatigue damage in connector welding [1]. Figure (1-1) shows the effect of composite action.

Although steel and concrete are the most commonly used materials for composite beams, other material such as pre-stressed concrete and timber can be used, also.

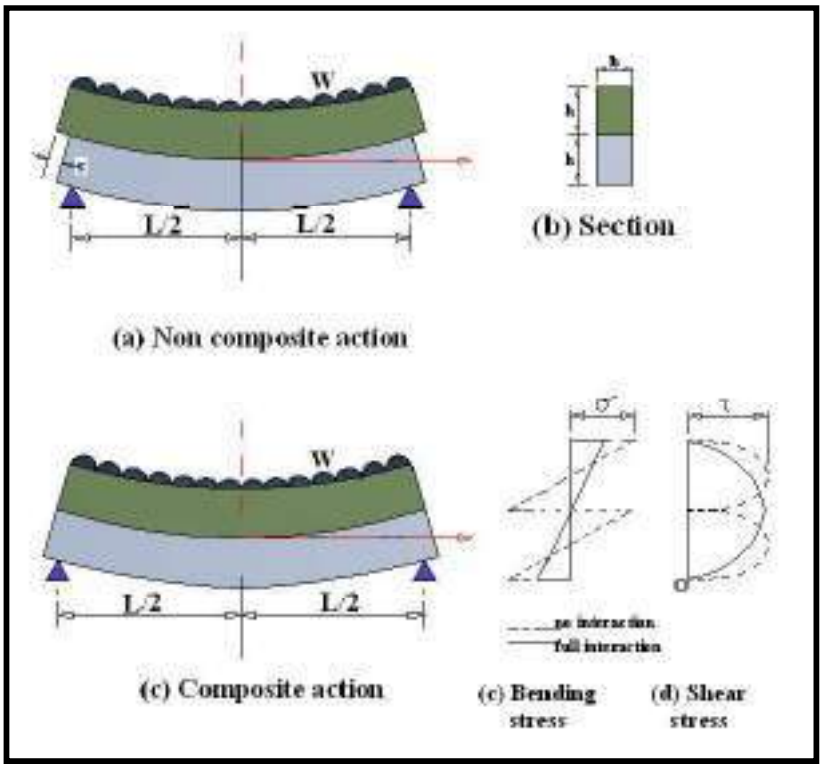

Figure (1-1) Composite action effect [2]

The advanced technology and other aspects of life aims to use everything available and efficient.

Aluminum alloys are used in a variety of structural engineering applications due to their high strength-to-weight ratio and durability [3].

Ferrocement has taken a significant place among components used for construction, for its specification of durability and strength, and its small thickness, which makes it a component suitable for constructing many light-weight structures [4].

The proper properties of ferrocement and aluminum in additional to composite action benefits have encouraged us to propose, fabricate and study composite beams consists of ferrocement and aluminum components.

So by the composite action between the two, their respective advantage can be utilize to the fullest extent.

1.2 Aluminum

Aluminum is the third most common element in the earth's crust, coming after oxygen and silicon. It makes up 8% of the crust's total mass and is the most abundant metal [5].

Pure aluminum is not suitable for structural applications because of the low values of its mechanical characteristics. In order for aluminum to be useful as a structural metal, it was essential to develop suitable alloys, However, many alloys are available with a large variety of excellent mechanical and physical qualities. The appropriate alloy depends on the specific application. The 6xxx series alloys are the most useful for structural applications because of their combination of strength, corrosion resistance, and weldability [5].

Generally the advantages of aluminum alloys are [6]:

a. Low density, of approximately one third of steel.
b. Good strength and toughness properties, also at very low temperatures.
c. Large variety of possible cross-sectional shapes of profiles and connection elements.
d. Good workability.
e. High corrosion resistance due to a tough oxide-layer.
f. Excellent to recycle without a decrease in quality .

The main characteristics of aluminum alloys differ from those of steel as follows [7]:

a. Aluminum alloys offer a wider range of strength than steel. Therefore the concept of a fourth dimension in metal construction seems to be more appropriate to aluminum alloys than to steel. Aluminum is very ductile ($\varepsilon_t \approx$ 40 %), but on the other hand its strength is very low for structural application ($f_{0.2}$=20 MPa). In order to increase strength, a cold – working process can be used; however, this process does not greatly increase strength ($f_{0.2}$=100 MPa),

and ductility is drastically decreased (up to one tenth of the initial value). Another way of increasing the strength of the material is to alloy aluminum with other element (AlMn, AlMg alloys). After this process, the strength can be higher than 100 MPa, with a ductility equal to ($\varepsilon_t \approx$ 10 %). The high strength can be obtained if heat treatment is applied. The strength goes up to $f_{0.2}$ =250 MPa in AlSiMg alloy, and can reach $f_{0.2}$=350-400 MPa in AlZn and AlCu alloys. In a comparison of the stress – strain curves of AlMgSi alloy and Fe360 steel in Fig. (1-2) it can be observed that aluminum alloys have a strain – hardening portion without a horizontal line corresponding to yielding. It is clearly shown that the ultimate elongation is lower than of steel and the ($f_t/f_{0.2}$) ratio is lower than that of steel (1.2 against 1.5). Both materials behave linear elastically up to the elastic limit, which basically represents the working range of structure. They differ, instead in inelastic behavior.

b. Aluminum is lighter than steel, the specific weight is (2700 kg.m^{-3}) equal to one third that of steel. A concise comparison can be made if the ratio (f/γ) termed the" strength ratio" between strength and specific weight is considered. Figure (1-3) shows that this comparison is extremely positive for aluminum alloys.

c. Young's modulus is one third that of steel, thus giving more frequent problems of deformation and of instability. When aluminum alloys under compression, owing to the small value of Young's modulus , buckling is more likely to occur than in steel structures. Elastic deflection becomes more of a factor than it is in steel. This is often a consideration in beam design.

d. The coefficient of thermal expansion of aluminum is twice that of steel. This means that the structure is more sensitive to thermal variations, and thus has higher deformation when it is not constrained. When a structure is constrained against thermal deformation, residual stress will be about 30 percent lower than those in steel structures since they are proportional to the product (αE). Aluminum is eminently suitable for cryogenic applications, because it is not

prone to brittle fracture at low temperature in the way that steel is. Its mechanical properties steadily improve as the temperature goes down.

e. Most of the alloys can be arc welded as readily as steel, using gas shielded processes. Welding speeds are faster. On other side the alloys sever from heat-affected zone (HAZ) softening at welds which tends to be a serious local drop in strength at welded joints in some alloys. The use of adhesive bonding is well established as a valid method for making structural joints in aluminum.
f. Extrusion process is the standard way of producing aluminum sections, is vastly more versatile than the rolling procedures in steel.
g. Aluminum components are more prone to failure by fatigue than are steel ones.
h. Aluminum does not rust and can normally be used unpainted. However, the strongest alloys will corrode in some hostile environments and may need protection.

1.2.1 Aluminum Applications

The main cases of structural applications belong to the following groups [8]:

a. Long-span roof system with small live loads compared with dead loads; they include reticular schemes of plane and space structures.
b. Structures located in inaccessible places far from the fabrication shop; so the transport economy and ease of erection are of extreme importance. It is the case of prefabricated elements such as electrical transmission towers, stair cases, provisional bridges, which can be carried by helicopter completely assembled.
c. Structures situated in corrosive or humid environments; they cover many types, such as swimming pool roofs, river bridges, hydraulic structures and offshore superstructures.
d. Structures having moving parts; so that lightness means economy of power under service. They are mainly moving bridges.
e. Structures for special purposes, for which maintenance operations are particularly difficult and must be limited, as in case of masts, lighting towers,

sign motorway portals. An example of structural application of aluminum alloys is shown in Plate (1-1).

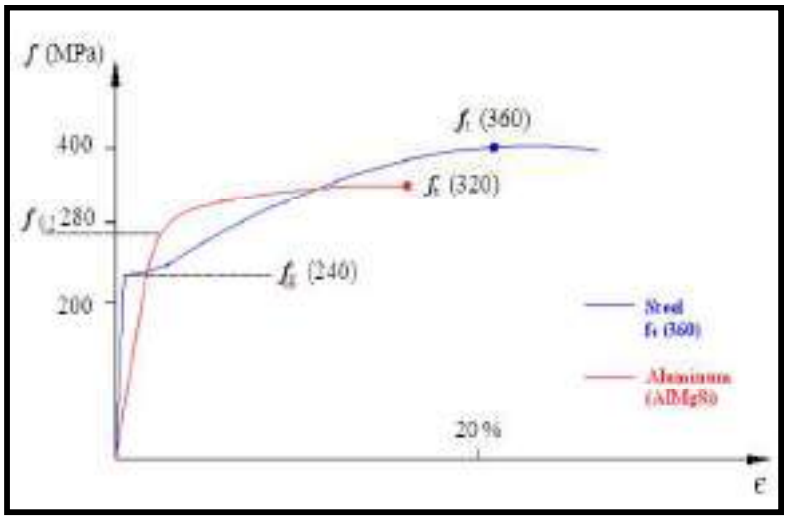

Figure (1-2) Stress-strain curves of AlMgSi alloy and Fe360 steel [7]

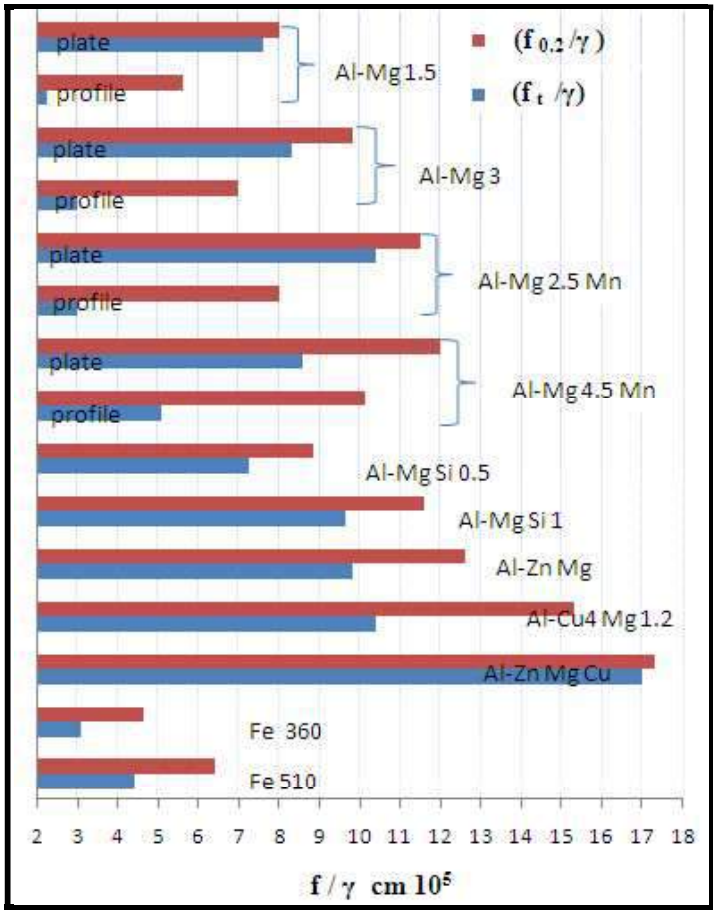

Figure (1-3) Comparison of strength ratio for aluminum alloy and steel [7]

Plate (1-1) Installation of an aluminum deck on aluminum beams [5]

1.3 Ferrocement

Ferrocement is a form of thin reinforced concrete structure in which a brittle cement-sand mortar matrix is reinforced with closely spaced multiple layers of thin wire mesh and /or small diameter rods, uniformly dispersed throughout the matrix of the composite [9].

Ferrocement has taken a significant place among components used for construction, for its specification of durability and strength, and its small thickness, which makes it a component suitable for constructing many light-weight structures.

From the architectural stand-point, ferrocement is very useful, since it can be molded into different shapes for different designs. These facts ensure a significant future for use of this component. For these reasons, a careful study of the characteristics of this component was made, to be able to determine its specifications from the structural engineering stand-point, to make it easier for use. The mechanical characteristics of ferrocement differ from those of reinforcement concrete as follows [9]:

a. Ferrocement can have homogenous-isotropic properties in the two directions; two way action and high level of redundancy as indeterminate systems are expected.

b. Ferrocement generally has a high tensile strength and a high modulus of rupture. Its tensile strength can be of the same order as its compressive strength

c. Ferrocement generally has a high reinforcement ratio in both tension and compression.

d. Ferrocement has a high specific surface of reinforcement, which is one to two orders of magnitude that of reinforcement concrete.

e. The cracking and multiple cracking process in ferrocement under tension differs from reinforced concrete.

f. The extensibility of ferrocement, that is its elongation to failure in tension, or its deflection to maximum load increases with an increase in the number of mesh layers used. Its ductility increases with an increase in the volume fraction and specific surface of reinforcement. Such behavior is different from that of reinforced concrete in bending, where generally a lower ductility is observed with increase in reinforcement ratio.

g. Ferrocement provides excellent leakage characteristics for applications in water tanks because of its very small crack width under service load.

h. Ferrocement has shown good durability under various environmental exposures.

i. Because of its smaller thickness, ferrocement provides poorer fire resistance than reinforcement concrete.

j. Ferrocement has a better impact and punching shear resistance than reinforced concrete because of the two direction reinforcement.

1.3.1 Ferrocement Applications

In its role as a thin reinforced concrete product and as laminated cement-based composite, ferrocement can be used in numerous applications, including[9]:

a. Agricultural applications: grain storage bins and silos, water tanks, lining for underground pits and irrigation channels pipes, shells for fish and chicken farms, and pedestrian bridges.

b. Rural energy applications: biogas digestors, biogas holders, incinerators and panels for solar energy collectors.

c. Water supply and sanitation: water tanks, sedimentation tanks, well casings, service modules, sanitary tanks, linings for swimming pools, and fuel tanks.

d. Housing applications: house, commonly centers, museums, mosque domes and other worship place, domes structures, precast housing element, wall panels, sandwich panels, corrugated roofing sheets, hollow-core slabs, permanent formwork and repair and rehabilitation of existing housing.

e. Building Industry: Roofing element, wall element, lintels, beams, and columns. An example of housing applications is shown in Plate (1-2).

Plate (1-2) Two story house units under construction in Baghdad [10]

1.4 Why Using Ferrocement and Aluminum in Composite beam

To select a particular structural material for a given application, its properties are evaluated and compared with other competing materials.

The following points reflect powerful properties of aluminum and ferrocement which will be active when utilizing those materials in composite action.

1. High strength to weight ratio is a contributed character for ferrocement and aluminum and courages us to study ferrocement aluminum composite beam.

2. Ferrocement is strong in compression and aluminum is susceptible to buckling in compression and strong in tension, so by the composite action between the two materials, one can utilize their respective advantage to the fullest extent.
3. Ferrocement thickness is (5 to 50 mm); thinner than reinforced concrete.

1.5 Adhesive bonded connections

The most interested point in the field of this new suggested composite structures is in adhesive bonded connections between ferrocement and aluminum beam. The use of epoxy-resins allows many problems related to the traditional connecting system to be solved [7].

The use of epoxy-resins could be profitable tools for optimizing some connection problems as well as for maximize economy.

Generally the advantages of using Adhesion bonded connections are:

(a) Avoiding aluminum corrosion due to contact with concrete .
(b) Avoiding notch produced by mechanical connectors.
(c) Enabling the use of pre-cast slabs.
(d) Reduction of local buckling of aluminum section.
(e) Avoiding of block failure which is a potential limit state for connected plates with mechanical fasteners.
(f) Eliminating concentrated stresses .
(g) Eliminating the risk of fatigue damage in connector.
(h) Avoiding the reduction of aluminum strength due to the heat of connectors welding.

1.6 Objective of Study

The purpose of the study is to generate data and provide information about the structural behavior of the proposed ferrocement aluminum composite beams .

The study consists of two parts; the first part is to investigate experimentally the structural behavior of ferrocement aluminum composite

members. Simply supported beams were tested. The main variables considered in the study were the shape, depth and thickness of the aluminum section as well as span length. Adhesive bonded connection is examined.

The second part deals with the analysis of the tested beams theoretically. The analysis is made by using the available ANSYS version 11.0 code to simulate the ferrocement – aluminum composite beams. Also, a plastic analysis is done by using a suggested method to determine the ultimate capacity of such beams.

The validity of the used methods of analysis is examined by comparing their results with the experimental ones.

1.7 Thesis Layouts

The thesis is organized in six chapters. The first one gives a general introduction on composite beam, aluminum structural alloy and ferrocement. Chapter two presents the literature review concerning the aluminum beams, ferrocement members and composite beams. Chapter three deals with the experimental work in which the properties and testing of materials used in investigation, details of tested beams, instrumentations, and test program are illustrated. The finite element, three dimensional models are presented in chapter four in which the basic finite elements relationships, derivation of the governing equilibrium equations, and the mathematical modeling of the materials used in the tested composite beam are shown. Chapter five includes the results relating to the structural behavior of tested composite beams. The main conclusions derived from this study and suggestions for the futures works are presented in chapter six.

CHAPTER TWO

REVIEW OF LITERATURE

2.1 General

This chapter aims to provide a brief review of previous investigations of structural behaviour of aluminum beams, ferrocement as structural members and composite beams.

2.2 Aluminum Beams

Aluminum is easily the second most important structural metal, yet few designers seem to know much about it. Since the 1940s, the aluminium rapidly became more important. Researchers have been slow to investigate what it has to offer and how to design with it.

In 1994, Brown et al. [11] investigated the collapse behaviour of lightweight aluminium girders, suitable for transportable bridging systems. They described the theoretical and experimental behavior of the transverse web stiffeners of welded aluminium alloy plate girders loaded predominantly in shear. The theory was based on a mathematical model that assumes a non-linear shear stress distribution at the boundaries of the adjacent web panels. The experimental investigation consisted of a series of tests in which l0 fabricated plate girders were loaded to failure; careful tests of material properties are also reported.

In 1996, Mazzolani et al. [12] presented a comprehensive parametric analysis to compare different approaches in the design of slender aluminium alloy sections. They applied different design criteria to a set of sections which adequate represent the most important types of slender aluminum alloy sections.

They examined the reliability of the procedures proposed by the codes considering also the different computational cost required by each method.

In 1997, Mazzolani et al. [13] outlined the theoretical steps of a semi-empirical method for evaluating the rotation capacity of aluminium alloy members subjected to non uniform bending. The approach was represented by the extension to aluminium alloy members of the semi-empirical methods proposed for evaluating the rotation capacity of steel members. The moment curvature relationship of aluminium alloy members was represented by means of Ramberg-Osgood type relation. This allowed with reference to the classical three-point bending test, the derivation in closed form of the curvature diagram. Furthermore, a closed form integration of the curvature diagram was performed, providing a relation for evaluating the rotation corresponding to the occurrence of local buckling. The study included also experimental evaluation of the non-dimensional stress corresponding to the attainment of the local buckling. The testing needs for this evaluation were outlined, and both the preliminary test results and the planned activity were presented.

In 1999 Moen et al. [14] presented an experimental program for evaluating the rotational capacity of aluminum beams subjected to a moment gradient loading. The study was focused on local buckling and on the tensile failure susceptibility. Results were compared with design codes. Beams of different tempers, cross sections, and lengths were tested. Some beams were welded, whereas others were unwelded. Uniaxial tensile tests revealed a pronounced plastic anisotropy in the extruded beams. Tests for the reduced strength zone near welds indicated a local ultimate strength in the order of 67% of the parent material yield strength in alloy AA 6082-T6. Nevertheless, the local failure mode was ductile. The strain-hardening behavior of the material and compression flange width thickness ratio were found to have a strong influence on both the moment capacity and the rotational capacity of aluminum beams. The magnitude of the moment gradient had a significant influence on rotational capacity, whereas the effect on the moment capacity was not very pronounced

in the experiments. Welded members suffered a tremendous loss of rotational capacity owing to premature tensile failure. Moreover, the tests provided a calibration basis for numerical modeling.

In 2001, Mazzolani et al. [15] presented a numerical study to assess the rotational capacity of aluminum alloy members. In order to investigate the effects of some governing parameters on the inelastic response of aluminum beams under moment gradient, a wide parametric analysis was carried out. This was based on the use of a FEM code ABAQUS/Standard. Reference was made to hollow rectangular cross sections, focusing on the influence of the flange slenderness, the strain hardening of the material, the shape factor of the section, the web stiffness, and member compactness. The investigations concerning these factors were considered separately as well as their interaction. Also, the susceptibility of aluminum beams to tensile failure, which might produce a limitation of member deformation capacity, was analyzed. The results, which have been obtained for two different alloy tempers, showed the importance of some of the foregoing parameters on both buckling strength and rotational capacity of aluminum beams, emphasizing the need to improve the present guidelines provided by the European code on aluminum structures relating to cross-sectional classification.

In 2004, Mazzolani et al. [16] devoted an extensive numerical analysis program to the evaluation of the inelastic response of I-shaped aluminium alloy beams in non-uniform bending. By using a numerical model implemented in the implicit FE code ABAQUS/Standard and largely calibrated with experimental tests, the main geometrical and mechanical parameters influencing the plastic behaviour of such beams were investigated. The results obtained in this study confirmed the important role of the material hardening which, in addition to the local slenderness of compressed elements, has a strong influence on both ultimate moment and rotational capacity of the member. Moreover, it was shown that the influence of the other parameters, namely flange-to-web slenderness ratio, moment gradient, web slenderness and sectional area ratio, on

the plastic capacity of the considered beams in terms of strength and deformability was of a secondary importance even if it is not negligible. On the whole, the results, which were obtained for two different tempers, emphasized the need to improve the present guidelines provided by the European code for aluminium structures relating to cross-sectional classification. More accurate class limits for outstand elements, which were able to account for the most important influential parameters on the plastic behaviour, were therefore proposed.

In 2006, Zhu1 et al. [17] presented a test program on aluminum alloy thin-walled square and rectangular hollow sections in combined axial compression and minor axis bending. A total of six series of tests was conducted that included 27 beam-column and 4 pure bending tests. The test specimens were manufactured by extrusion using 6061-T6 heat-treated aluminum alloy in three different cross sections having the clear width-to-thickness ratio ranged from 31.3 to 81.3. The beam-column specimens were compressed between pinned ends at different eccentricities in order to obtain an interaction curve for each series of tests. Pure bending tests were conducted for each test series to determine the bending capacities of the specimens. Local and overall initial geometric imperfections of the specimens were measured. Material properties were obtained from tensile coupon tests. The observed failure modes of the beam-column tests included local buckling, flexural buckling, interaction of local and flexural buckling, and material yielding in the heat-affected zone. The test strengths were compared with the design strengths calculated using the American, Australian/New Zealand, and European specifications for aluminum structures. Beam-column interaction curves were plotted for each test series. It was shown that the beam-column design strengths and bending capacities predicted by the three specifications were generally conservative.

In 2006, Manganiello**a*** ***et al.*** [18] devoted an extensive numerical study to the evaluation of the inelastic flexural behaviour of aluminium alloy structures. The main aim of the research was to determine the required ductility

for applying simplified methods of plastic analysis (i.e. plastic hinge method) to structural systems made of materials characterized by a continuous hardening and with limited deformation capacity. Therefore, the cross-section rotational capacity necessary to attain predefined levels of load bearing capacity is evaluated for different structural schemes and then compared to the available rotational capacity corresponding to fixed thresholds of ultimate cross-section curvature. The influence of both geometrical (cross-section shape factor and structural scheme) and mechanical (material hardening and ultimate deformation capacity) parameters was taken into account. The parametric analysis was performed by using a numerical model implemented in the implicit non-linear FE code ABAQUS/Standard and calibrated on available experimental tests. On the basis of the above analysis, the limit values for the rotational capacity of a cross-section in bending necessary to guarantee adequate inelastic redistribution of internal forces for continuous beams and framed structures were given. Finally, new indications for the application of the modified plastic hinge method included in Eurocode 9 were provided.

In 2006, Ming et al. [19] presented an investigation of the nonlinear deformation of aluminum bending members using the finite-element analysis (FEA). Most design codes adopted a simple linear analysis for the calculation of deflections, therefore, in this study the plastic adaptation coefficient, which can be used to limit the residual deflection, was introduced, and the influence of residual deflection was investigated. A method for evaluating the plastic adoption coefficient was proposed. The study also showed the load-deflection curve of aluminum bending members and the influence of several parameters. A semi-empirical formula was derived, and some numerical examples were solved by FEA. The coefficients of the semi-empirical formula were modified by the FEA results using the nonlinear fitting method. Based on these results, two improved design methods for strength and deformation of aluminum bending members were proposed. Through the comparison with test data, these methods were proved to be suitable for structural design.

In 2007 , Koltsakisa et al. [20] performed a numerical approach to the mechanical behaviour of aluminium beams, both extruded and welded at the web–flange junction. The studied beams were taken to be short so as to ensure that their design is dominated by shear. In order to investigate the effects of the weld and the consequent existence of a heat-affected zone (HAZ), both welded and extruded beams of identical geometric characteristics were studied. Three alloys, 6063-T6, 6005A-T6 and 7020-T6, were chosen because of their varying strength characteristics, as well as the different severity of mechanical degradation that each one undergoes in the HAZ. The numerical investigation was performed in the framework of small displacements, and the possibility of lateral buckling was excluded. All the studied cases were qualified as Class-I cross sections for normal actions. The Ramberg–Osgood stress–strain relation was used to describe the hardening of the material. The results obtained by means of finite element models were compared to those of classical beam theory and to the resistance checks of Eurocode 9.

In 2007, Wanga et al. [21] predicted the structural behaviour of welded and un-welded I-section aluminium members subjected to four-point bending by Finite element analyses. A modeling procedure using shell elements was established, where careful modeling of the inhomogeneous material properties due to welding is an important ingredient. A material model comprising anisotropic plasticity and ductile fracture was adopted. The yield function and work hardening parameters for the heat-affected zone, weld and base material were determined based on material tests and experimental data available in the literature. The numerical simulations comprised explicit analyses for a basic, relatively coarse mesh and implicit analyses for the same basic mesh and a refined mesh. Simulations were performed with perfect and imperfect geometries, since some beams fail by local buckling. The numerical results were compared with existing experimental data, and, in general, good agreement with the experimental results was obtained. However, the solutions were found to be

mesh dependent for members failing by strain localisation and fracture in the tension flange.

In 2007, Young et al. [22] assessed the web crippling design rules in the current American Aluminum Design Manual, Australian/New Zealand Standard, and European code for aluminum structures. Test strengths of aluminum square and rectangular hollow sections under end-two-flange (ETF) and interior-two-flange (ITF) loading conditions were compared with the design strengths (capacities) obtained using the aforementioned specifications, Fig.(2-1). The test strengths were also compared with the design strengths obtained using the unified web crippling equation as specified in the North American Specification for cold-formed steel structural members. It is shown that the design strengths predicted by the aforementioned specifications were either quite conservative or unconservative, but in general the predictions were unreliable resulting from reliability analysis. Hence, two different unified web crippling equations for aluminum square and rectangular hollow sections under ETF and ITF loading conditions were proposed. The proposed unified design equation (A) used the same technique as the North American Specification for the unified web crippling equation with new coefficients of C, CN and Ch determined based on the test results obtained in this study. The proposed unified design equation (B) was similar to the unified web crippling equation in the NAS Specification, and the effect of the ratio N/h was also considered, where N is bearing length and h is the depth of the flat portion of web. Generally, it was shown that the proposed unified web crippling equation (B) compares well with the test results.

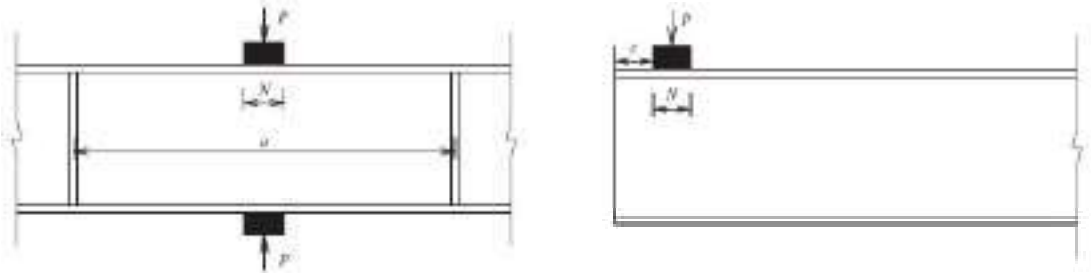

(a) **(b)**

Figure (2-1) Load applications specified in EC9 Code Part 1.1. (a) ITF, (b) ETF

In 2008, Bambach [23] outlined experimental and analytical investigations of metal beams subjected to transverse blast loads. The study presented an experimental study of 73 aluminium square hollow sections subjected to transverse blast loads by application of explosives. Four different section slenderness values and three different lengths were investigated, resulting in a wide range of length/depth ratios typical to façade structures. A semi-empirical analytical solution was presented whereby existing theory developed by others for solid metal sections was modified to account for local section deformations that occur in blast loaded hollow sections. The technique considered both the energy dissipated in local deformations and the resulting reduction in the section-bending modulus, and furnished a solution that bounds the experimental results with reasonable accuracy. A general design procedure was outlined that may be based on a final permanent deformation or a failure load, and the limitations of such a procedure were discussed.

In 2009, Zhou et al. [24] presented a series of tests on high strength aluminum square hollow sections subjected to concentrated bearing load. A total of 64 web-bearing tests was conducted. The test specimens were fabricated by extrusion using 6061-T6 heat-treated aluminum alloy. The tests were carried out under end and interior loading conditions, where the specimens were seated on a fixed solid steel base plate. These tests closely simulated the support condition of the floor joist members seated on solid foundation. The test results were compared with the design strengths obtained using the American Aluminum Design Manual and European code for aluminum structures. It was shown that the design strengths predicted by these codes are either quite conservative or unconservative. Furthermore, the Australian Standard AS4100 and British Standard BS5950 Part 1 were used for aluminum square hollow section with sharp corners. The design rules of steel codes were modified to predict the web-bearing strength based on this study. It was shown that the design strengths calculated using the modified web-bearing design rules are generally conservative and agree well with the experimental results.

Furthermore, the critical values of web slenderness were proposed beyond which web buckling governs.

In 2009, Zhu et al. [25] presented experimental and numerical investigation for aluminum alloy flexural members. The tests were performed on ten different sizes of square hollow sections subjected to pure bending. Material properties of each specimen were obtained from tensile coupon tests. A nonlinear finite-element model was developed and verified against the pure bending tests. Stress-strain relationships obtained from tensile coupon tests were incorporated in the finite-element model. The verified finite-element model was used for a parametric study of aluminum alloy beams of square hollow sections. A comparison of the experimental and numerical bending strengths with the design strengths calculated using the current American, Australian/New Zealand, and European specifications for aluminum structures was presented. The bending strengths were also compared with the design strengths predicted by the direct strength method, which was developed for cold-formed carbon steel members. Design rules were proposed for aluminum alloy square hollow section beams based on the current direct strength method. Reliability analysis was performed to evaluate the reliability of the design rules.

2.3 Ferrocement Members

The use of Ferrocement as roofing and slab elements has been a subject of investigation by many researchers.

In 1971, Rao et al. [26] studied the behavior of ferrocement in flexure. The variable parameters involved were wire mesh aperture, percentage of steel and diameter of wire of square woven mesh. It was stated that specimens with small wire aperture resulted in higher ultimate bending stress and modulus of elasticity for the same steel percentage, which seems to be more effective than the other parameters.

In 1972, Lee et al. [27] carried out tests on beams, one-way and two-way slab specimens. Chicken wire mesh was used in the investigation. The modulus

of elasticity in the cracked and uncracked stages was predicted. They mentioned that in the cracked range, the contribution of mortar in the tension zone was neglected. The agreement between experimental and theoretical values was good. The ultimate moment was determined by assuming rectangular stress distribution in the compression zones. The contribution of skeletal steel in the calculation was also accounted.

In 1974, Alwash [28] tested ferrocement beam specimens reinforced with square wire mesh and different layers of wire mesh were used. Tested beams were simply supported and subjected to third point concentrated loads. He concluded that it is possible to predict some of ferrocement properties on the basis of reinforced concrete concept. Also, it was found that the period of load application of beams can be characterized by three limits. The first limit was the first crack, the second was the first visible crack and the third was the failure. The first crack and the first visible crack were limits which define the behavior of ferrocement beams. In the first crack no visible cracks can be observed. The variations of these limits were found to be given by the specific surface of the tensile reinforcement.

In 1977, Balaguru et al. [29] conducted testes on ferrocement beam specimens. All specimens were 457mm long,130mm wide, and 13mm thick. Three types of wire meshes with square opening were used which include welded reinforcement of (12.6 mm) opening and woven reinforcement of (12.6 mm) and (6.3 mm) opening. The diameter of wires were (1.07 mm for 12.6 mm opening and 0.635 mm for 6.3 mm opening).Two, four and six layers of wire mesh in each three specimens for each type of mesh, with W/C and sand cement ratios by weight of 0.55 and 2.0 were used. A four point loading arrangement with 381mm span and 130 mm constant bending moment zone was used. The investigation was conducted to predict deflection and crack width for ferrocement members under flexure. The results included:

1- The stress –strain curve of mortar in compression and tensile stress-strain curve of meshes were obtained.

2- A mathematical model to predict the moment-curvature and the load-deflection curve of ferrocement beam for given properties of the constituent materials was developed.
3- Empirical and analytical relationship between crack widths and steel stresses were proposed.

In 1980, Fernandes et al. [30] presented a work conducted to evaluate the merits of ferrocement as a roofing material. Effects of the type of wire mesh and amount of transverse wire mesh reinforcement have been studied. Test results of six panels were presented and compared with results from a similar study on asbestos panels. The experimental results showed that panels made of hexagonal mesh yielded larger deflection for the same load than the panels made of square mesh. The effect of transverse wire mesh reinforcement was more pronounced in the higher load ranges than in the lower load ranges, and the load carrying capacity of ferrocement panel was much higher than that of asbestos panel.

In 1985, Mansur et al. [31] presented a study on flexure of lightweight ferrocement slab. An experimental investigation was carried out on one way ferrocement slabs. In their slabs the major variables were thickness of the slabs, number of the layers of wire mesh, and density of the mortar. Steel fibers of short length and small diameters were also added to the matrix to study their influence on the cracking behavior, ductility and ultimate strength of the slabs. Galvanized woven wire mesh of 8.5 mm square grid with a wire diameter of 0.87 mm was used as reinforcement. 12 slabs with 2.5m and 0.4m wide specimen were selected, and the test was divided into three groups according to the thickness of slab (90, 75 and 50mm). Tests were conducted under third point loading over a simple span of 1.8m. The load was applied by hydraulic jack and deflection readings were taken at 0.2 kN increment of the load. The results of these tests have indicated that there was a reduction in uncracked stiffness as the density of mortar or volume fraction of reinforcement is decreased. The conventional reinforced concrete theory was modified for the inclusion of wire mesh reinforcement in the analysis of the slabs. In general, the theoretical

predictions were found to be in a good agreement with the experimental values.

In 1988, Mansur [32] presented analytical and experimental investigation of the ultimate load behavior of ferrocement in flexure. The experimental program comprised of a series of tests in which the thickness of member was systematically varied for an equal volume fraction of reinforcement. Test results indicated that the ultimate rotation capacity of a member decreases with increasing the thickness and that the welded wire mesh as reinforcement provided better curvature ductility than an equivalent amount of woven wire mesh. However, within the practical range of member thickness, both types of reinforcement furnished sufficient ductility to justify a rigid-plastic analysis at collapse. Three methods of ultimate strength analysis have been evaluated by comparing with a large number of available test data. Of the three methods, the rigid – plastic analysis appeared to be marginally better. Using this method, design charts have been developed for typical ferrocement section.

In 1999, Al-Salihi et al. [33] presented a design method of ferrocement element in flexure. A total of twenty-one ferrocement specimens of (1000x90x38mm) were tested in bending. Three different types of steel mesh were investigated. The amount of reinforcement of 0.5, 1.0, and 1.5 percent relative to section area was attempted. It was stated that the thin section of ferrocement exhibits moment capacity in excess of that computed on the basis of ultimate strength theory.

In 1991, Basunbul et al. [34] studied the flexural behavior of ferrocement sandwich panels. The parameters considered in the experimental investigation were the number of wire mesh layers, the skeletal steel, the web mesh reinforcement and the number of webs. Ultimate moment capacities were computed analytically using conventional reinforced concrete theory. The analytical results were compared with the experimental results by tests on 12 sandwich panels. Cracking behavior and failure patterns for all panels were also obtained and compared.

In 2001, Wang et al. [35] studied bending response of hybrid ferrocement plates with meshes and fibers. They found that for ferrocement and laminated cementitious composites, increasing the number of mesh layers was not an efficient way to improve the modulus of rupture (MOR); moreover, at high reinforcement ratio severe spalling of matrix cover and delamination of extreme tensile layer were likely to lead to premature failure. Adding discontinuous fibers to the matrix provides a remedy to these drawbacks. In this paper, the bending response of hybrid ferrocement thin plates reinforced with meshes and fibers was reported and compared with conventional ferrocement composite with meshes and plain mortar. Three types of meshes, including two expanded steel meshes and one Kevlar FRP mesh, combined with two types of synthetic fibers, namely Spectra and PVA fibers, were experimentally investigated. The test results showed that even at a high volume fraction of 6.73%, the expanded steel mesh can still be effectively used as reinforcement of ferrocement and a MOR exceeding 60 MPa was achieved. Compared with the specimens using plain mortar, the presence of fiber resulted in substantial increase in MOR, significant reduction in crack spacing and in turn crack width, prevention of cover spalling even at large deflection, and considerable improvement in shear capacity. An increase of the toughness and energy absorption to failure by up to 250% was also observed when a ductile fiber reinforced matrix was used with the FRP meshes. Non-linear analysis was employed to predict the MORs of the composites, and good agreement was observed.

In 2003, Nassif et al. [36] presented experimental and analytical investigation of ferrocement–concrete composite beams. The composite beams were made of reinforced concrete overlaid on a thin section of ferrocement (cement paste and wire mesh). In particular, the method of shear transfer between composite layers was examined. Various types of beam specimens with various mesh types (hexagonal and square) were tested under a two-point loading system up to failure. Results from experimental data were compared to those from nonlinear analysis as well as a finite element study to model the

overall non-linear behavior. Results showed that the proposed composite beam has good ductility, cracking strength and ultimate capacity.

In 2005, Hago et al. [37] studied the ultimate and service behavior of ferrocement roof slab panels. The test results of six simply supported roof slab panels were presented. The parameters of study included the effect of the percentage of wire mesh reinforcement by volume and the structural shape of the panels on the ultimate flexural strength, first crack load, crack spacing and load-deformation behavior. The results indicated that the use of monolithic shallow edge ferrocement beams with the panels considerably improves the service and ultimate behavior of the panels, irrespective of the number of steel layers used.

In 2008, Rao et al. [38] presented an experimental study on the strength and behavioral aspects of voided ferrocement channel type units for precast beams. As these beams are lighter in weight, they find their place in seismic resistant design of structures. Eight channel type ferrocement units were tested by four points loading. The variable parameter included the number of layers of wire mesh. The flexural strength of the voided channels was compared with that of solid channels too. The test results indicated that the drop in flexural strength with the voids is very negligible compared to the decrease in the weight of the member. The Moment curvature response of the voided members under flexural loading was improved with the post ductility of the member with increase in the number of mesh layers.

In 2009, Aboul-Anen et al. [39] studied the composite action between the ferrocement slabs and steel sheeting. The paper presented the experimental models of ferrocement slabs with and without steel sheeting and their numerical models using the finite element method. Finite element models were developed to simulate the behavior of the slab through nonlinear response and up to failure, using the ANSYS Package. Additionally, the comparison between the theoretical and experimental models was presented and discussed.

In 2010, Ahmed [40] studied the fracture behavior of ferrocement beams under flexural loading. The influence of different factors on the strength and deformation characteristics was examined and assessed. The factors studied are the volume fraction of mesh reinforcement, presence of initial crack, and alignment of mesh layers. A series of 8 bending specimens reinforced with square wire meshes were tested under two central concentrated loads. Deflection, mouth opening displacement, crack width, and crack length were recorded from the first application of load up to failure. A finite element program for analysis of beams has been developed to calculate the resulted deformation, and a fracture program has been developed based upon the linear elastic fracture mechanics equations to estimate the stress intensity factor. A comparison between the theoretical and experimental results has been made. The results appeared to have good agreement. The calculated stress intensity factor for specimens with high volume fraction of mesh reinforcement reached to about (40MPa. $mm^{1/2}$), while for specimens with low volume fraction it was (12MPa. $mm^{1/2}$).

2.4 Composite Beams

Composite beams were widely used in the early 1900s. Many researchers investigated the behavior of the composite beams .

Since the early fifties of the previous century, numerous experimental and theoretical works have been carried out to understand the behaviour of composite beams. The following review will concentrate on the pervious works conducted on simply supported composite beams with different material such as concrete, steel, timber and aluminum.

In 1964, Chapman et al. [41] studied the behavior of seventeen simply supported steel concrete composite T-beams under static and distributed loads. The amount of shear connectors (welded studs) was varied within the range which might be contemplated for design purpose and the effect of interface slip on elastic and ultimate behaviour was observed. It was found that the use of

ultimate load design for a composite section may lead to working stresses approaching the yield stress, because of the large shape factor. He suggested that the shear connection should be designed to carry the horizontal shear force existing in the beam at ultimate load. For this purpose it was recommended that 80 percent of the experimentally determined capacity of shear connectors should be used. In the case of uniformly loaded beams, a uniform spacing of shear connectors was proved to be satisfactory, despite the triangular distribution of external shear force.

In 1969, Pincus [42] studied the behavior of timber concrete composite beams using an epoxy resin compound to bond the horizontal concrete flange to the vertical wood stem. Epoxy glues have ideal characteristics such as rapid curing, good adhesion, high strength and superior chemical resistance. The epoxy glue formed the shear transfer surface between the two materials and simulates the constructional procedure of placing precast and reinforced concrete slab on simply supported deep timbers which have a fresh coat of epoxy glue on their top surface. No appreciable slip between the two materials was found prior to final failure, indicating true composite action.

In 1980, Hirst et al. [43] analyzed composite beams to show how it is possible to modify the material properties to standard finite element to make them equivalent to connecting system on composite construction. The analysis was applied in the elastic range and also to predict the load deflection characteristics of a composite beam up to ultimate load. Two dimensional representations using eight nodded curved parabolic isoparametric in plane stress elements were adapted. The stiffness of the connecting elements was determined on the assumption that they deformed essentially in shear and bending. A partial interaction was introduced by reducing the stiffness and capacity of the connecting elements.

In 1989, Saadatmanesh et al. [44] examined experimentally the behaviour of prestressed, composite steel-concrete beams. Two beams were tested, one subjected to positive bending moment and the other to negative

bending moment. The load was plotted against the deflection, and strains in the concrete, steel beams and prestressing bars. The values predicted with the equations of internal forces equilibrium and compatibility between the deformations of the bars and the composite beam were found to correlate well with the measured data.

In 1997, Mohamad Ali et al. [45] applied a linear partial interaction analysis to determine the deflection at mid-span of simply supported steel concrete composite beams with partial shear connection under different cases of loading. The results were presented in a general form and so arranged that these deflections were defined as ratios of the corresponding defections of the equivalent fully composite beams. It was found that such an arrangement leads to expressions that have the same numerical values. Consequently, a general design chart was constructed which facilitates the determination of the central deflection of simply supported composite beams with partial shear connection.

In 1999, Jasim et al. [46] presented a simplified method to evaluate the deflections at mid-points of the spans of simply supported and continuous beams having partial shear connection. A simple expression, which gives the deflection of partially composite beam as a ratio of the corresponding deflection of the equivalent fully composite beam, was derived. This expression explicitly gives the increase in deflection of partially composite beams as compared with the fully composite one. This increase was defined by one term depending upon a factor that varies with a single variable. A chart to evaluate this factor was constructed. The chart was proved to be more suitable for determining the deflection than those suggested in pervious work.

In 2003, Baskar et al. [47] presented an experimental investigation on steel-concrete composite plate girders subject to the combined action of shear and bending. All girders were simply supported at the ends and subjected to central concentrated load thus providing constant shear along the span and maximum bending moment at the mid-span. Six composite plate girders have been tested to failure in order to study their ultimate load behaviour. Two

different web-depth to thickness (d/t) ratios and two different moment/shear ratios have been considered. Attention was focused on the variation in tension field action in web panels due to composite action between the steel girder and concrete slab. Extensive strain measurements have been made on the web panels in order to obtain a detailed picture of tension field action. The ultimate load carrying capacity and the tension field width of composite plate girders were found to increase significantly compared to the bare steel girders.

In 2005, Liang et al. [48] used the finite element method to investigate the flexural and shear strengths of simply supported steel-concrete composite beams under combined bending and shear. A three dimensional finite element model has been developed to account for geometric and material nonlinear behavior of composite beams, and verified by experimental results. The verified finite element model was then employed to quantify the contributions of the concrete slab and composite action to the moment and shear capacities of composite beams. The effect of the degree of shear connection on the vertical shear strength of deep composite beams loaded in shear was studied. Design models for vertical shear strength including contributions from the concrete slab and composite action and for the ultimate moment–shear interaction were proposed for the design of simply supported composite beams in combined bending and shear. The proposed design models provided a consistent and economical design procedure for simply supported composite beams.

In 2006, Brunner et al. [49] used Swiss adhesive SIKA in timber-concrete-composite structures. The adhesive SIKA is capable of bonding the concrete both wet and hardened. Within the framework of the project, the wet process was investigated. The first project phase was concerned with the possible displacement of the adhesive when the fresh concrete is poured onto the wet adhesive. Key parameters such as the concrete type and the falling height of the concrete were analyzed. After the adhesive had been freshly applied onto the wood, a certain time interval was allowed for the adhesive to stiffen before the concrete was poured: this "stiffening time" also proved to be a key parameter.

After the production parameters had been optimized, a number of timber concrete- composite slabs were cast and tested in bending. The test results fully met the expectations.

In 2007, Abbas [50] investigated the structural behaviour of simply supported composite beams, in which a concrete slab is connected with steel I-beam by means of headed stud shear connectors. The study consisted of two parts, the first part was the experimental work in which ten composite beams, designed to fail in bending, were tested. Varied degrees of shear connection were used. Regions of positive bending moment and negative (hogging) bending moment were taken into account. Two types of loading, central point load and two point loads were considered. The behaviour of beams under loading was observed. Ultimate loads, concrete and steel strains, deflections, end slip, and mid span uplift, were recorded. The reduction of the degrees of shear connection from 100 % to 33.3 % caused increasing of strains, mid span deflection, end slip, and uplift. The values recorded for the case of sagging bending regions were lower than those recorded for the hogging bending regions. In the second part of the study, the tested beams were analyzed using nonlinear one dimensional and three dimensional finite element models. The adopted finite element models were found to predict the deflections, strains, slip distribution, and uplift distribution, in a reasonable agreement with the test results.

In 2008, Bouazaouia et al. [1] investigated the bonding connection in steel–concrete composite beams for the case of static loading and high-strength concrete. The 3-point bending test performed on a large beam confirmed that bonding is very efficient: the elastic domain is followed by a non-linear behaviour with noticeable ductility. The measurements were generally close to the numerical results provided by beam models or the FE model. It was found that the composite beam model which does not take into account slip and shear deflection could be used for engineering design purposes. However all the studied beam models did not allow a very accurate prediction of the behaviour close to the interface and the behaviour at failure in the case of shear failure.

Non-linear FE approach may be more suitable but requires realistic failure criterion for all the materials.

In 2010, Salih [51] investigated the structural behavior of simply supported timber – concrete composite beams. The study consisted of two parts; the first part was the experimental work which consists of investigations of push – out specimens and composite beam specimens. In the second part of the study, the tested beams were analyzed using nonlinear one dimensional finite element and three dimensional finite element models. Two types of connectors (suggested BNAIL and Hilti – Dowels connectors) were considered. The failure of beam specimens with BNAIL and Hilti – Dowels connectors under sagging bending moment was flexural tensile failure by the development of flaw in the timber beam. In beams under hogging bending moments, the failure was characterized by excessive crack widths in the tension zone of concrete slab. The adopted finite element models were found to predict the ultimate load in a good agreement with the test results.

2.4.1 Aluminum in Composite Beams

In 1987 and 1989, Bruzzese et al. as cited in [7] carried out experimental tests on composite aluminum and concrete beams at the engineering Faculty of Naples. The main goal has been to investigate the basic aspects of the bending behavior of this kind of structures, by checking the influence of both the connection system and transverse confining of a concrete slab. The adopted structural scheme was simply supported beam. Two test procedures have been followed, testing under controlled load and testing under controlled displacement. The first type of test was carried out on two models. The test conditions were determined to ensure purely flexural behavior in middle gauge length. The two beams with 150 cm span were varied only in terms of stirrup spacing in slab, 65 mm in first model and 130 mm in the second model. The ultimate limit state was reached with consecutive loading and complete unloading cycles. The first specimen collapsed as a result of both concrete compression failure at the slab upper edge and tensile cracking in lower one. At

85 percent of ultimate load, longitudinal cracking occurred symmetrically along the slab axis, located near the connector pairs. The collapse mode was entirely different in the second specimen owing to an irregular mechanism, clearly related to the wider inter axis of the slab stirrups. This constructional details affected the inelastic response of the structure and its ultimate strength to such an extent that longitudinal cracks occurred rather early, at 64 percent of the ultimate load. The main features of the test behavior was the wide knee in the load displacement curve corresponding to the hardening character of aluminum alloy. The second type of test was designed to avoid some of the problems that occurred in the experiments, particularly with regard to the effect of shear actions. For this reason, the specimen ends were suitably strengthened by a full section concrete cast, so to obtain a true composite section in the central region only. This was carefully designed and manufactured with 50 mm regularly spaced 1.5 mm diameter steel hoops. Furthermore, a displacement controlled loading procedure was used to investigate closely the bending behavior after the maximum load bearing capacity had been reached, when the load bearing capacity drops as far as displacement increase. The test showed a quite satisfying agreement with experimental values in both the elastic and plastic ranges, with an exact prediction of ultimate load bearing capacity.

In 1991, Triantafillou [52] investigated the hybrid structural aluminum components, in which a principal aluminum structure is reinforced with unidirectional carbon fiber reinforced polymer CFRP composite laminates, Fig.(2-2). In this study an analysis was conducted on the problem of minimum weight design of CFRP-reinforced thin-walled rectangular aluminum sections subjected to given strength and stiffness constraints. The problem was formulated within the framework of classical nonlinear optimization analysis. It was shown that at the optimum design various local failure mechanisms occur simultaneously, while stiffness rarely controls. The experimental results supported the accuracy of the calculations and provided additional information on the flexural behavior of hybrid aluminum/CFRP members.

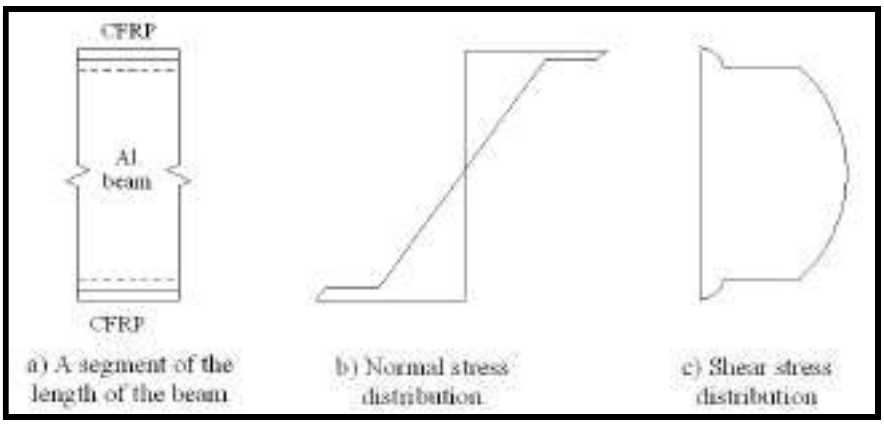

Figure (2-2) The stress distribution in aluminum / hybrid beam

In 1998, Taylor et al. [53] tested combined member of extruded aluminum hollow box sections with steel section inserted. They riveted together to form a combined member increasingly used as the basis for the production of skeletal structures ranging from shelters on transport routes to larger covered walkways at airports, hospitals and industrial compounds. The research work was carried out on the stress and deflection behavior of a typical riveted combined member investigated using the finite element method and supported by experimentation. The effect of the fit between the steel section and the aluminum section was given particular attention. The results of a parametric study were presented and combined with wind excitation criteria and design curves were proposed. Conclusions were drawn on the engineering value of the use of aluminum/steel combined members including the implications for the design of light aluminum/steel structures.

2.5 Concluding Remarks

From the previous literature review, the following points may be noted:

1- No works related to the behavior of ferrocement-aluminum composite beams.
2- Some materials utilized to strengthen aluminum beams such steel plate and CFRP.
3- The use of epoxy as a shear connectors in composite beams is still limited.
4- Many material investigated as components of composite beams such as steel and concrete, timber and concrete.

CHAPTER THREE

EXPERIMENTAL PROGRAM

3.1 Introduction

The experimental work was carried out at the Construction Materials Laboratory of the College of Engineering at the University of Basrah. The Construction Materials Laboratory of Amarah technical institute is also utilized to conduct some tests.

The main purpose of the test program is to generate data and provide information about the structural behavior of ferrocement aluminum composite beams. The tested ferrocement aluminum composite beams are of 1.2 m and 2.4 m overall length and consist of ferrocement slab, 0.05 m depth and 0.4 m breadth, and four different aluminum sections. The two components, ferrocement slab and aluminum beam are connected together by epoxy adhesion layer (Sikadur 31) of about 3 mm thickness.

The main variables considered in the study were the aluminum section shape, depth and thickness of the aluminum section as well as span length. Adhesive bonded connection was examined. Sixteen specimens were tested under three point load with different configurations and three specimens were used for push out test.

This chapter describes the experimental work objectives, details of specimens, their construction, material properties, the instrumentation utilized, and the testing procedures. The full details aluminum beams and ferrocement-aluminum composite beams are summarized in Table (3-1) and Table (3-3). Typical specimens configuration are shown in Fig. (3-1).

Table (3-1) Details of aluminum beams

No.	Design-ation	Section	Weight Kg/m.l	Full depth, D mm	length, mm	Flange width, B mm	Flange thicken-ss, t_f	Web thicken-ss, t_w mm	Aa mm^2	Calculat-ed Ia mm^4
1	S1	20x5x0.4 cm	5.12	200	1200	50	4	4	1936	8560725
2	S2	10x5x0.4 cm	3	100	1200	50	4	4	1136	1441259
3	S3	10x5x0.3 cm	2.29	100	1200	50	3	3	864	1121192
4	S4	16x10-6x0.5 cm	4.87	160	1200	100,60	6	5	1800	4943467

Table (3-2) Details of ferrocement - aluminum composite beams

No	Designat-ion	Aluminum section	Weight Kg/m.l	Length (L) mm	Full depth, mm
1	S1-F1.2	S1	49.12	1200	253
2	S1F1.2#	S1	49.12	1200	253
3	S1F1.2	S1	49.12	1200	253
4	S2F1.2	S2	47	1200	153
5	S3F1.2	S3	46.29	1200	153
6	S4F1.2	S4	48.87	1200	213
7	S1F2.4	S1	49.12	2400	253
8	S2F2.4	S2	47	2400	153
9	S3F2.4	S3	46.29	2400	153
10	S4F2.4	S4	48.87	2400	213

Designations; SiFj # -

S : Aluminum section.

i : Type of aluminum section.

F: Ferrocement slab.

j : Length of beam (m).

S F : Aluminum - Ferrocement Composite beam.

(-) : There is no adhesion between beam components.

(#): Test was conducted after only one day of applying the adhesive epoxy layer.

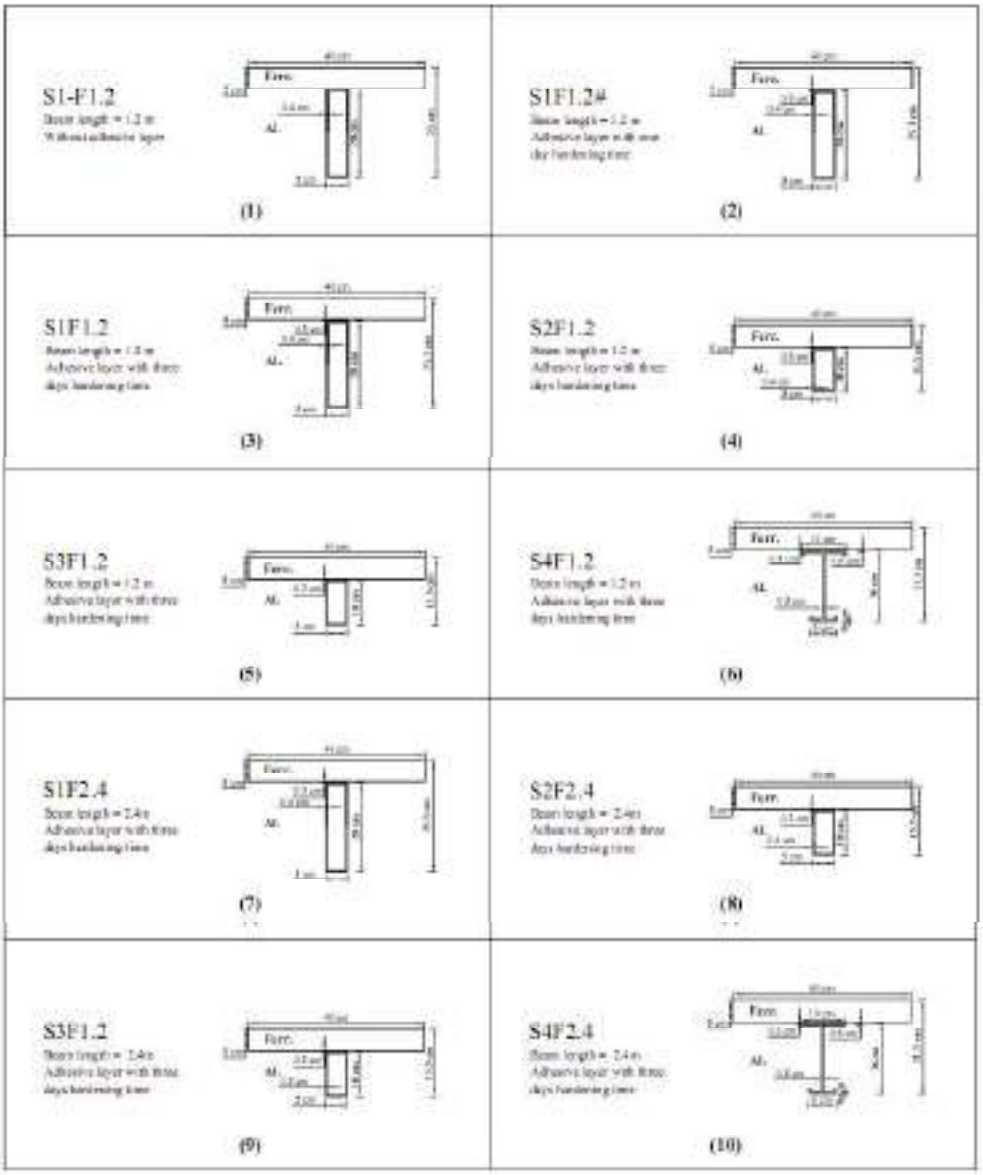

Figure (3-1) Details of ferrocement - aluminum composite beams

3.2 Aluminum

Pure aluminum is weak, with a tensile strength ranging from about 90 to 140 N/mm^2 depending on the temper. It is employed for electrical conductors and for domestic products (such as pans, cans, packaging), but for serious structural use it has to be strengthened by alloying. The strongest alloys have a tensile strength of over 500 N/mm2. There are around ten basic alloys in which wrought material (plate, sheet, sections) is produced. Unfortunately, each of these alloys appears in a vast range of different versions, so that the full list of actual specifications is long. The newcomer therefore finds material selection less simple that it is in structural steel, and there is also the alloy numbering system to contend with [5], see Appendix A.

There are many advantages of using aluminum alloys, such as high strength-to-weight ratio, lightness, corrosion resistance, good workability and ease of production. Aluminum can also be recycled, which gives environmental advantages. However, many alloys are available with a large variety of excellent mechanical and physical qualities.

The appropriate alloy depends on the specific application. The 6xxx series alloys are the most useful for structural applications because of their combination of strength, corrosion resistance, and weldability. Alloys in this group contain *magnesium* and *silicon* in proportions that form magnesium silicide (Mg*2*Si). These alloys have a good balance of corrosion resistance and strength. The 6xxx series alloys are also very readily extruded, so they constitute the majority of extrusions produced and are used extensively in building, construction, and other structural applications [54].

Structural Aluminum Alloy sections produced by Jordanian aluminum industry have been used in this investigation. The geometrical details are shown in Table (3-2). Figure (3-2) and Plate (3-1) show sections used in this study.

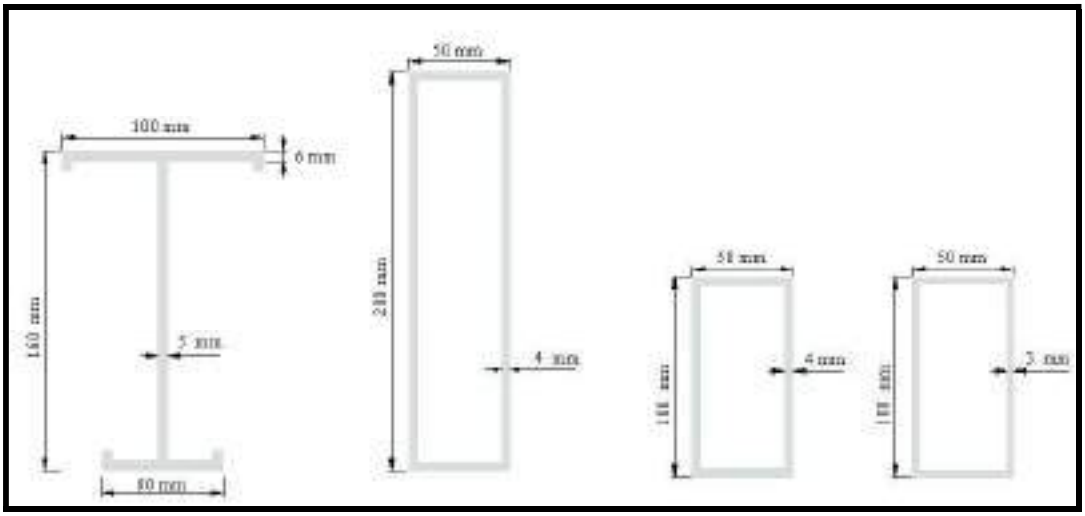

S4 **S1** **S2** **S3**

Figure (3-2) Aluminum sections used in the study

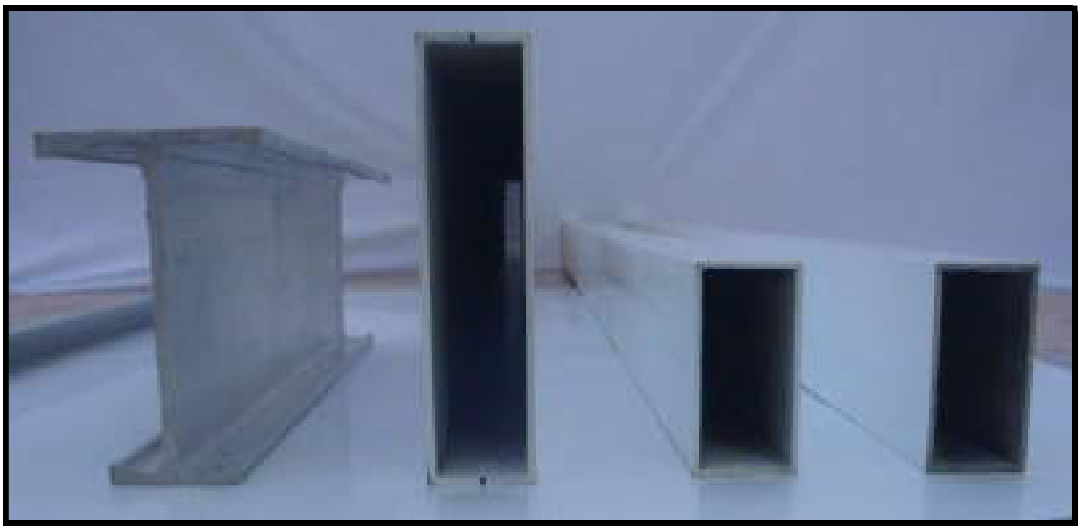

Plate (3-1) Aluminum sections used in the study

3.2.1 Mechanical Properties

Aluminum material standards quote two levels of stress, both of which must be attained for a batch of material to be accepted:

$f_{0.2}$ minimum value of the 0.2% proof stress (or '0.2% offset') and

f_u minimum tensile strength (or 'ultimate stress').

The mechanical properties of the aluminum were determined by using tensile coupon. The tensile coupons were taken from the center of the web plate in the longitudinal direction of the aluminum beams. The tensile coupons were prepared and tested according to the American Society for Testing and Materials standard (B557M-ASTM 2003-Standard: Test Methods of Tension Testing Wrought and Cast Aluminum- and Magnesium-Alloy Products)[55]. In the tensile test 12.5 mm wide coupons of 50 mm gauge length were used as shown in Fig. (3-3).They were tested under direct tension by 5 kN capacity Bench-Top testing machine model BT-1000. The material properties obtained from the tensile tests are summarized in Table (3-3), which includes the measured initial Young's modulus (E_0), the static 0.2% tensile proof stress $f_{0.2}$, the static tensile strength f_u and the elongation after fracture. This is typically measured on a gauge-length of 50 mm and gives a crude indication of ductility. The compressive proof stress not recorded, and it is normally assumed to be the same as in tension [5].

Figure (3-4) shows the typical stress-strain for aluminum alloy indicating the different stress levels and Figs. (3-5) and (3-6) show samples of the stress-strain curve for box and I – section, respectively.

Plates (3-2), (3-3) and (3-4) show tensile test coupons before and after test and test arrangement, respectively.

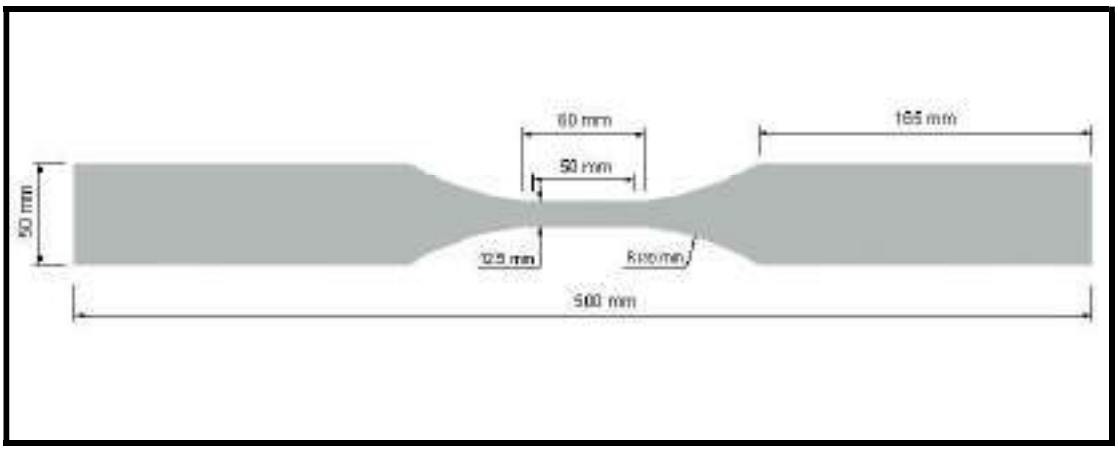

Figure (3-3) Geometrical details of aluminum tensile coupons

Table (3-3) Mechanical Properties of Aluminum Alloy

Section style	Specimens	$f_{0.2}$ yield stress (MPa)	Ultimate stress (MPa)	E (GPa)	Fracture elongation (%)	Specific elongation[5] (%)
Box	a1	184.66	224.42	64.65	6.87	6-14
	a2	186.76	220.58	63.37	6.98	
	a3	182.29	225.5	65.54	7.09	
I-Shape	b1	192.24	219.11	68.01	11.9	
	b2	188.35	221.23	67.97	12.11	
	b3	187.76	226.32	66.14	11.68	

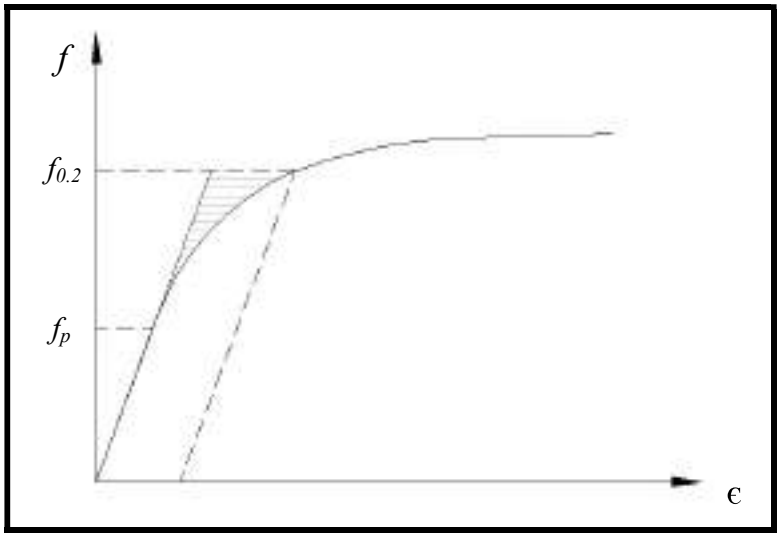

Figure (5-4) Typical stress - strain relationship for aluminum alloy

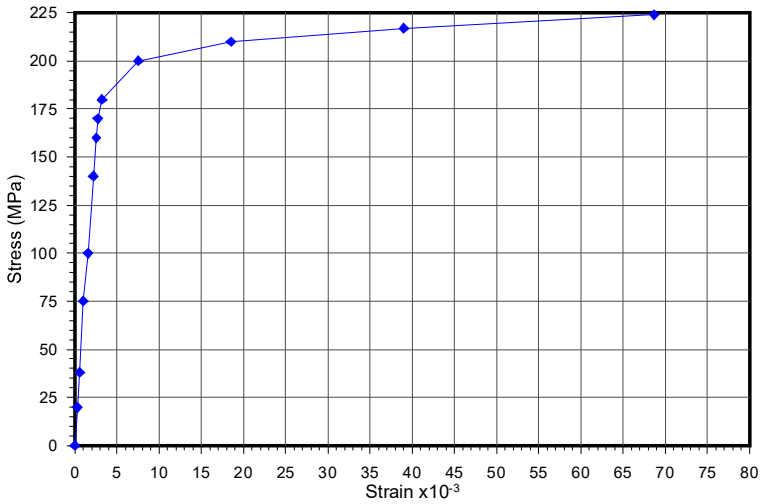

Figure (3-5) Stress - strain relationship for aluminum alloy,a_1

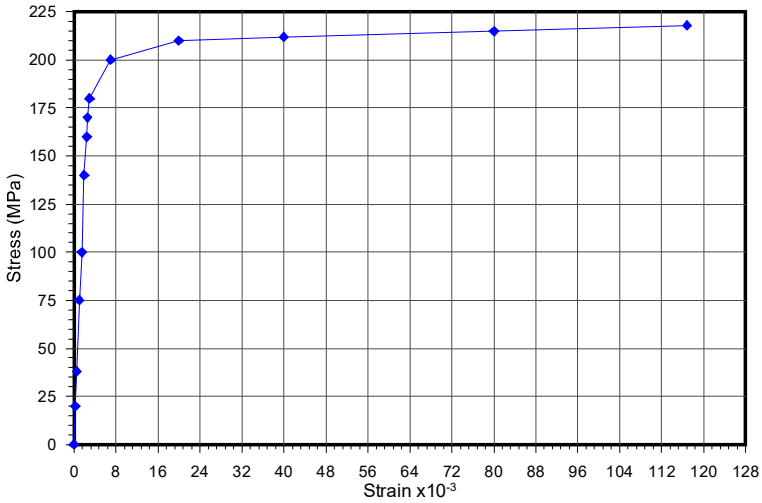

Figure (3-6) Stress - strain relationship for aluminum alloy,b_1

Plate (3-2) Aluminum alloy tensile coupons before test

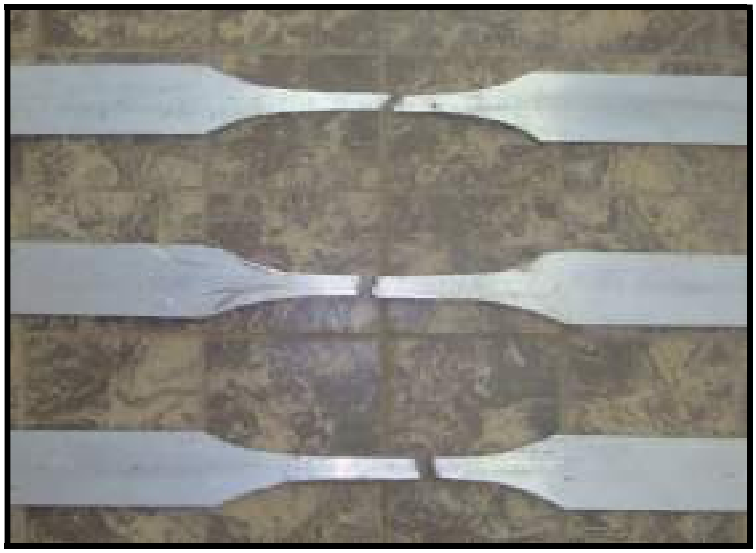

Plate (3-3) Aluminum alloy tensile coupons after test

Plate (3-4) Test arrangement for aluminum alloy tensile coupons

3.2.2 Aluminum Alloy Chemical Analysis

Structural aluminum alloys (6xxx series alloys) contain *magnesium* and *silicon* in proportions that form magnesium silicide (Mg*2*Si) as main ingredients of alloy base. It contains other elements such as Iron, Copper, Manganese, Chromium, Zinc, Titanium, and other elements[5]. The test was conducted at the Chemical Laboratory of the College of Engineering, according to the American Society for Testing and Materials standard (E 34 -ASTM 2003- Standard Test Methods for Chemical Analysis of Aluminum and Aluminum-Base Alloys)[56]. Table (3-4) shows the weight percentage of main ingredients of the used structural aluminum alloys.

Table (3-4) Main ingredients of structural aluminum alloy

Section	Chemical elements	Composition, wt%
Box	Al	95.02
	Mg	0.32
	Si	0.35
I	Al	95.91
	Mg	0.21
	Si	0.33

3.3 Ferrocement

Ferrocement is a form of thin reinforced concrete in which a brittle cement-sand mortar matrix is reinforced with closely spaced multiple layers of thin wire mesh and /or small diameter rods, uniformly dispersed throughout the matrix of the composite. Ferrocement has taken a significant place among components used for construction, for its specification of durability and strength,

and its small thickness, which makes it a component suitable for constructing many light-weight structures [57]. The same materials (cement, sand, water and wire mesh) were used for all ferrocement segments throughout this investigation and they are detailed below with their tests.

3.3.1 Cement

Ordinary Portland cement was used throughout this investigation. The whole quantity required was brought to the laboratory and stored in a dry place. The physical properties of cement used throughout this work are presented in Table (3-5).The setting time test is conducted according to ASTM C191[58]. The compressive strength test is accomplished according to ASTM C109 [59]. The chemical composition of it are presented in Table (3-6). Results indicate that the cement conforms with the Iraqi standard No. 5/1984 [60].

Table (3-5) Physical properties of ordinary Portland cement

Physical and Mechanical Properties	**Test Result**	**Limits of Iraqi specification No.5/1984**
Compressive strength, N/mm²		
3 – day	16.9	≥ 15.00
7 – day	34.1	≥ 23.00
Setting time, h:minutes		
Initial setting	02:31	≥ 00: 45
Final setting	03:19	≤ 10: 00
Standard consistency, %	27.92%	
Fineness Specific surface area (by Blaine method), cm²/gm	3011	≥ 2300

Table (3-6) Chemical composition of cement

Components		Results	Requirement according to Iraqi specification No.5/1984	
			Minimum	Maximum
Silicon Dioxide	SIO2	21.14%		
Aluminum Trioxide	AL2O3	4.00%		
Ferric Oxide	Fe2O3	3.05%		
Calcium Oxide	CaO	62.69%		
Magnesium oxide	MgO	2.11%		5%
Sulphate	SO3	2.32%		3%
potassum oxide	K2O	0.66%		
Sodium Oxide	Na2O	0.18%		
Insoluble Residue	Ins.Res.	1.14%		1.50%
Loss on Ignition	LOI	3.38%		4%
Freelime	FL	0.84%		
Lime Saturation Factor	LSF	91.2	66	102
Silicon Ratio	SM	2.66%		
Alumina Ratio	AM	1.61%		
Tricalcium Silicate	C3S	50.59%		
Dicalcium Silicatr	C2S	22.44%		
Tricalcium Aluminates	C3A	7.82%		
Tetracalcium Aluminoferrate	C4AF	9.27%		

3.3.2 Fine Aggregate (Sand)

Natural silica sand brought from Al-Zubair area was used as a fine aggregate in this research. The sieve analysis test was conducted according to ASTM C-136 [61]. Table (3-7) shows the grading of sand used in this work. Results indicate that the sand conforms to Iraqi specification No. 45/1984 [62].

Table (3-7) Sieve analysis of sand

Sieve size mm	Percent Passing		
	Sand used	Limits of Iraqi Specification No. 45/1984	ASTMC33-86
4.75	100	90-100	90-100
2.36	93	75-100	80-100
1.18	67	55-90	50-85
0.60	48	35-59	25-60
0.30	22	8-30	10-30
0.15	3	0-10	2-10
Sulfate content	0.09 %	< 0.5%	-

3.3.3 Water

Potable water was used for casting and curing the ferrocement elements during work.

3.3.4 Steel Wire Mesh

Locally available steel wire mesh of 12 mm square opening with average wire diameter of (1 mm) has been used in this investigation. Figure (3-7) shows the geometry and dimensions of the mesh type used throughout this work.

Several tensile coupons of the wire were made from mesh and tested under direct tension by 5 kN capacity Bench-Top testing machine model BT-1000. The tensile coupons were prepared and tested according to ACI 549.1R-93[63] as shown in Fig. (3-8).

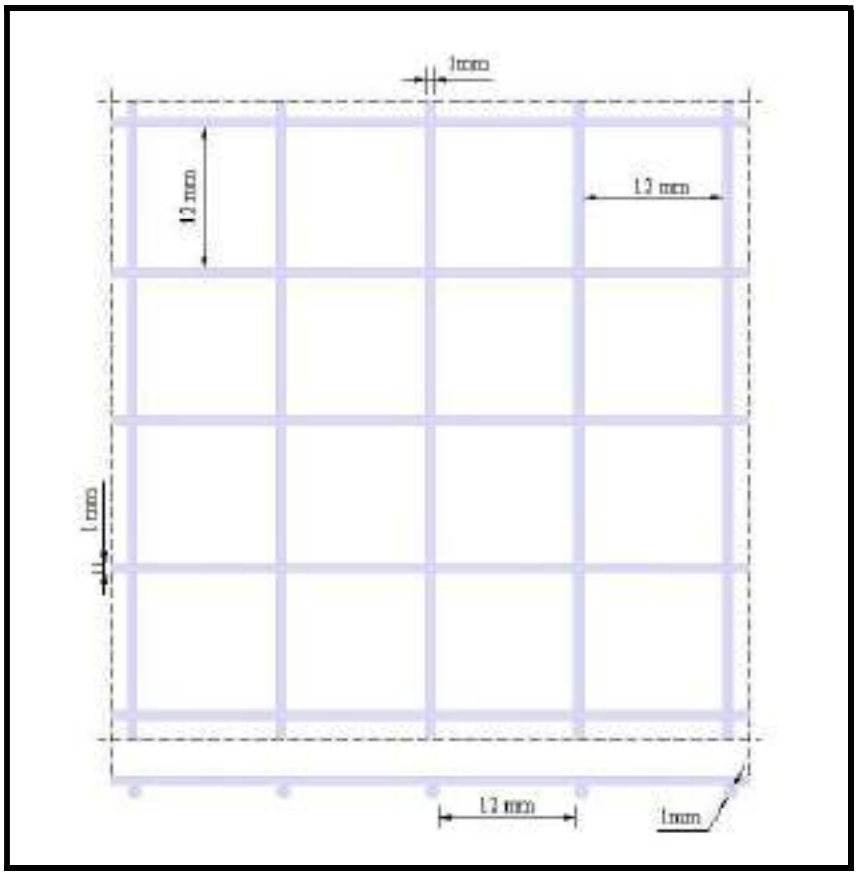

Figure (3-7) Details of steel wire mesh

The test specimens were prepared by embedding both ends of a rectangular coupon of mesh in mortar over a length at least equal to the width of the sample. The mortar-embedded ends serve as pads for gripping. The free (not embedded) portion of the mesh represents the test sample.

The average yield stress f_y, the ultimate strength f_{ul}, and modulus of elasticity E_s were determined. Table (3-8) shows the geometric and strength characteristics of used wire mesh.

The yield strain of the mesh reinforcement should be taken as the strain at the point of intersection of two lines, one drawn through the initial portion of the stress-strain curve and the other drawn through the final portion of the curve [9].

Figure (3-9) shows the typical stress-strain relationship for wire mesh indicating the different stress levels and Fig. (3-10) shows a sample of the test results. Plates (3-5) to (3-8) show tensile test coupons fabrication, configuration after test and test arrangement, respectively.

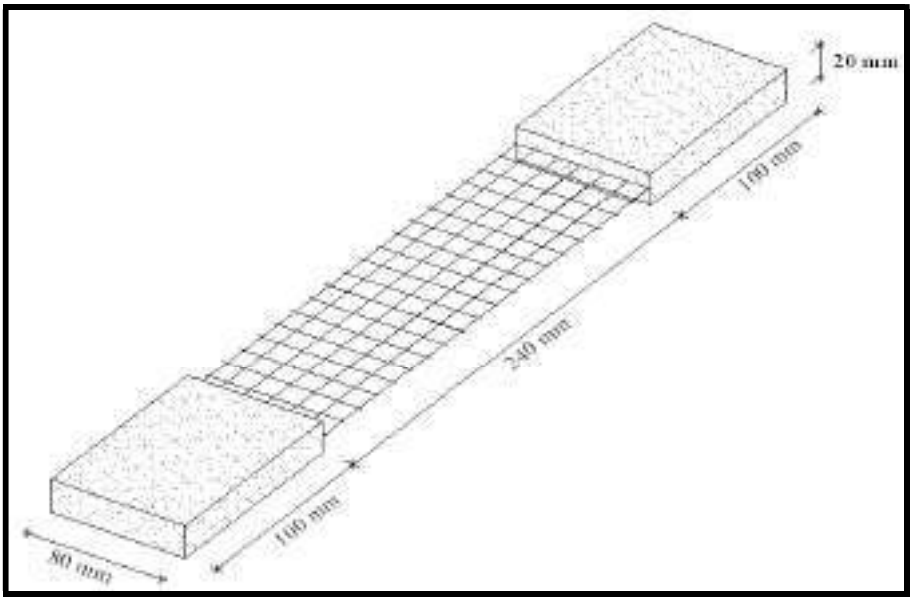

Figure (3-8) Details of wire mesh tensile coupons

3.3.5 Direct Tensile Tests of Ferrocement Elements

Tensile strength of ferrocement was obtained by using several tensile coupons of the ferrocement made from mesh and matrix (mortar capsulated wire mesh). The tensile coupons specimens were tested using the Universal Testing Machine (MARUI) 20 ton capacity. They were prepared and tested according to ACI 549.1R-93[63] as shown in Fig. (3-11). The test specimens were prepared by embedding a rectangular coupon of mesh in mortar over their length. They were additionally reinforced at their ends for gripping. The middle half of the test specimen was instrumented to record elongations.

Table (3-8) Properties of wire mesh

Specimens	Wire diameter (mm)	f_y (MPa)	f_{ul} (MPa)	Modulus of elasticity (MPa)
w1	1	406	588	89400
w2	1	410	602	89500
w3	1	394	583	88910

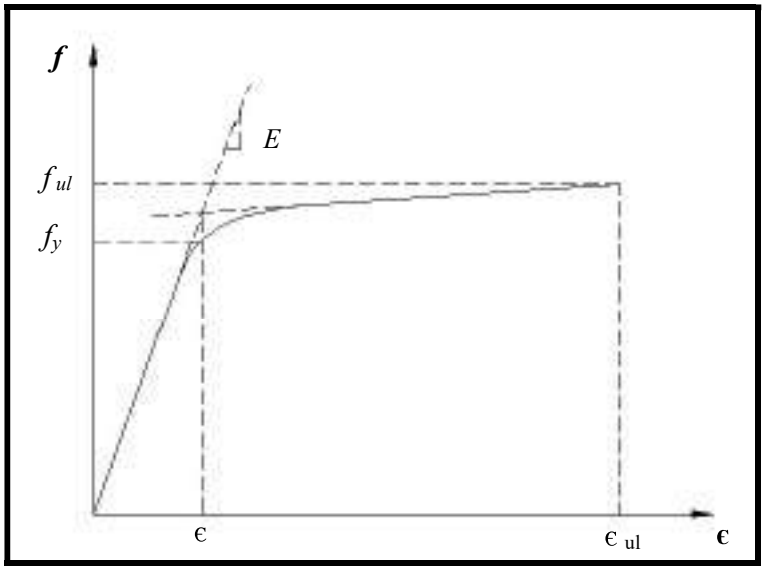

Figure (3-9) Typical stress-strain relationship for wire mesh[63]

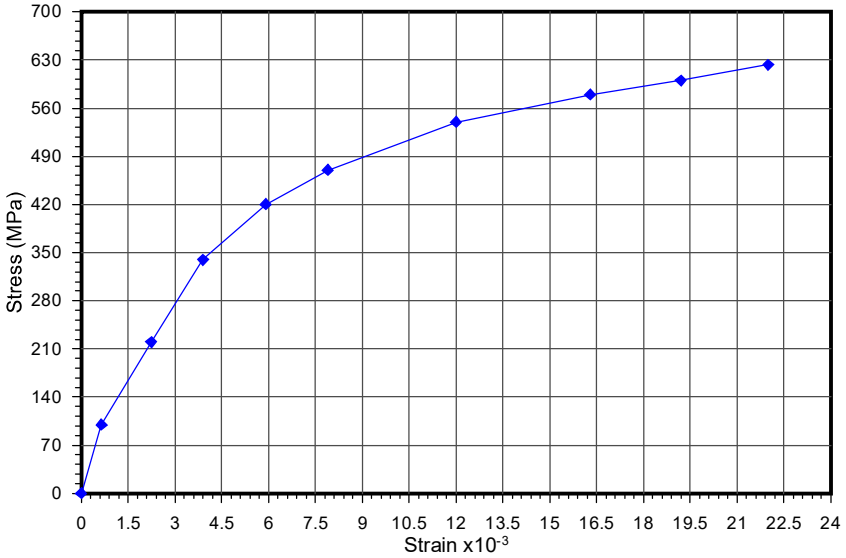

Figure (3-10) Stress –strain relationship for wire mesh, w_1


Plate (3-5) Fabrication details of wire mesh tensile coupons specimens

Plate (3-6) Wire mesh tensile coupons

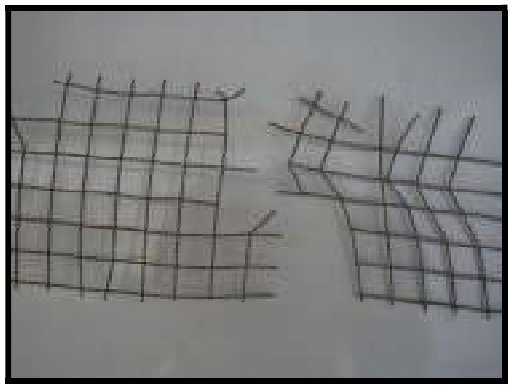

Plate (3-7) Failure mode of wire mesh

Plate (3-8) Test arrangement for wire mesh tensile coupons

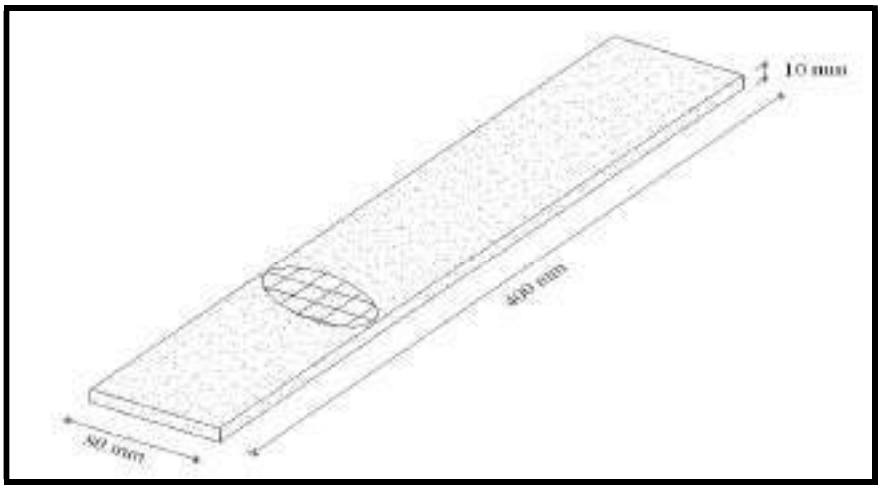

Figure (3-11) Details of ferrocement elements tensile coupons

A plot of the load-elongation curve upto failure was used to estimate the effective modulus of the mesh system as well as its yield and ultimate strengths.

Figure (3-12) shows the typical stress-strain relationship for ferrocement element indicating different stress levels and Fig. (3-13) shows a sample of the test results. Plates (3-9) to (3-12) show tensile coupons specimens, their fabrication, their configuration after test and test arrangement, respectively.

3.3.6 Cement Mortar

The sand-cement mortar was mixed in the ratio of one part by weight of cement to two parts of sand. The water-cement ratio used was (0.5).

3.3.6.1 Mix Design

The hydraulic cement matrix for ferrocement was designed according to standard mix design procedures for mortar and concrete [9]. Three trial mixes were examined depending on the water cement ratio (w/c). The cement sand ratio was kept as constant 1:2 based on experiments carried out on the ferrocement by other researches. All the mixes were batched in a horizontal pan type mixer. For each mix six 50mm cubes were cast. The cubes were kept in water until the date of testing. Three of the six cubes were tested at age of 7 days while the other at the age of 28 days. Details of these mixes properties are given in Table (3-10). Mix2 was chosen in this investigation, because of its relevant strength and workability.

Table (3-9) Ferrocement tensile strength

Specimens	f_y (MPa)	f_u (MPa)
t1	3.9	5.1
t2	3.8	5.21
t3	4.3	6.12

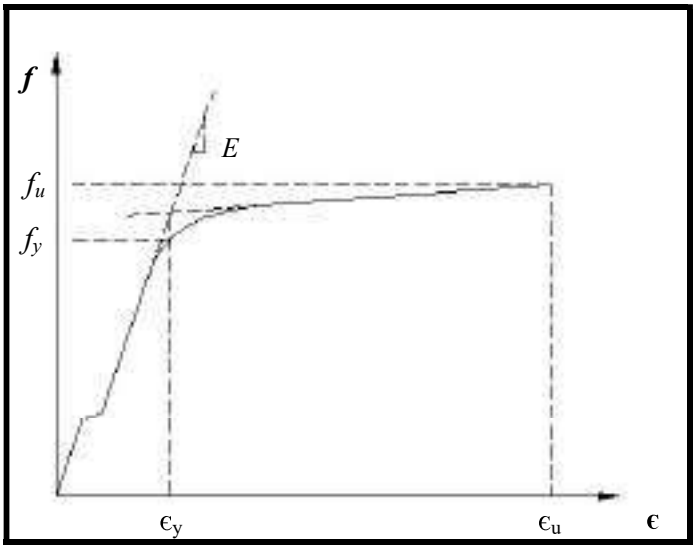

Figure (3-12) Typical stress-strain relationship for ferrocement element [63]

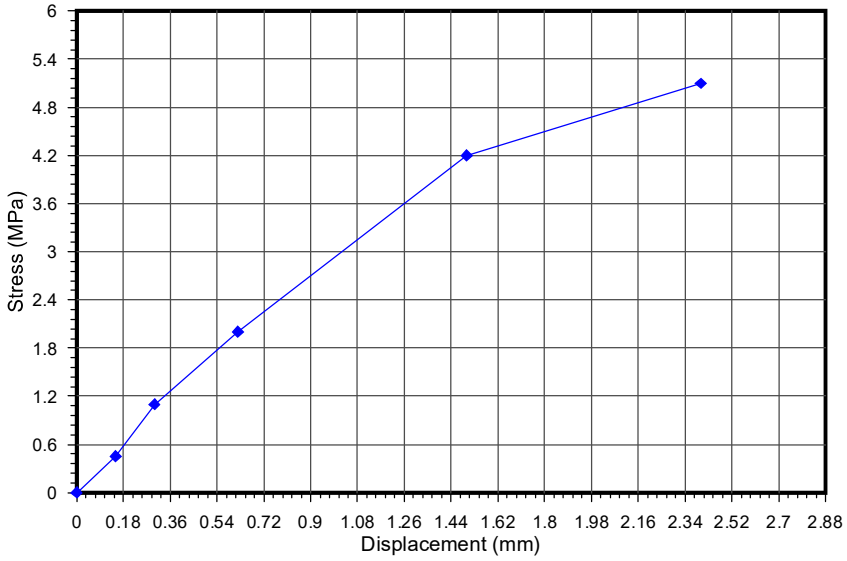

Figure (3-13) Stress –strain relationship for ferrocement element, t_1

Table (5-6) Experimental comparison of tested aluminum and composite beams

No.	Beams designation	Aluminum beam				Composite beam		Ratio, (P_3/P_1)
		Section	Shape factor	Ultimate load,P_1 (kN)	Service load,P_2 (kN)	Ultimate load,P_3 (kN)	Service load,P_4 (kN)	
1	S1-F1.2	S1	27.41	95.12	63.41	97.08	64.72	1.02
2	S1F1.2#	S1	27.41	95.12	63.41	125.03	83.35	1.31
3	S1F1.2	S1	27.41	95.12	63.41	149.05	99.37	1.57
4	S2F1.2	S2	13.40	28.44	18.96	76.49	50.99	2.69
5	S3F1.2	S3	18.02	21.87	14.58	53.44	35.63	2.44
6	S4F1.2	S4	18.3	77.27	51.51	139.25	92.83	1.80

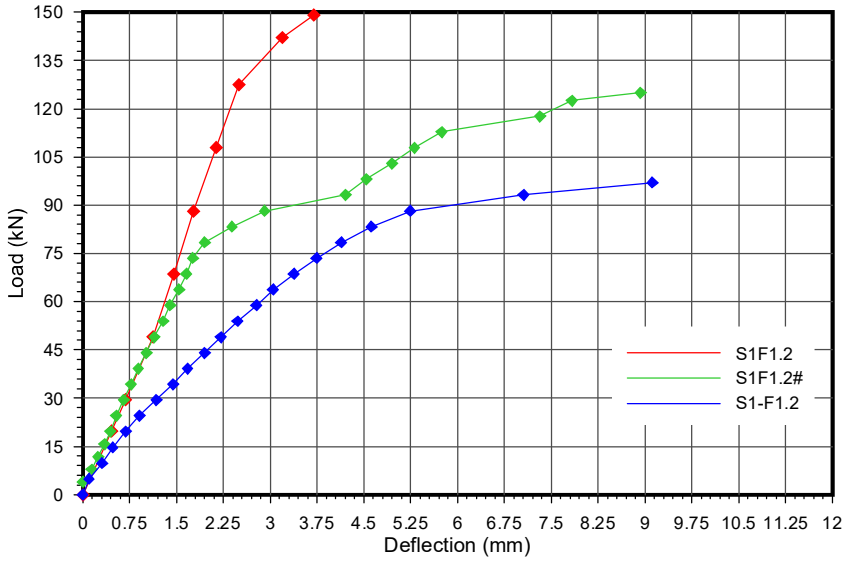

Figure (5-11) Variation of midspan deflection with load for different conditions between the components of composite beams – Experimental work

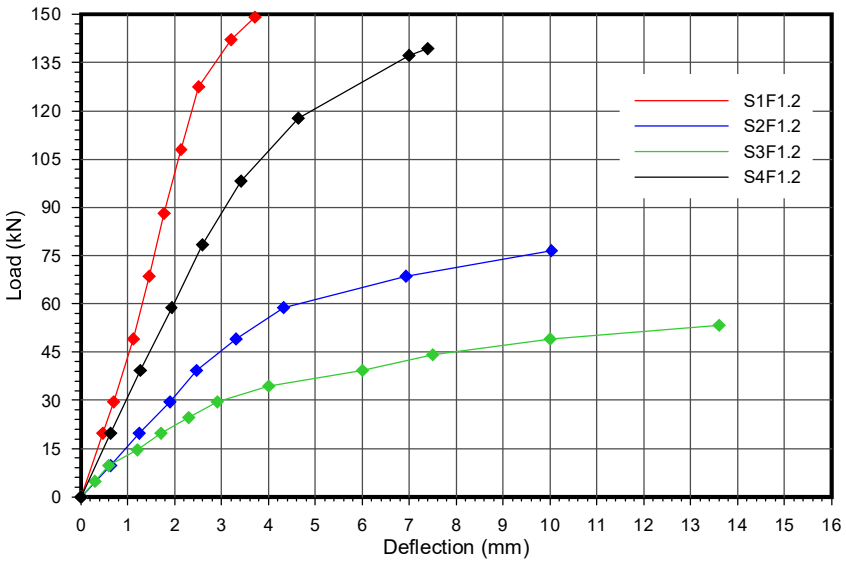

Figure (5-12) Variation of midspan deflection with load for composite beams with 1.2 m length – Experimental work

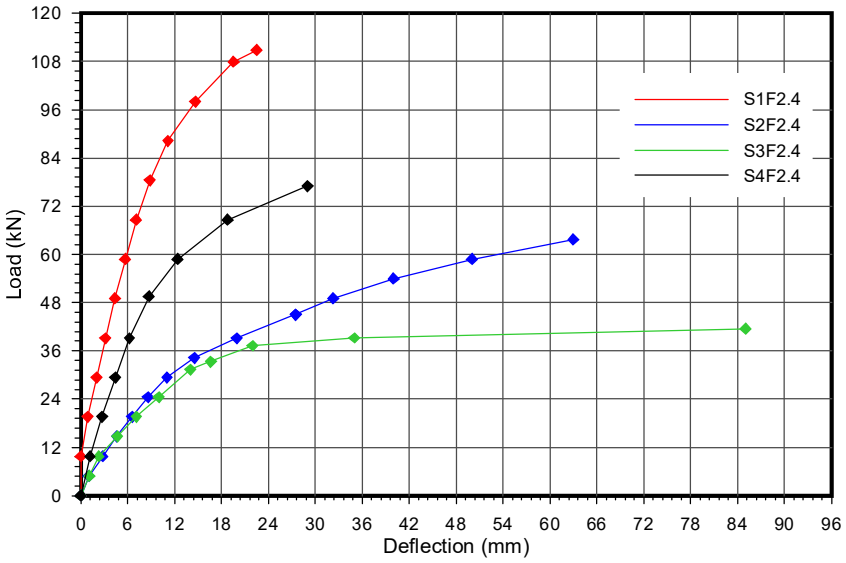

Figure (5-13) Variation of midspan deflection with load for composite beams with 2.4 m length – Experimental work

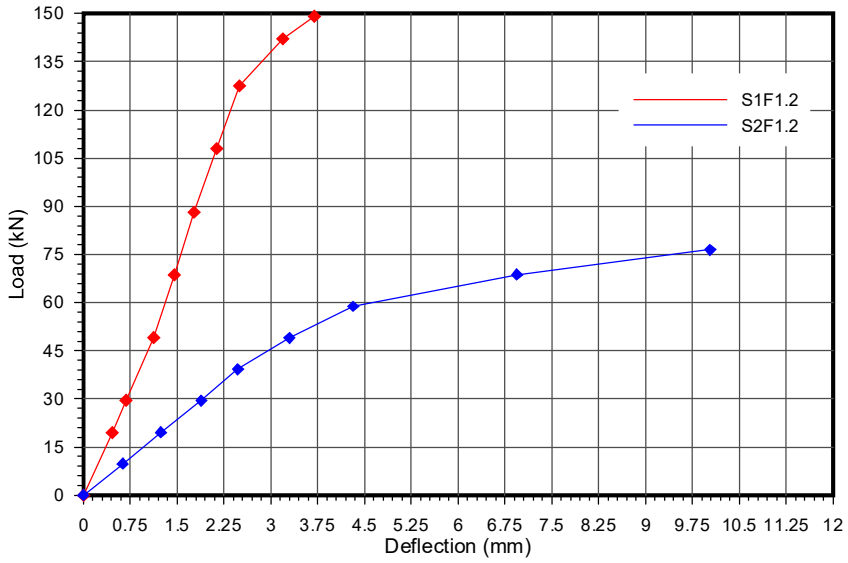

Figure (5-14) The effect of aluminum beam depth on variation of midspan deflection with load for composite beams with 1.2m length – Experimental work

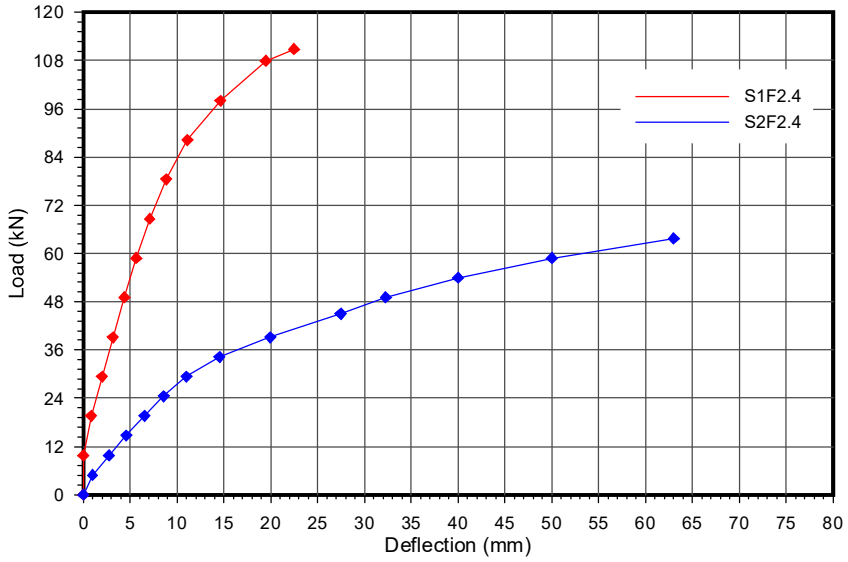

Figure (5-15) The effect of aluminum beam depth on variation of midspan deflection with load for composite beams with 2.4 m length – Experimental work

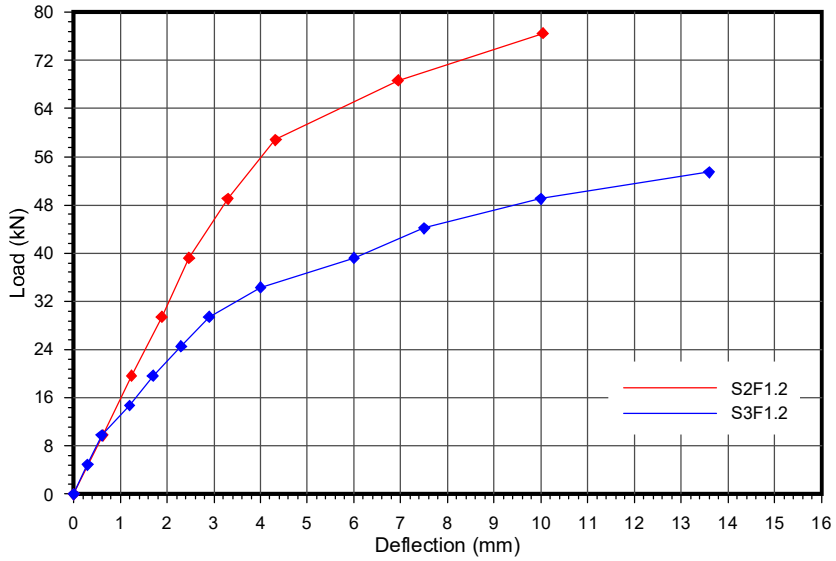

Figure (5-16) The effect of aluminum beam wall thickness on variation of midspan deflection with load for composite beams with 1.2m length – Experimental work

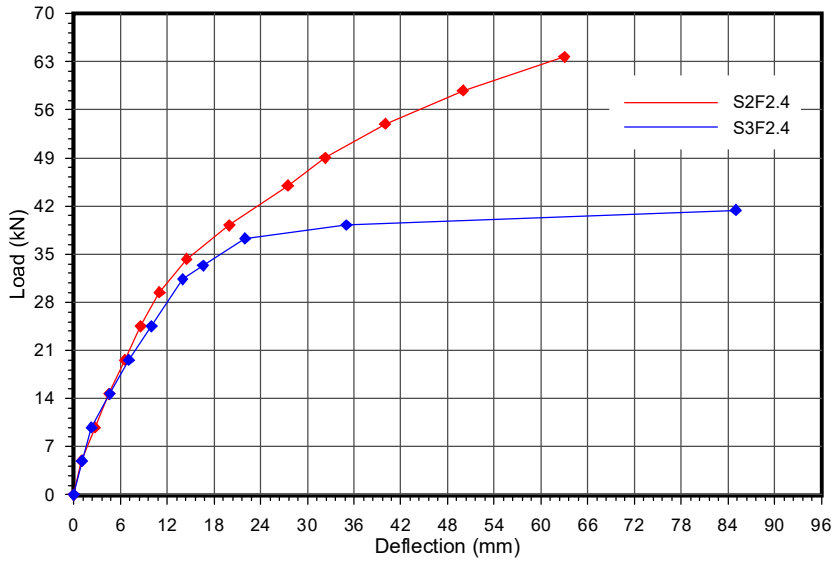

Figure (5-17) The effect of aluminum beam wall thickness on variation of mid-span deflection with load for composite beams with 2.4 m length – Experimental work

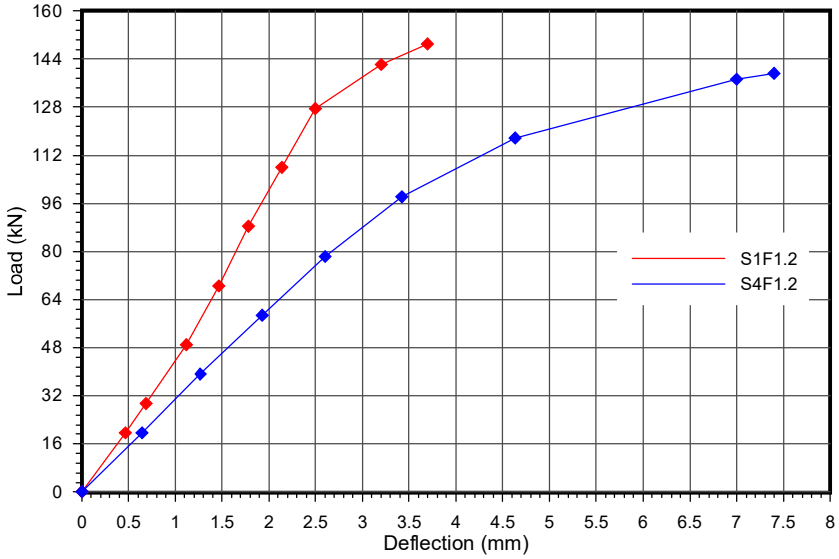

Figure (5-18) The effect of aluminum beam shape on variation of midspan deflection with load for composite beams with 1.2 m length – Experimental work

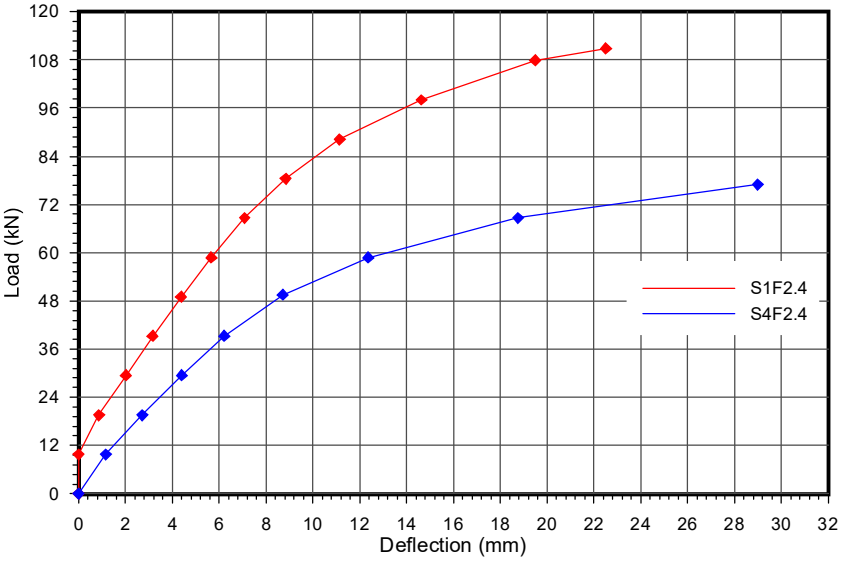

Figure (5-19) The effect of aluminum beam shape on variation of midspan deflection with load for composite beams with 2.4 m length – Experimental work

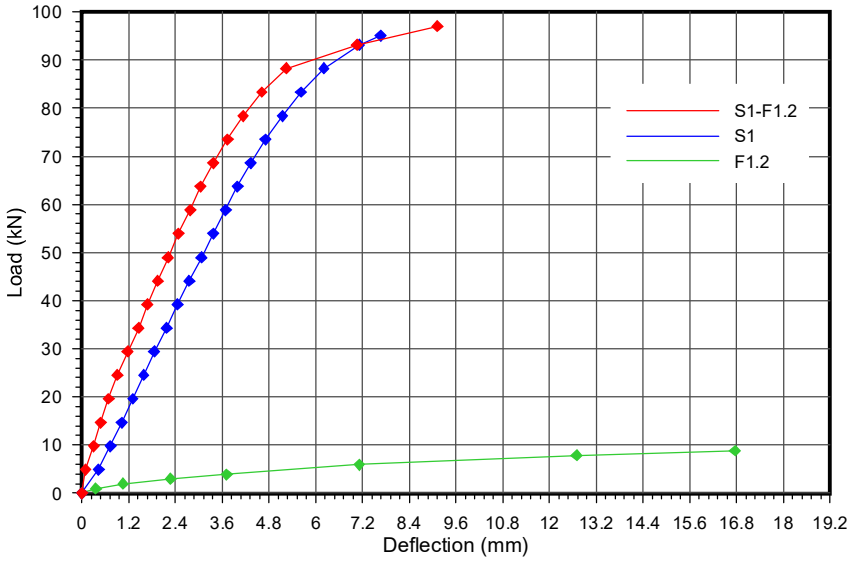

Figure (5-20) Comparison of load-mid span deflection relationships of composite section with its components for S1-F1.2 – Experimental work

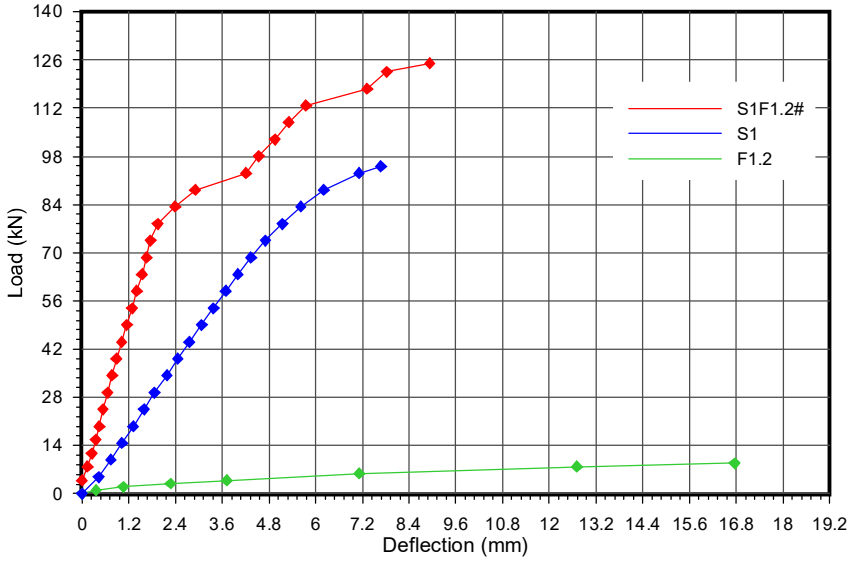

Figure (5-21) Comparison of load-mid span deflection relationships of composite section with its components for S1F1.2# – Experimental work

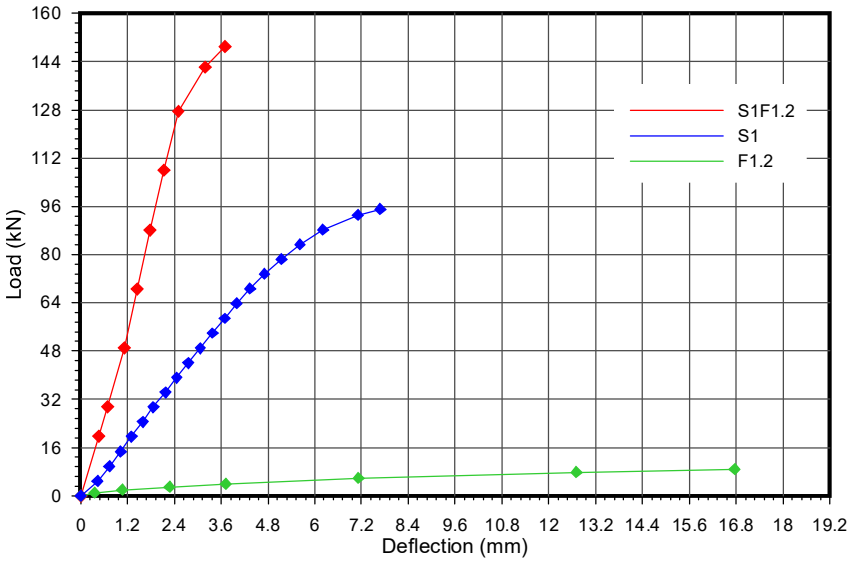

Figure (5-22) Comparison of load-mid span deflection relationships of composite section with its components for S1F1.2 – Experimental work

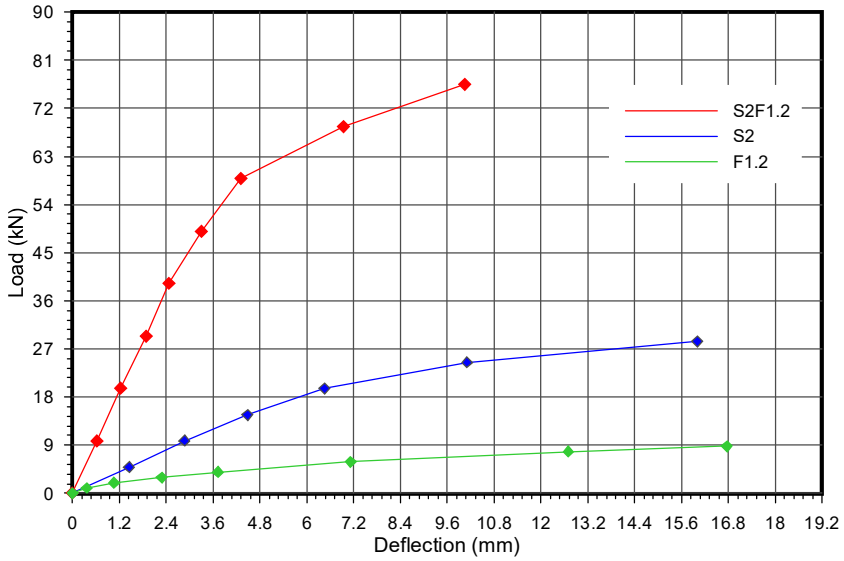

Figure (5-23) Comparison of load-mid span deflection relationships of composite section with its components for S2F1.2 – Experimental work

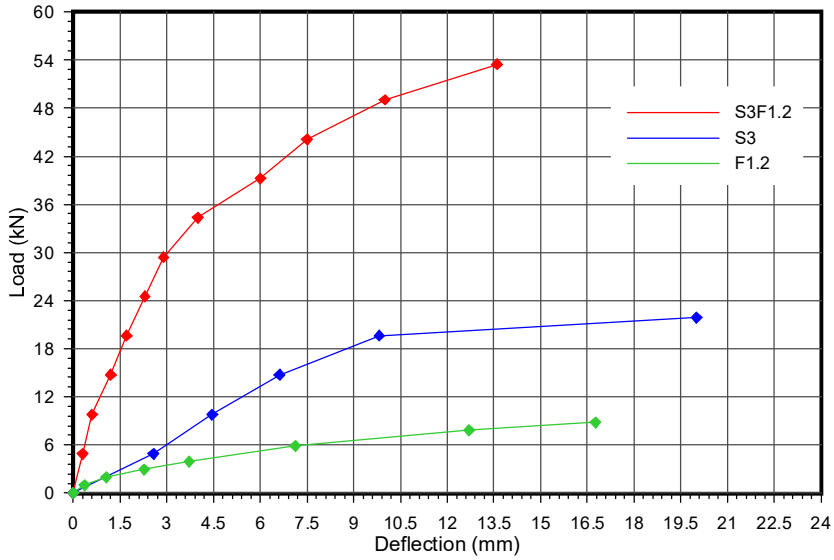

Figure (5-24) Comparison of load-mid span deflection relationships of composite section with its components for S3F1.2 – Experimental work

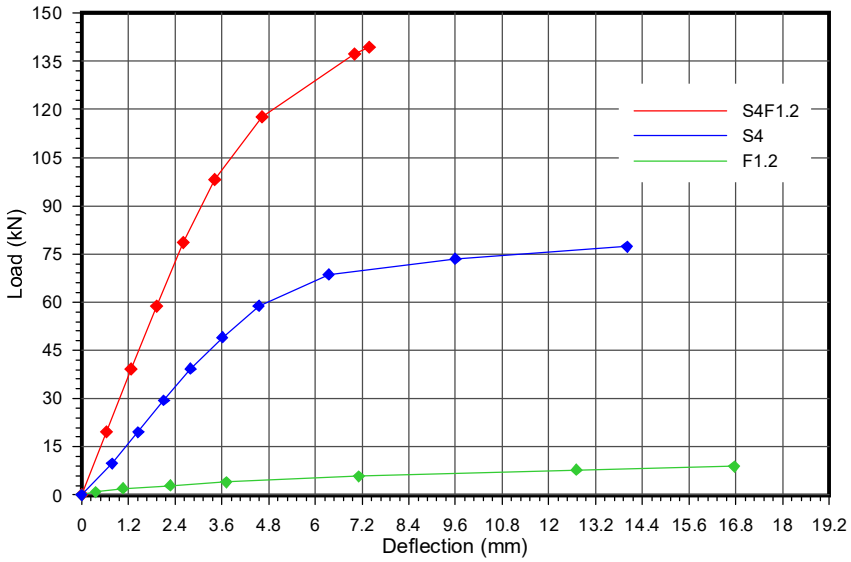

Figure (5-25) Comparison of load-mid span deflection relationships of composite section with its components for S4F1.2 – Experimental work

5.2.4.3 End slip

The variation of the experimentally measured values of the end slip between the ferrocement slab and aluminum beam with load are summarized in Table (5-7).

The load versus end slip relationships for the tested composite beams are presented in Figs. (5-26) to (5-34).

Figure (5-26) illustrates the efficiency of adhesive epoxy layer after three days of hardening where slip value remains so small and approaches to zero (0.012 mm) as compared with beams tested after one day of epoxy hardening (1.91 mm) or that without adhesive layer (2 mm).

Figures (5-27) and (5-28) show a comparison between the values of end slip for beams of 1.2 m and 2.4 m length.

For composite beams (S1F1.2) and (S1F2.4) which have the same cross section and different lengths, the extrapolated deflection at ultimate load is (3.7 mm) for (S1F1.2) and (22.5 mm) for (S1F2.4), Table (5-5), while the end slip shows very little variation, (0.012 mm) for (S1F1.2) and (0.014 mm) for (S1F2.4). This finding is true for all other sections with different lengths.

The influence of end slip upon midspan deflection is very small as the end slip values is also very small for all tested composite beams.

The relationship between deflection increment Δv and maximum slip δ, ($\Delta v = 10\delta$) [78] for composite beams is considered to show slight slip effect upon midspan deflection. Table (5-8) shows the small values of Δv calculated for tested beams.

It can be observed that using glue provides adequate bond between the two components of composite beam. Measurements also show that the connection could be considered to be perfect as the slip remains very small

during the test (0.013 to 0.06 mm). This proves that the adhesive layer could efficiently replace the conventional connectors used in composite beams.

During test the end slip for all tested beams occurred without any indication of separation between ferrocement slab and aluminum beam .

Figures (5-29) to (5-34) clearly show that the parameters including thickness, depth and section shape of aluminum beam have slightly affected the end slip values.

Table (5-7) End-slip of tested composite beams

No.	Beams designation	Ultimate load, P_{ul} (kN)	Extrapolated end-slip at ultimate load (mm)	Service* load (kN)	End-slip at service load (mm)
1	S1-F1.2	97.08	2.000	64.72	0.950
2	S1F1.2#	125.03	1.910	83.35	0.345
3	S1F1.2	149.05	0.012	99.37	0.004
4	S2F1.2	76.49	0.035	50.99	0.015
5	S3F1.2	53.44	0.055	35.63	0.021
6	S4F1.2	139.25	0.023	92.83	0.011
7	S1F2.4	110.81	0.014	73.87	0.004
8	S2F2.4	63.74	0.044	42.49	0.012
9	S3F2.4	41.45	0.060	27.63	0.024
10	S4F2.4	76.98	0.033	51.32	0.009

* Service load = (2/3) Ultimate load

Table (5-8) End-slip effect upon deflection for composite beams

No.	Beams designation	Extrapolated deflection at ultimate load (included slip effect) mm	Extrapolated slip (δ) at ultimate load mm	Deflection increment due to slip, Δv =10δ mm
1	S1F1.2	3.70	0.012	0.12
2	S2F1.2	10.04	0.035	0.35
3	S3F1.2	13.60	0.055	0.55
4	S4F1.2	7.40	0.023	0.23
5	S1F2.4	22.50	0.0135	0.135
6	S2F2.4	63.00	0.044	0.44
7	S3F2.4	85.00	0.06	0.6
8	S4F2.4	29.00	0.0325	0.325

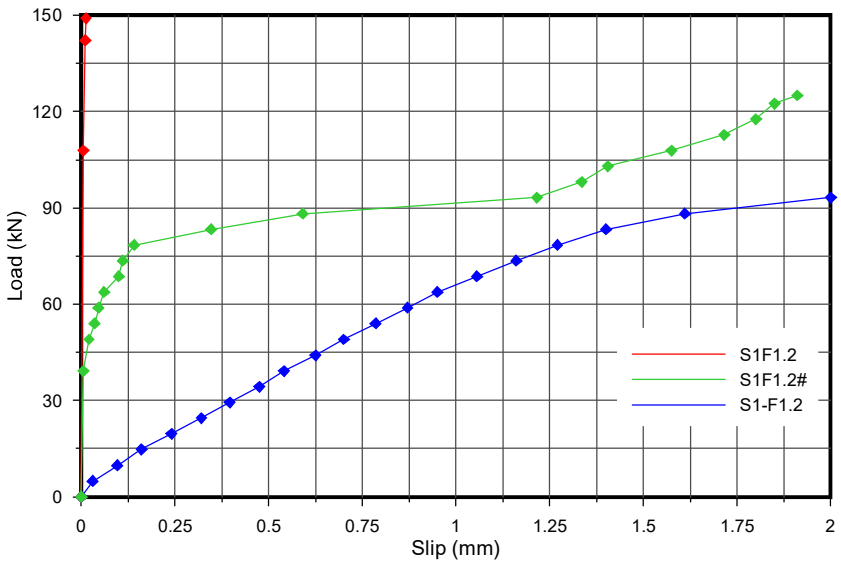

Figure (5-26) Variation of end slip with load for different conditions between the components of composite beam – Experimental work

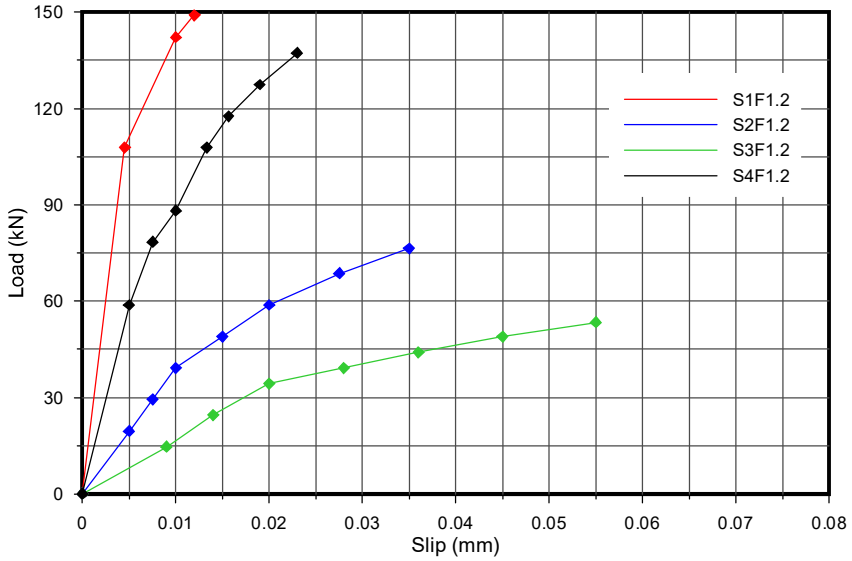

Figure (5-27) Variation of end slip with load for composite beams with 1.2 m length – Experimental work

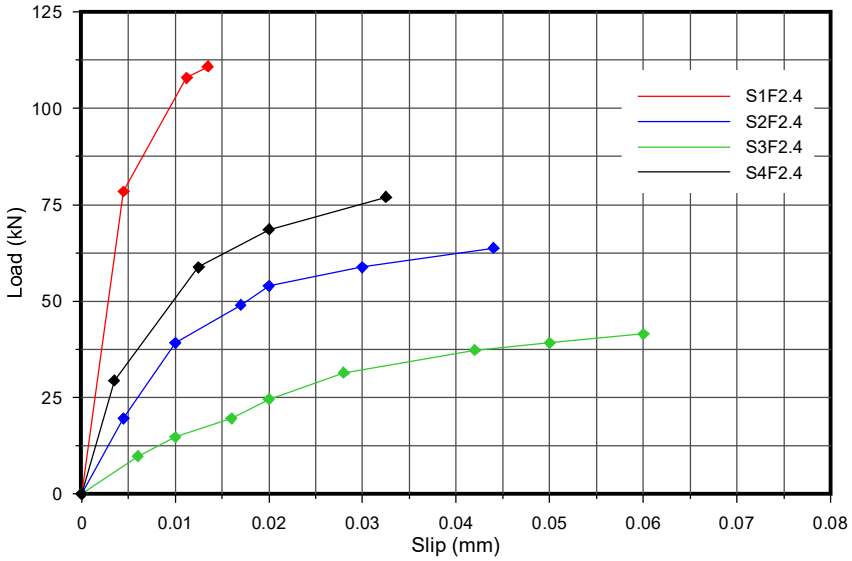

Figure (5-28) Variation of end slip with load for composite beams with 2.4 m length – Experimental work

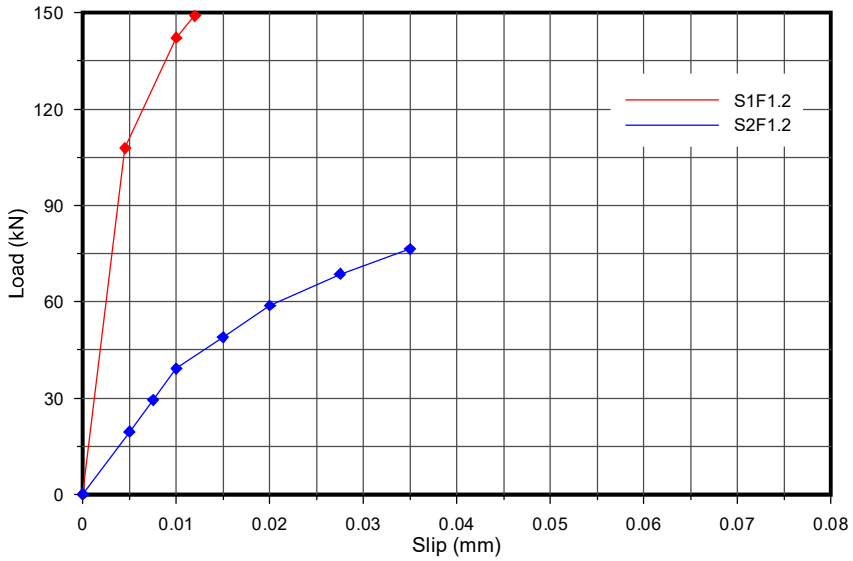

Figure (5-29) The effect of aluminum beam depth on variation of end slip with load for composite beams with 1.2 m length – Experimental work

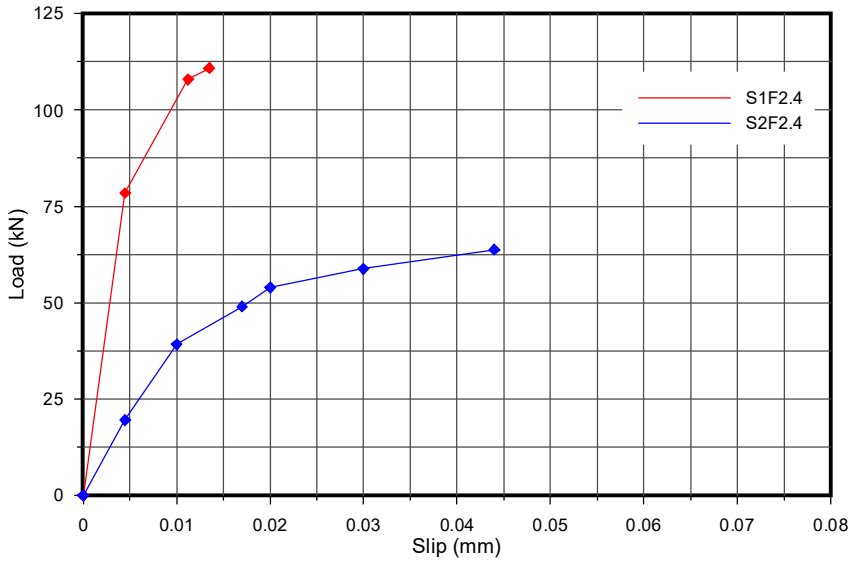

Figure (5-30) The effect of aluminum beam depth on variation of end slip with load for composite beams with 1.2 m length – Experimental work

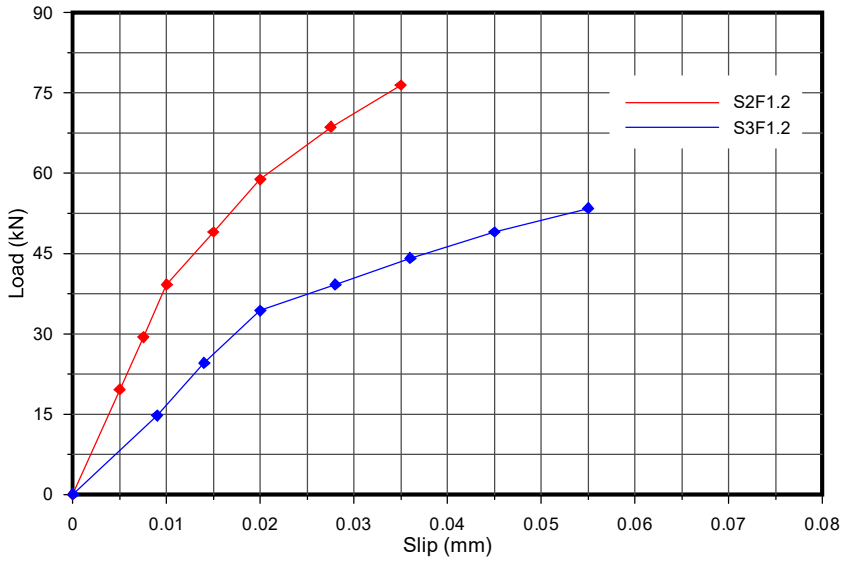

Figure (5-31) The effect of aluminum beam thickness on variation of end slip with load for composite beams with 1.2 m length – Experimental work

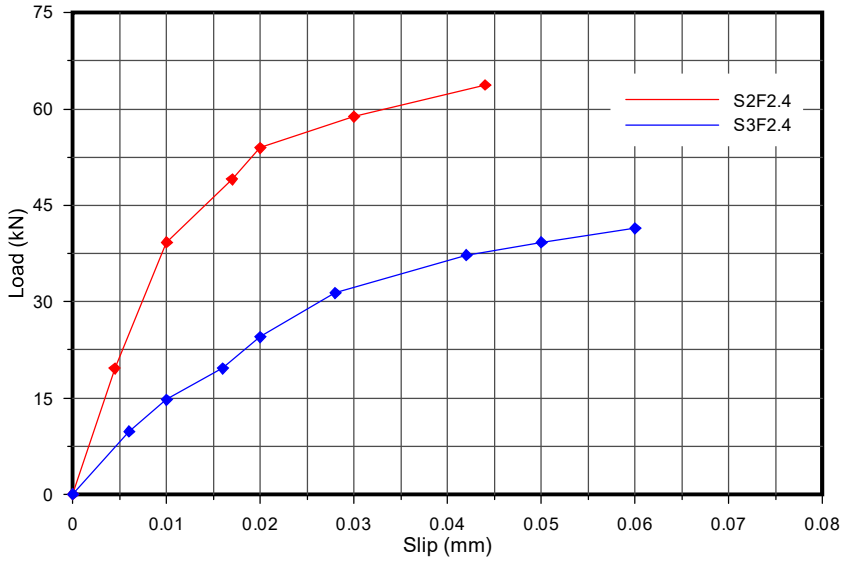

Figure (5-32) The effect of aluminum beam thickness on variation of end slip with load for composite beams with 2.4 m length – Experimental work

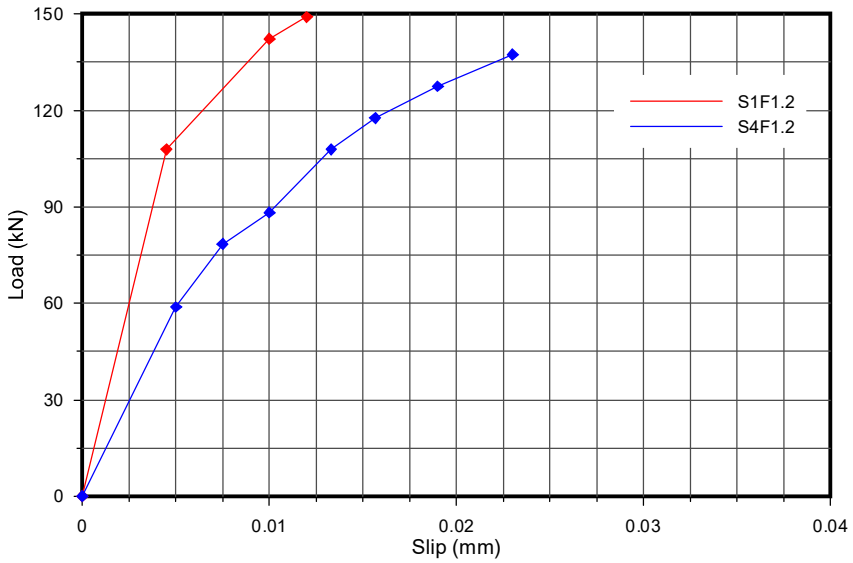

Figure (5-33) The effect of aluminum beam shape on variation of end slip with load for composite beams with 1.2 m length – Experimental work

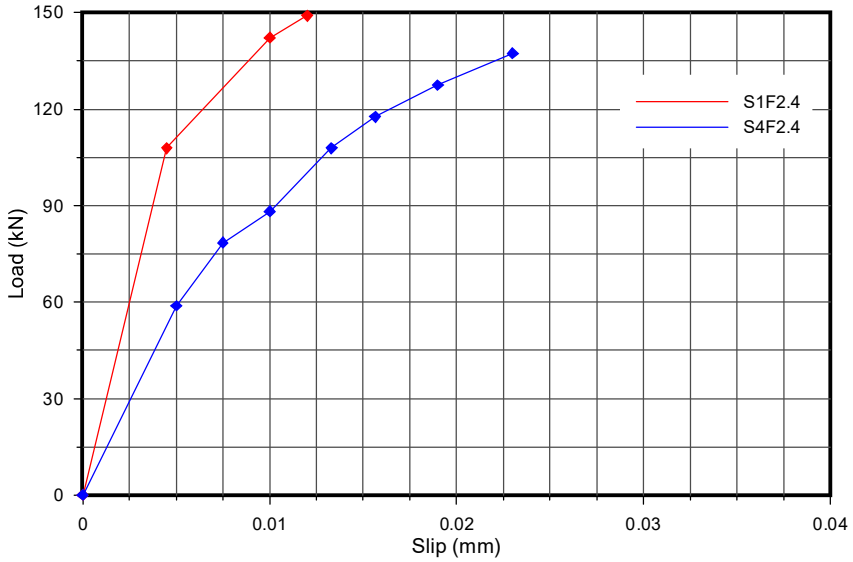

Figure (5-34) The effect of aluminum beam shape on variation of end slip with load for composite beams with 2.4 m length – Experimental work

5.2.4.4 Midspan uplift

When the load is applied, two regions of negative and positive uplift are developed. The negative uplift usually occurs near the supports, while the positive uplift occurs at the mid span region, and the length of the negative uplift region is small as compared with the length of the positive uplift region.

The variation of the experimentally measured values of the central uplift between the ferrocement slab and aluminum beam with load are summarized in Table (5-9)

The load versus uplift relationships for the tested composite beams are shown in Figs. (5-35) to (5-42).

The variation of midspan uplift with load for composite beams with various conditions between the components of composite beam, with (S1) as aluminum section, is illustrated in Fig. (5-35).

The comparison of this figure with Figs. (5-11) and (5-26) clearly depicts that the global response of uplift with load is the same as those of deflection or slip with load.

The loss of contact between ferrocement slab and aluminum beam is not noticed and there is no indication of separation accompanied with vertical uplift. For beams with ferrocement splitting failure mode, the separation occurs after the sudden slip increase at the ultimate failure load.

Comparison between Figs. (5-36) and (5-37) and Fig. (5-2) shows that for the composite beam with aluminum sections having more flexural ductility, S2 and S3 aluminum sections, uplift is larger than for beams with S1 and S4 aluminum sections.

Figures (5-38) and (5-39) show the variation of central uplift with load for composite beams with different depths of used aluminum beams, 200 mm

for S1 and 100 mm for S2.

It is evident from these figures that the uplift at ultimate load increases from (0.2 mm) to (0.6 mm) with increase ratio of 66.67 % for 1.2 m composite beams length and from (0.25 mm) to (0.96 mm) with increase ratio of 73.95 % for 2.4 m composite beams length when the depth of aluminum box section decrease from (200 mm) to (100 mm).

Figures (5-40) and (5-41) show the variation of central uplift with load for composite beams with different wall thickness of used aluminum beams, 4 mm for S2 and 3 mm for S3.

It can be seen that the uplift at ultimate load increases from (0.6 mm) to (0.9 mm) with increase ratio of 33.34% for 1.2 m composite beams length and from (0.96 mm) to (1.60 mm) with increase ratio of 40% for 2.4 m composite beams length when the thickness of aluminum box section decreases from (4 mm) to (3 mm).

Figures (5-42) and (5-43) show the variation of central uplift with load for composite beams with different aluminum section shapes. The shape factors are 27.4 and 18.3 for S1 as box section and S4 as I section, respectively.

It can be seen that the uplift at ultimate load increases from (0.2 mm) to (0.31 mm) with increase ratio of 35.48 % for 1.2 m composite beams length and from (0.25 mm) to (0.36 mm) with increase ratio of 30.56 % for 2.4 m composite beams length when the shape factor of aluminum section decreases from (27.4) to (18.3).

In general from Figs.(5-38) to (5-43), it can be seen that the composite beam with stiffer aluminum beam exhibited less midspan uplift.

Table (5-9) Midspan uplift of tested composite beams

No.	Beams designation	Ultimate load, P_{ul} (kN)	Extrapolated midspan uplift at ultimate load (mm)	Service load* (kN)	Midspan uplift at service load (mm)
1	S1-F1.2	97.08	10.50	64.72	6.30
2	S1F1.2#	125.03	9.65	83.35	0.74
3	S1F1.2	149.05	0.20	99.37	0.09
4	S2F1.2	76.49	0.60	50.99	0.14
5	S3F1.2	53.44	0.90	35.63	0.25
6	S4F1.2	139.25	0.31	92.83	0.11
7	S1F2.4	110.81	0.25	73.87	0.09
8	S2F2.4	63.74	0.96	42.49	0.20
9	S3F2.4	41.45	1.60	27.63	0.17
10	S4F2.4	76.98	0.36	51.32	0.11

* Service load = (2/3) ultimate load

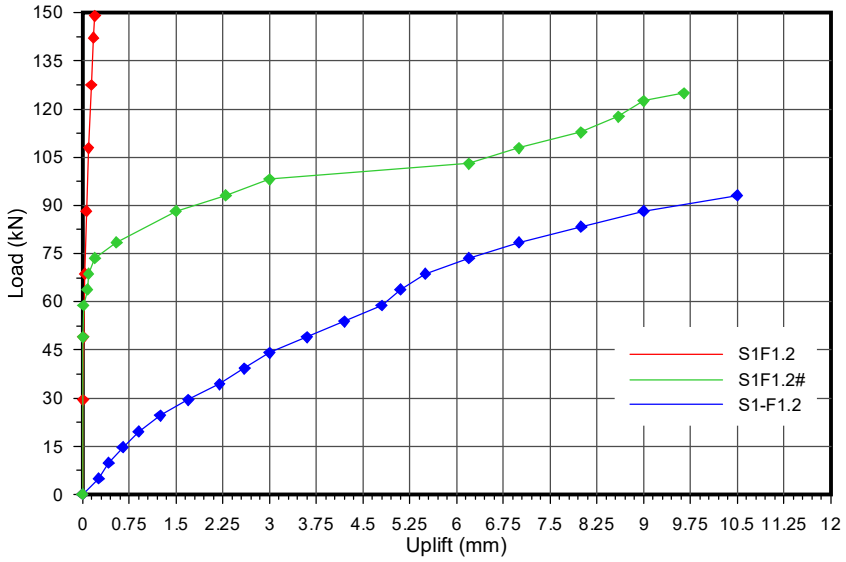

Figure (5-35) Variation of central uplift with load for different conditions between the components of composite beam – Experimental work

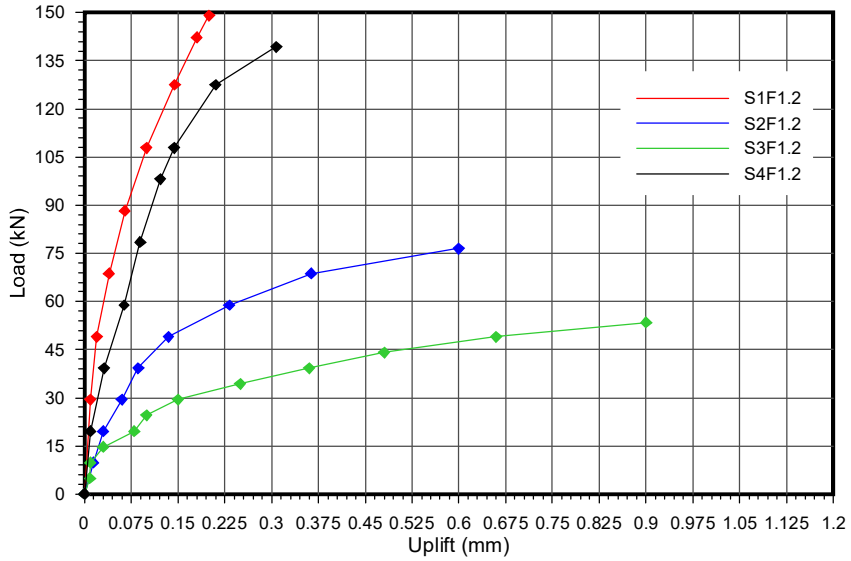

Figure (5-36) Variation of central uplift with load for composite beams with 1.2 m length – Experimental work

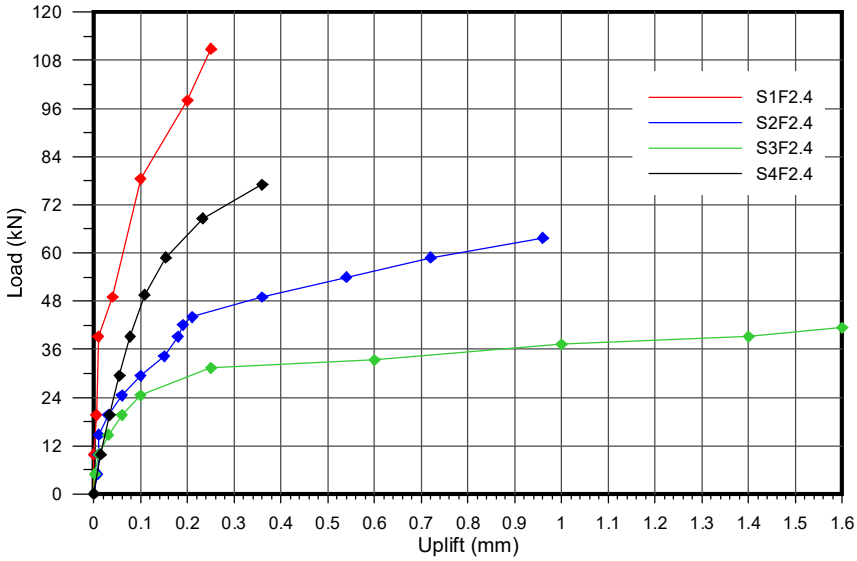

Figure (5-37) Variation of central uplift with load for composite beams with 2.4 m length – Experimental work

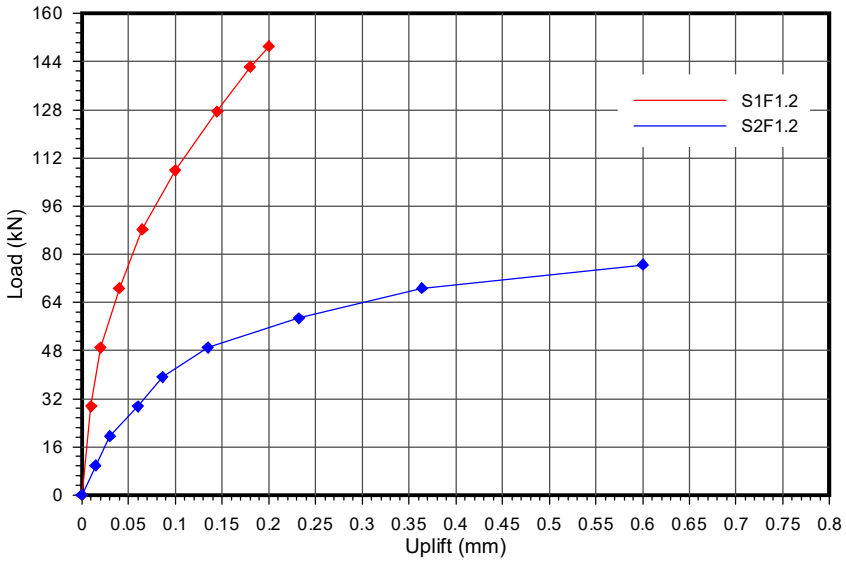

Figure (5-38) The effect of aluminum beam depth on variation of central uplift with load for composite beams with 1.2 m length – Experimental work

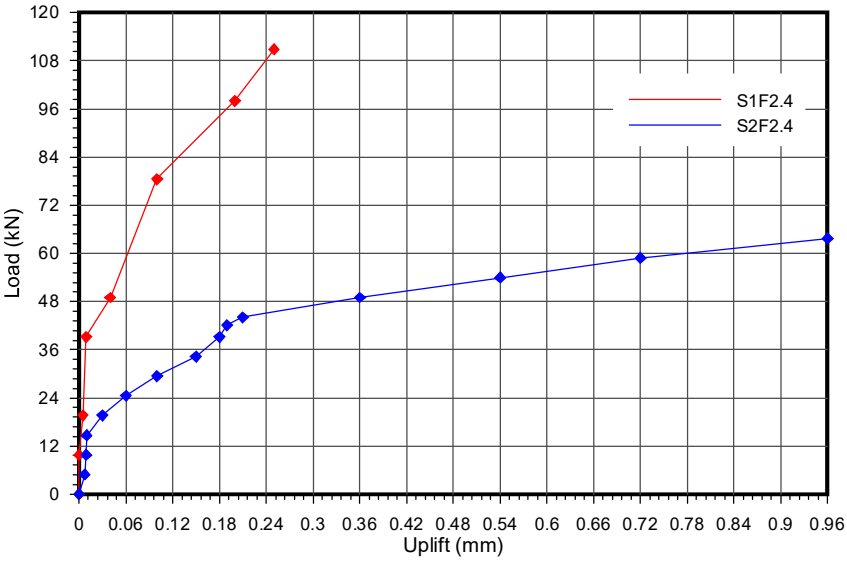

Figure (5-39) The effect of aluminum beam depth on variation of central uplift with load for composite beams with 2.4 m length – Experimental work

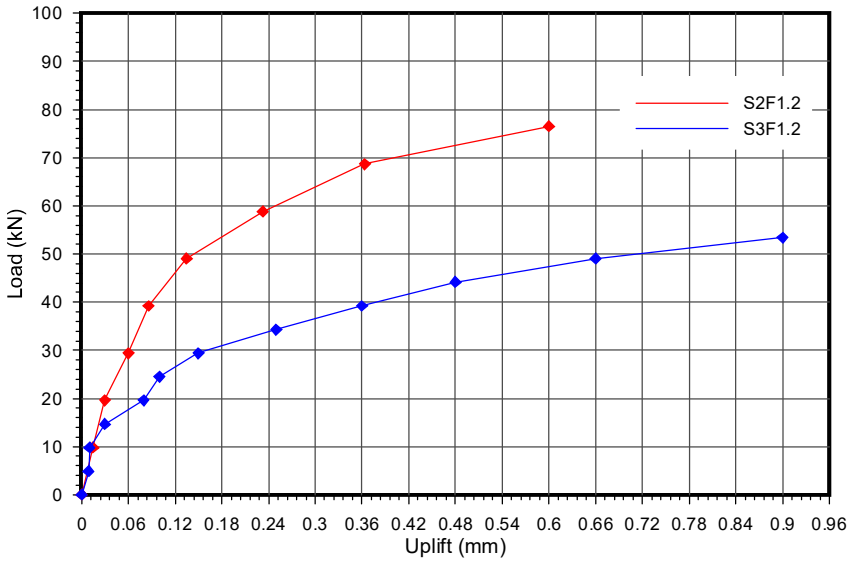

Figure (5-40) The effect of aluminum beam thickness on variation of central uplift with load for composite beams with 1.2 m length – Experimental work

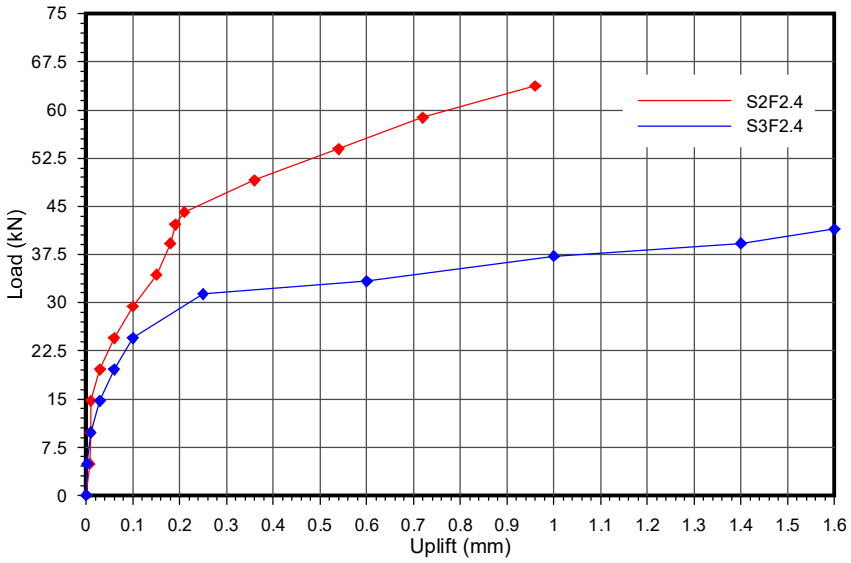

Figure (5-41) The effect of aluminum beam thickness on variation of central uplift with load for composite beams with 2.4 m length – Experimental work

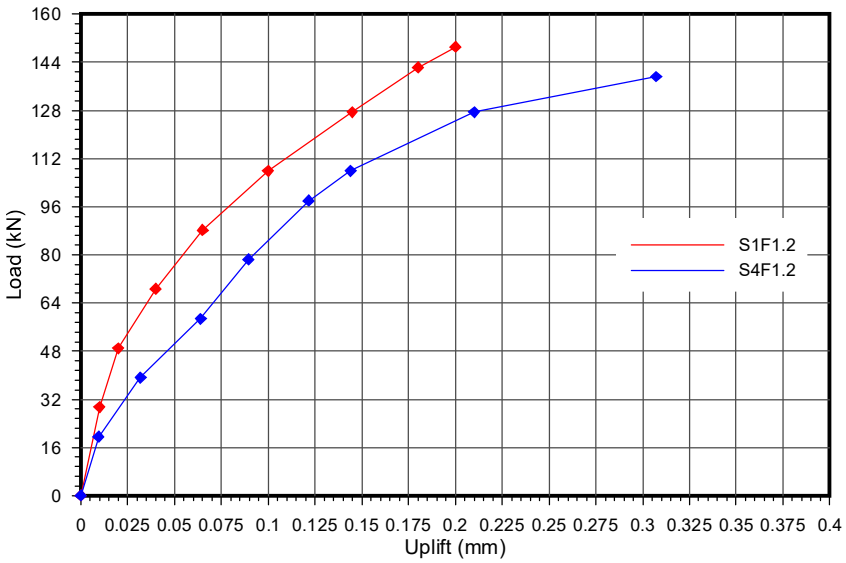

Figure (5-42) The effect of aluminum beam shape on variation of central uplift with load for composite beams with 1.2 m length – Experimental work

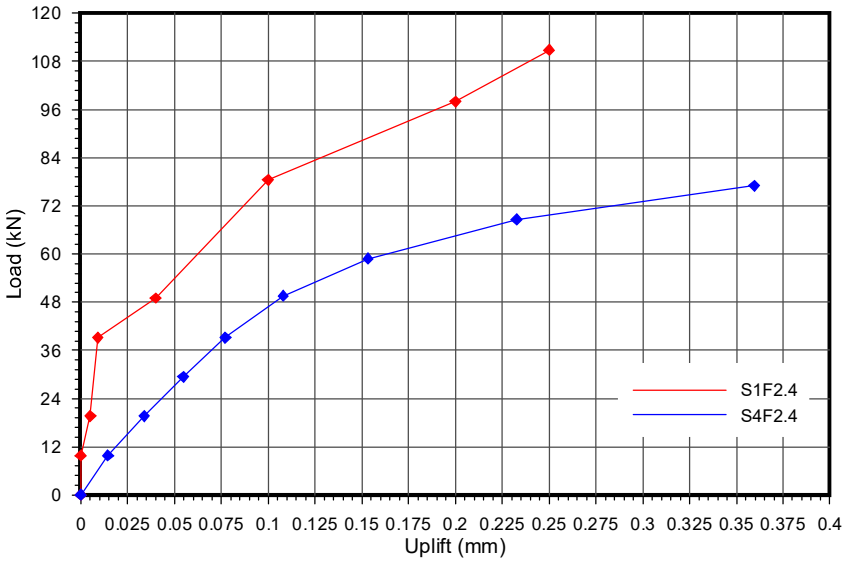

Figure (5-43) The effect of aluminum beam shape on variation of central uplift with load for composite beams with 2.4 m length – Experimental work

5.2.4.5 Strain distribution

Strains were measured in eight levels (four levels in the ferrocement slab and four levels in the aluminum beam) across the depth of the composite beam. This was done at two locations along the beam span as explained previously in section (3-7).

Very small strains were recorded at the first stage of loading up to onset of cracks in ferrocement when a sudden increase in the strains were taken place, thereafter the strains increased almost linearly with increasing the load.

The strain values at ultimate loads are extrapolated and summarized with those for service loads in Table (5-10).

Figures (5-44) to (5-53) show the strain distribution across the depth of tested beams for intermediate load values in the linear stage and ultimate loads.

Figures (5-44) and (5-45) illustrate the effect of connection condition upon composite action. The beam with no connection between components (S1-F1.2) shows individual behavior for its components, Fig. (5-44). While composite beam with one day period of hardening of adhesive epoxy layer behaves as one unit at small values of load and under higher load values the beam components tend to behave individually, Fig. (5-45).

Figures (5-46) to (5-53) clearly show the benefit of shear connection for tested composite beams where very low strain difference values (slip strain) at the interface between the ferrocement slab and aluminum beam are noted.

In all specimens, except for (S1F1.2), strains larger than (0.003) are measured at topmost fibers of ferrocement slab. No crushing was observed at strain (0.003).

Although the strains at bottommost fibers of aluminum beam sometime exceed the yield strain of aluminum, (0.014) for box section and (0.016) for I-section, but they do not reach elongation strain, (0.07) for box section and (0.12) for I section.

Table (5-10) Midspan strains of tested composite beams

No.	Beams designation	Ultimate load, P_{ul} (kN)	Extrapolated compressive strain in Ferr. (Top most fiber) at ultimate load($x10^{-3}$)	Extrapolated tensile strain in Al. (Bottom most fiber) at ultimate load ($x10^{-3}$)	Inter-mediate load in the linear stage (kN)	Compressive strain in Ferr. (Top most fiber) at intermediate load in the linear stage load ($x10^{-3}$)	Tensile strain in Al. (Bottom most fiber) at intermediate load in the linear stage load ($x10^{-3}$)
1	S1-F1.2	97.08	-3.30	25.00	64.72	-0.57	12.95
2	S1F1.2#	125.03	-3.10	20.50	83.35	-1.22	1.65
3	S1F1.2	149.05	-2.62	3.55	99.37	-1.55	2.35
4	S2F1.2	76.49	-4.09	10.75	50.99	-1.19	2.94
5	S3F1.2	53.44	-8.93	32.02	35.63	-0.90	3.03
6	S4F1.2	139.25	-9.68	18.35	92.83	-1.70	3.53
7	S1F2.4	110.81	-9.22	16.68	73.87	-1.92	5.46
8	S2F2.4	63.74	-12.90	60.17	42.49	-2.35	12.86
9	S3F2.4	41.45	-4.80	27.00	27.63	-0.60	2.95
10	S4F2.4	76.98	-8.60	24.09	51.32	-0.79	4.50

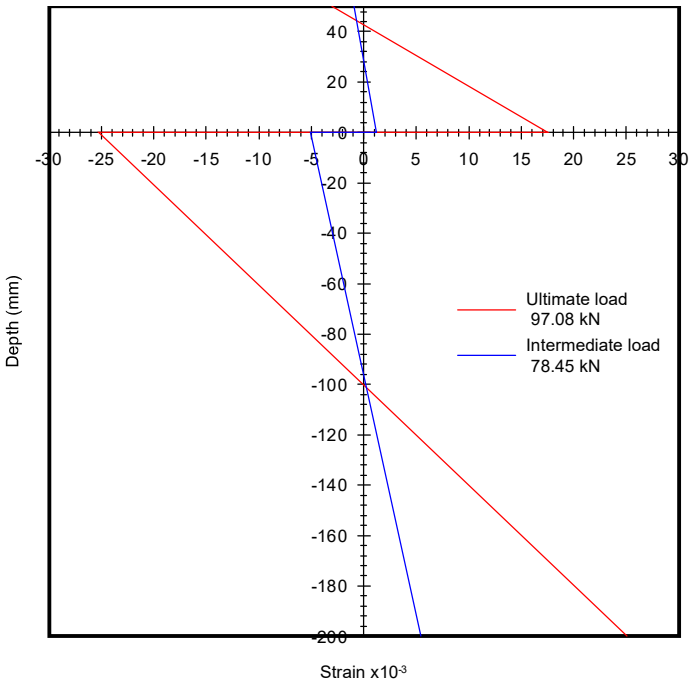

Figure (5-44) Strain distribution at mid-span for S1-F1.2 under ultimate load and intermediate load value in the linear stage - Experimental work

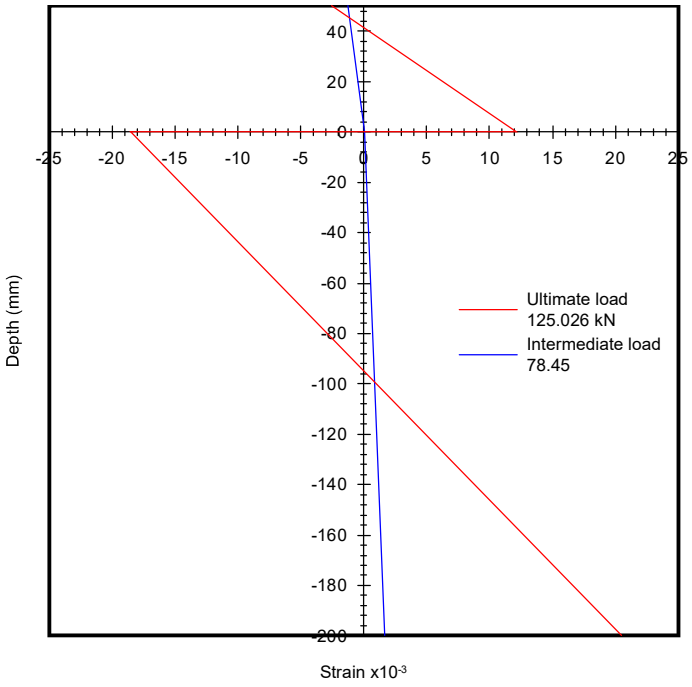

Figure (5-45) Strain distribution at mid-span for S1F1.2# under ultimate load and intermediate load value in the linear stage - Experimental work

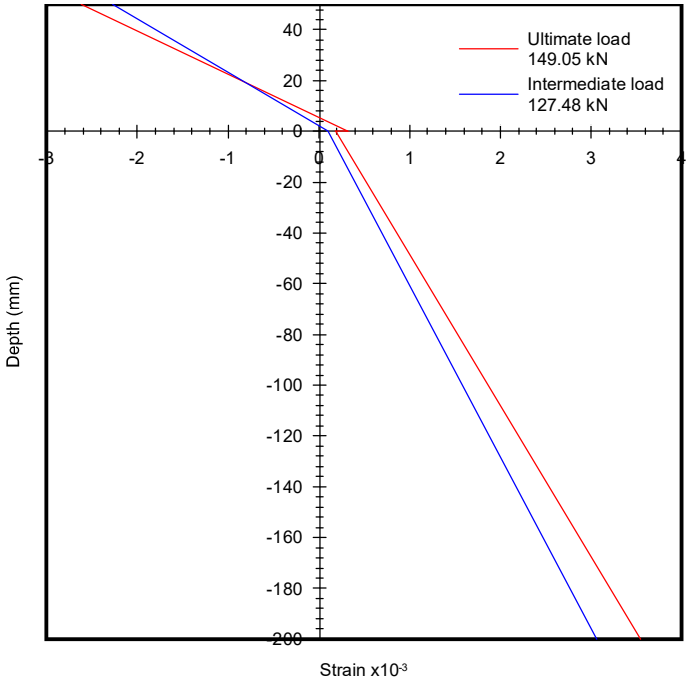

Figure (5-46) Strain distribution at mid-span for S1F1.2 composite beams under ultimate load and intermediate load value in the linear stage - Experimental work

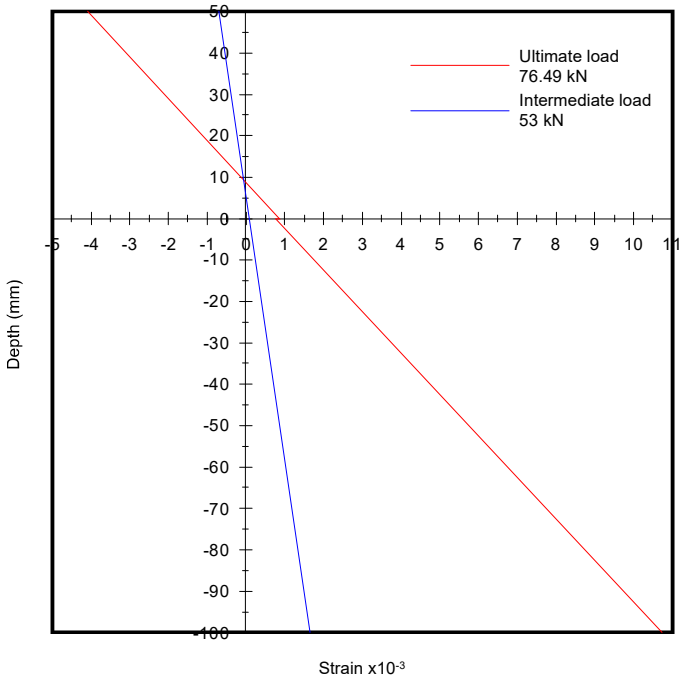

Figure (5-47) Strain distribution at mid-span for S2F1.2 composite beams under ultimate load and intermediate load value in the linear stage - Experimental work

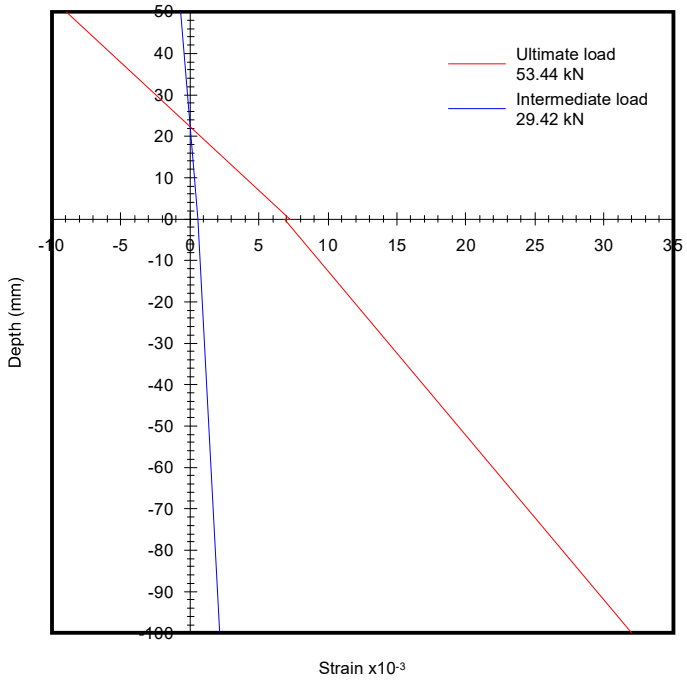

Figure (5-48) Strain distribution at mid-span for S3F1.2 composite beams under ultimate load and intermediate load value in the linear stage - Experimental work

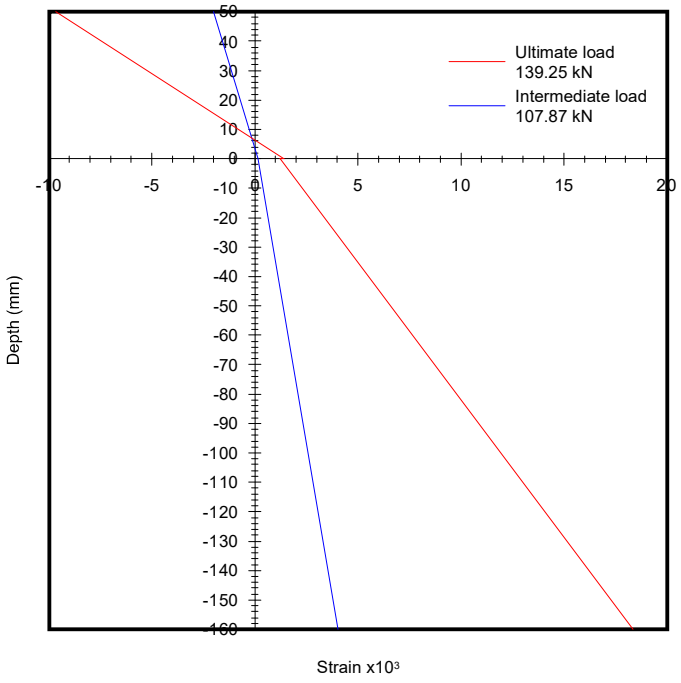

Figure (5-49) Strain distribution at mid-span for S4F1.2 composite beams under ultimate load and intermediate load value in the linear stage - Experimental work

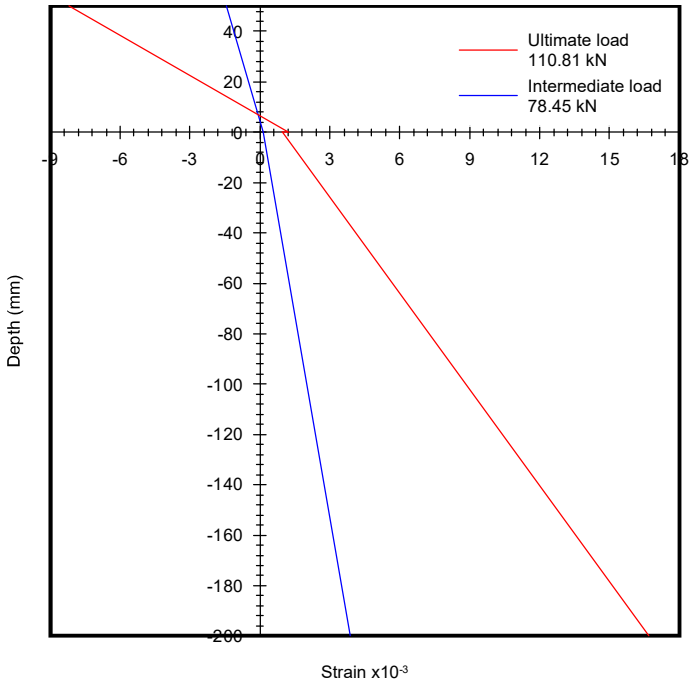

Figure (5-50) Strain distribution at mid-span for S1F2.4 composite beams under ultimate load and intermediate load value in the linear stage - Experimental work

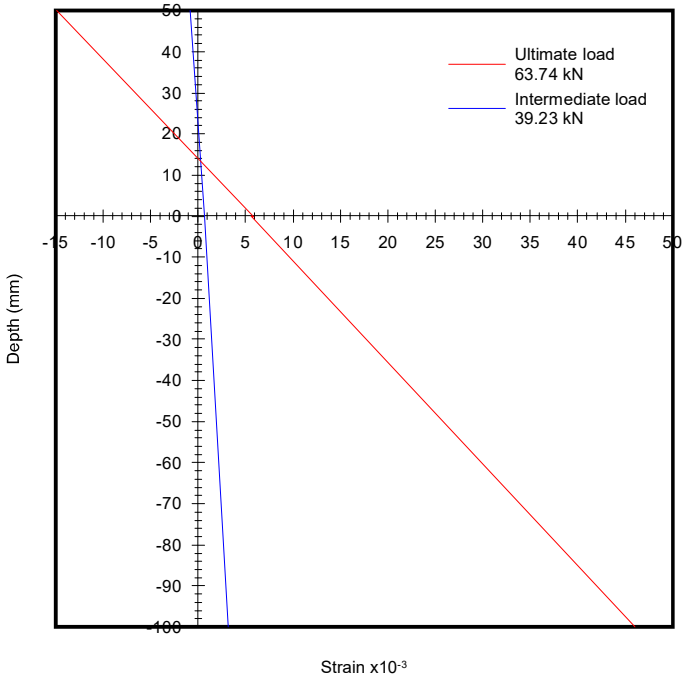

Figure (5-51) Strain distribution at mid-span for S2F2.4 composite beams under ultimate load and intermediate load value in the linear stage - Experimental work

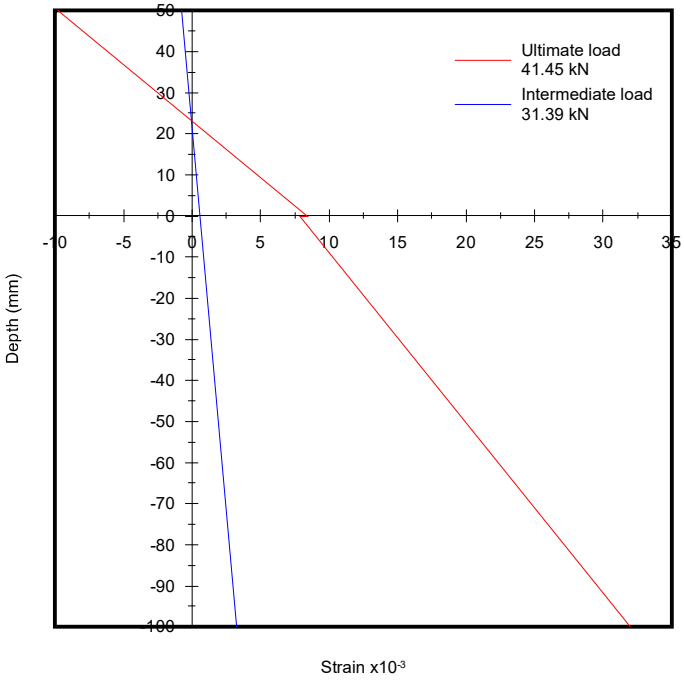

Figure (5-52) Strain distribution at mid-span for S3F2.4 composite beams under ultimate load and intermediate load value in the linear stage - Experimental work

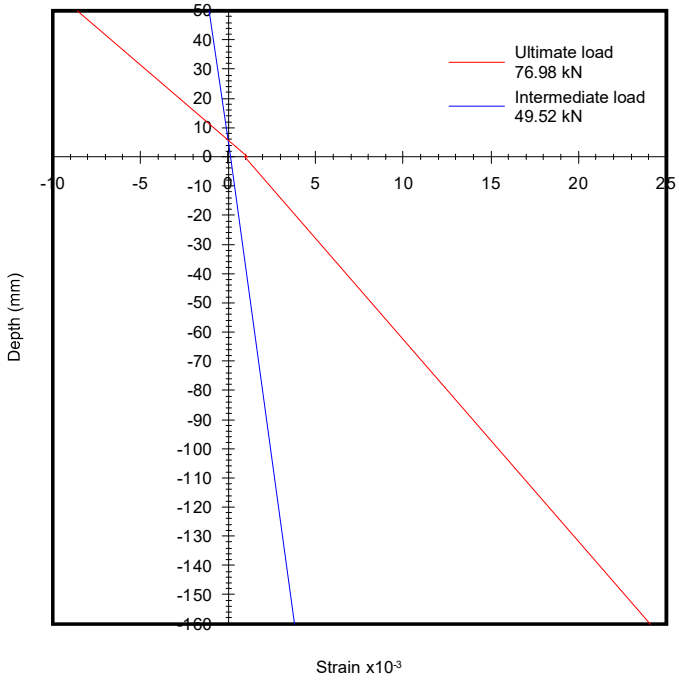

Figure (5-53) Strain distribution at mid-span for S4F2.4 composite beams under ultimate load and intermediate load value in the linear stage - Experimental work

5.3 Finite Element Analysis

In the present section, the tested beams have been analyzed using three dimensional finite element models. The main objectives of the analysis are to check the accuracy of the adopted finite element models to predict the overall behavior of the tested beams, and to get more information about stresses and strains developed in the beams.

In nonlinear analysis, the total load applied to a finite element model is divided into a series of load increments called load steps. At the completion of each incremental solution, the stiffness matrix of the model is adjusted to reflect nonlinear changes in structural stiffness before proceeding to the next load increment. The ANSYS program (ANSYS version 11.0) uses Newton-Raphson equilibrium iterations for updating the model stiffness.

5.3.1 Finite Element Discretization

The analysis of composite beams using three dimensional finite element model is achieved through the use of ANSYS version 11.0 computer code, see Appendix B.

As an initial step, a finite element analysis requires meshing of the model. In other words, the model is divided into a number of small elements, and after loading, stress and strain are calculated at integration points of these small elements. An important step in finite element modeling is the selection of the mesh density. A convergence of results is obtained when an adequate number of elements is used in a model. This is practically achieved when an increase in the mesh density has a negligible effect on the results. Therefore, in this finite element analysis a convergence study was carried out to determine an appropriate mesh density.

A number of response parameters was compared, including deflection of the beam, tensile strain at the bottom fiber of the beam, and compressive strain at the top fiber of the beam. The three parameters were determined at the midspan of the beam. Only one half of the beam is modeled, taking advantage

of symmetry. Three different numbers of elements (1224), (2372) and (4076) are used to examine the convergence of the results..

Comparison of the results is summarized in Table (5-11), and the convergence of three response parameters is shown in Fig. (5-54) .

As shown in Fig. (5-54), the results started to converge with a model have (2372) .

Table (5-11) Convergence of results

No.	Numbers of elements	Solution time (minute)	Midspan deflection (mm)	Compressive strain in ferrocement (top most fiber)	Tensile strain in aluminum section (bottom most fiber)
1	1224	10	6.8	-0.0025	0.0067
2	2372	41	9.12	-0.0062	0.0123
3	4076	104	10.09	-0.0066	0.015

5.3.2 Finite Element Model

The third model of convergence study is adopted. In this model the half span of each beam is divided into 24 and 48 elements (in z-direction) for 1.2m and 2.4m length, respectively. The composite beam cross section (in y-direction) is divided into four elements for the ferrocement and twenty two, twelve, twelve and fifteen elements for aluminum beams (S1, S2, S3 and S4), respectively, (one element for each flange of the section). In x-direction, the ferrocement flange is divided into thirty three elements, the aluminum flange into five and eight elements for box and I sections, respectively, and the web into two and one element for box and I sections, respectively, as shown in Fig. (5-55). Three dimensional 8-noded brick elements are selected to represent the ferrocement slab and aluminum beam.

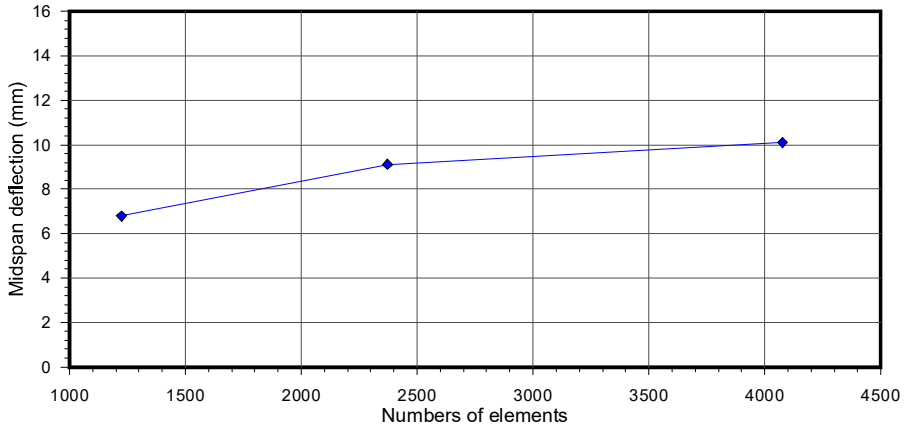

(a)

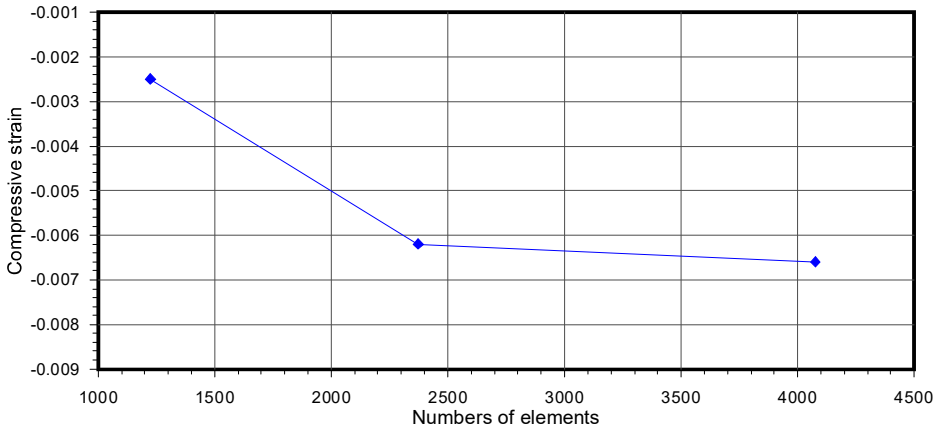

(b)

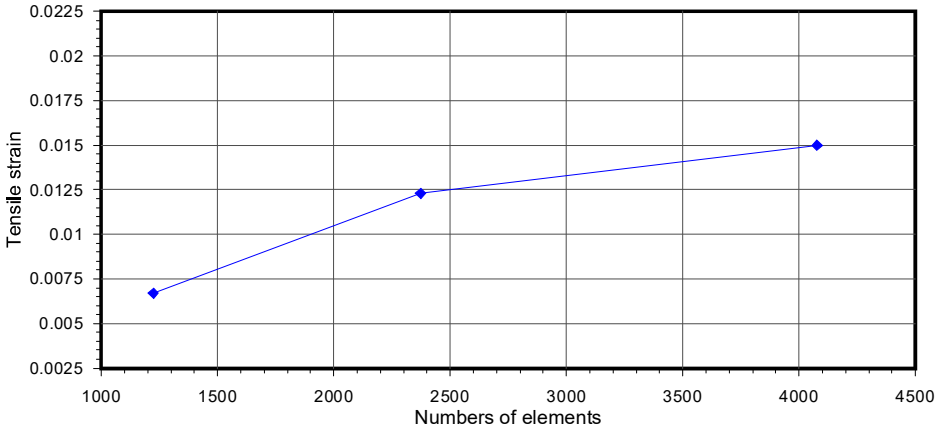

(c)

Figure (5-54) Results from convergence study: (a) mid-span deflection, (b) compressive strain, and (c) tensile strain

In general, the connectors are represented by spring elements at the interface between ferrocement and aluminum beam. Shell, cohesive zone, and nonlinear spring element are used as connectors representation and compared with the general case.

5.3.3 Loads and Boundary Conditions

It has been found that the simulation of the applied load and the supports has a significant effect on the results of the finite element analysis. In the experimental work of the present investigation, and to avoid premature local bearing failure of ferrocement and aluminum, bearing plates were used at the loading and reaction points.

To simulate the applied loads, loads (P) were distributed equally among the nodes lines within the loading plate and (P/2) on edge nodes lines. The applied loads configuration are shown clearly in Fig. (5-56).

Displacement boundary conditions are needed to constrain the model to get a unique solution. To ensure that the model acts in the same way as the experimental beam, boundary conditions need to be applied at points of symmetry, and where the supports and loadings exist.

Making use of symmetry, only one-half of the beam span was considered in the analysis. The symmetry boundary conditions were set first. The model being used is symmetric about one plane. The boundary conditions of symmetry are shown in Fig. (5-57).

Nodes defining a vertical plane through the beam midspan defines a plane of symmetry at which Z = 0. To model the symmetry, nodes on this plane must be constrained in the horizontal direction. These nodes, therefore, have a degree of freedom UZ = 0. The supports of the beams were simulated by preventing the vertical displacement of the nodes at the bearing plate position. The support was modeled in such a way that a roller was created. The translations UX and UY on a single line of nodes on the plate were given values of (0). By doing this, the beam will be allowed to rotate at the support. The support condition is shown in Fig. (5-58).

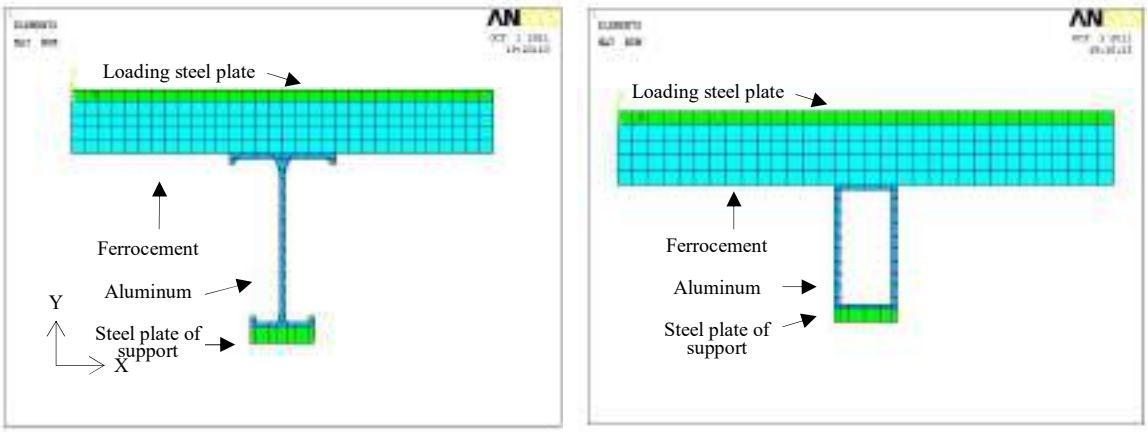

a-Front view

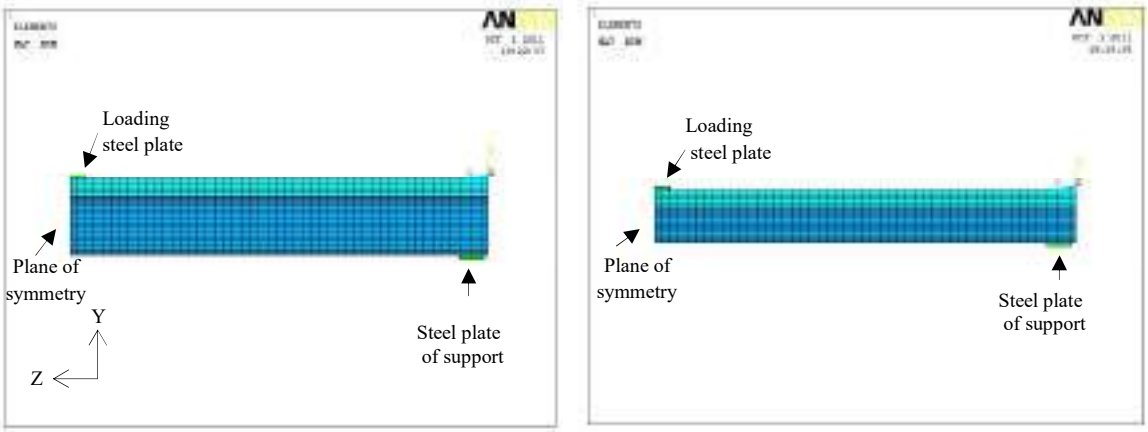

b-Side view

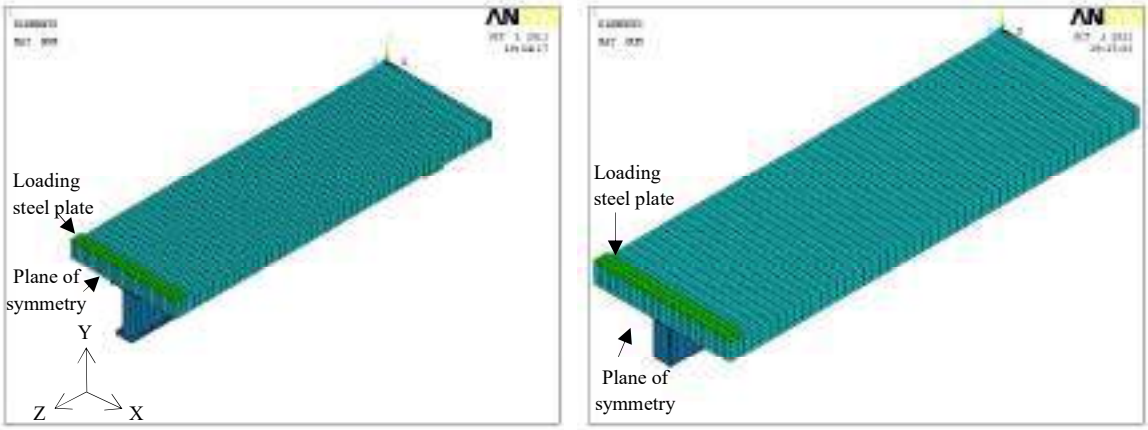

c- Isometric view

Figure (5-55) Discretization of the half span length of the composite beam

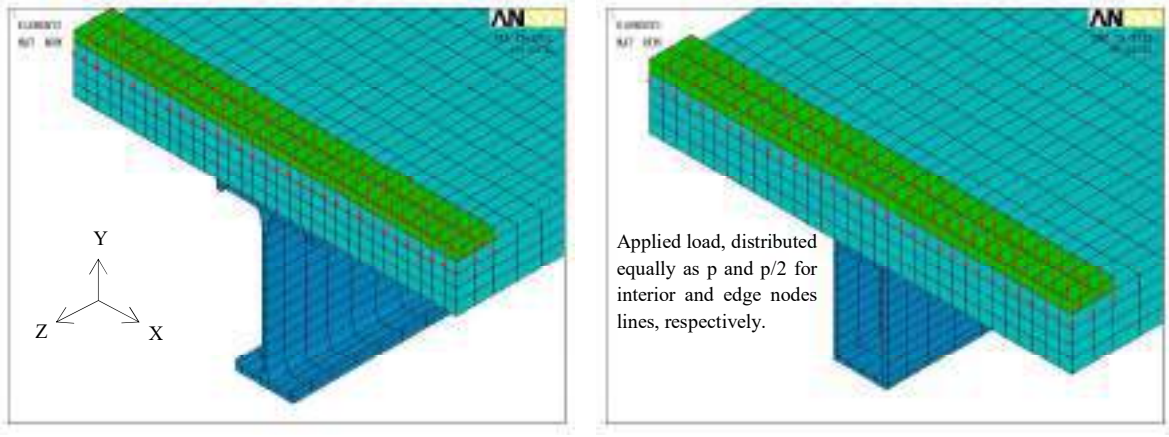

Figure (5-56) Distribution of applied loads

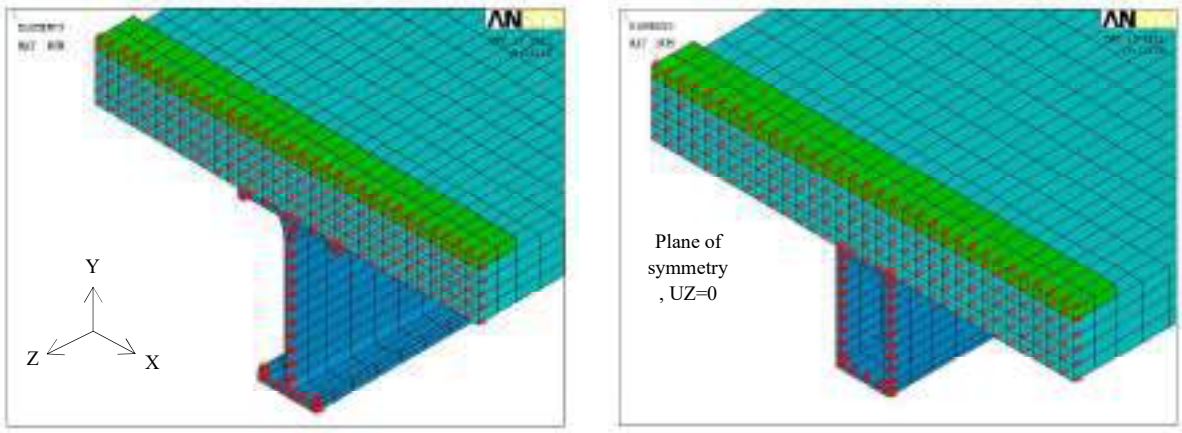

Figure (5-57) Boundary condition for symmetrical plane

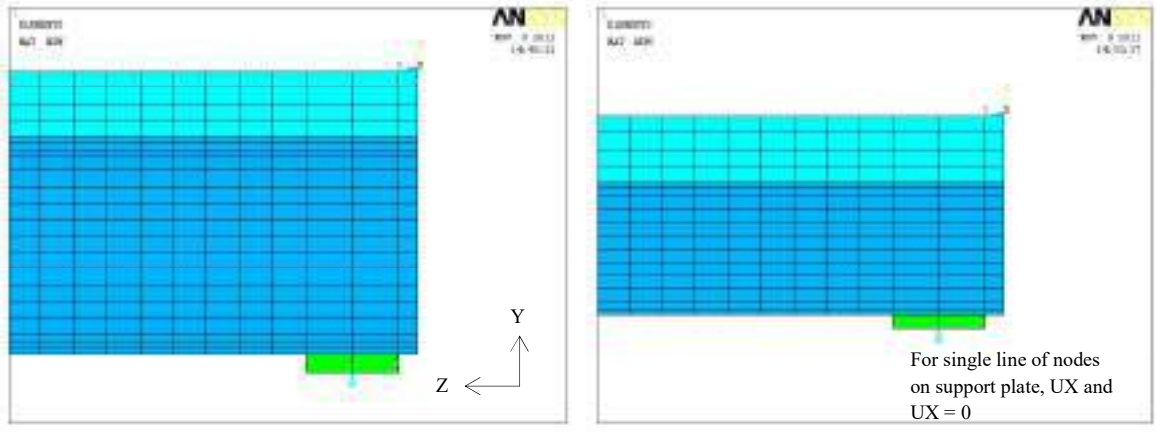

Figure (5-58) Boundary condition for supports

5.3.4 Adhesive Epoxy Layer Modeling

Epoxy adhesive layer have been used as a shear connector, but it is not clear how to behave or how to model so several models have been investigated.

Three models with different interface element types were used to simulate the adhesive epoxy layer for tested composite beam (S2F1.2) to include the slip effect. Another model with full interaction (without slip) between the two components of the beam was used for comparison (model 4).

Table (5-12) illustrates the comparison between the experimental and the theoretical results for ultimate load, deflection and end slip. Figures (5-59) and (5-60) show the results given by the used models for epoxy layer with respect to the load – midspan deflection and load – end slip relationships.

The model 1 which is COMBIN14 linear spring is adopted in this study because it gives closer results to experimental ones as well as the less solution iteration and so less solution time.

Table (5-12) Adhesive epoxy layer representation

Finite Element Analysis		**Ultimate load (kN)**	**Deflection (mm)**	**End slip (mm)**
Model No.	**Element type**			
1	COMBIN14	79.2	10.09	0.051
2	COMBIN39	82.5	13.10	0.09
3	INTER205	79.2	9.91	0.01
4	SOLSH190	85.8	12.83	-
Experimental results		76.49	10.04	0.035

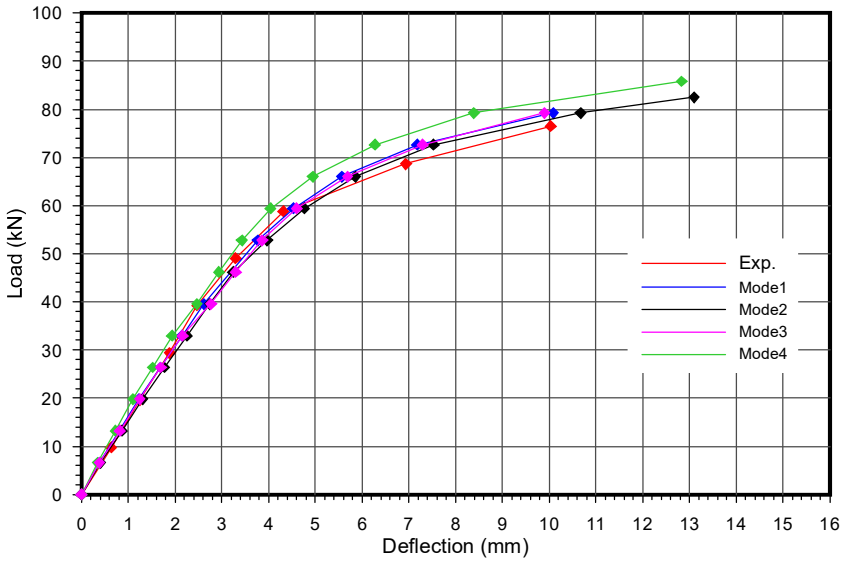

Figure (5-59) Variation of mid span deflection with load for different adhesive epoxy layer models

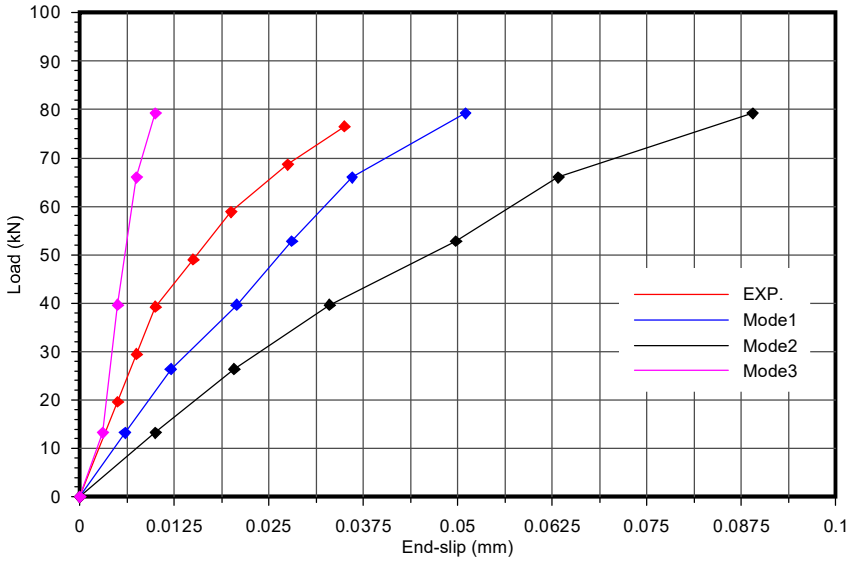

Figure (5-60) Variation of end slip with load for different adhesive epoxy layer models

5.3.5 Ultimate load

In the physical test under load control, collapse of a structure occurs when no further load increment can be sustained. This is usually indicated in the numerical test by successively increasing iterative displacements and a continuous growth in the dissipated energy. Hence, the convergence of the iterative process cannot be achieved. So The values of ultimate load obtained theoretically attribute to the solution divergence [79].

The ultimate load for each beam as tested and calculated by using the finite element method is shown in Table (5-13).

The finite element model is found to give ultimate loads closer to the experimental values .

The ratios of predicted to experimental values of ultimate load are 0.74 to 1.13 with an average value of 0.97 for beams with 1.2 m length and 1.17 to 1.49 with average value of 1.26 for beams with 2.4 m length. They are 1.07 to 1.15 with an average of 1.11 for ferrocement specimens and 0. 93 to 1.1 with an average of 1.02 for aluminum beams with 1.2 m length. Considering the strain hardening portion of the stress-strain relationship of aluminum in the theoretical evaluation of ultimate loads may be the reason behind obtaining very closer values for aluminum beams.

It is expected that the modeling strategy for the finite element analysis proposed in this study could be used for designing and analyzing ferrocement aluminum composite beams.

5.3.6 Deflection

Figures (5-61) to (5-76) illustrate the load-deflection relationships for tested beams. The experimental relationships alongside the theoretical ones are collected for each beam.

The finite element analysis is found to give close relationships to experimental results. Table (5-14) illustrates the comparison between the

experimental results and the theoretical ones for deflections at ultimate and service loads (2/3 the ultimate loads).

The ratios of experimental to predicted values of deflection are 0.92 to 0.89 with an average value of 0.91 for beams with 1.2 m length and 0.7 to 1.44 with average value of 0.99 for beams with 2.4 m length. They are 0.77 to 0.69 with an average of 0.73 for ferrocement specimens and 1.02 to 0.83 with an average of 0.93 for aluminum beams with 1.2 m length. This is because of the constraints theoretically stipulated on the deformation of beams.

5.3.7 End slip

The load-end slip relationships for all beams are depicted in Figs. (5-77) to (5-86). Good agreement between the experimental and theoretical results is achieved.

Table (5-15) illustrates the comparison between the experimental results and the theoretical ones. The theoretical and experimental investigations give small slip values for tested composite beams and it seems good to consider the used adhesive epoxy layer as a stiff shear connection as compared with classical connectors used in composite beam.

5.3.8 Strain

The load-strain relationships for all beams are depicted in Figs. (5-87) to (5-98).

The values of ultimate load for composite beams obtained theoretically are corresponding to the values of ferrocement slab strain of (0.0039-0.0125) which are larger than (0.003) value permitted by the code.

Table (5-16) illustrates the comparison between the experimental results and the theoretical ones. Figures (5-99) to (5-102) reveal the deformed shape and contours for longitudinal strain distribution at ultimate load for three samples comprising ferrocement slab, aluminum beam and composite beam.

Table (5-13) Ultimate and service loads of tested beams

No.	Beams designation	Ultimate load (kN)		Service load* (kN)		Ultimate P_{exp}/P_{th}
		Experimental (P_{exp})	Theoretical (P_{th})	Experimental (P_{exp})	Theoretical (P_{th})	
1	F1.2	8.83	8.25	5.88	5.50	1.07
2	F2.4	3.43	2.97	2.28	1.98	1.15
3	S1	95.12	86.73	63.41	57.82	1.10
4	S2	28.44	27.30	18.96	18.20	1.04
5	S3	21.87	21.98	14.58	14.65	0.99
6	S4	77.27	82.80	51.51	55.20	0.93
7	S1-F1.2	97.08	105.60	64.72	70.40	0.92
8	S1F1.2#	125.03	125.4	83.35	83.6	0.99
9	S1F1.2	149.05	132.00	99.37	88.00	1.13
10	S2F1.2	76.49	79.20	50.99	52.80	0.97
11	S3F1.2	53.44	72.60	35.63	48.40	0.74
12	S4F1.2	139.25	132.00	92.83	88.00	1.05
13	S1F2.4	110.81	92.40	73.87	61.60	1.20
14	S2F2.4	63.74	42.90	42.49	28.60	1.49
15	S3F2.4	41.45	34.65	27.63	23.10	1.20
16	S4F2.4	76.98	66.00	51.32	44.00	1.17

* Service load = (2/3) ultimate load

Table (5-14) Deflections of tested beams

No.	Beams designation	Deflection at ultimate load (mm)			Deflection at service* load (mm)		
		Experimental (d_{exp})	Theoretical (d_{th})	d_{exp}/d_{th}	Experimental (d_{exp})	Theoretical (d_{th})	de_{xp}/d_{th}
1	F1.2	16.76	21.71	0.77	7.12	3.50	2.03
2	F2.4	20.89	30.10	0.69	8.11	6.8	1.19
3	S1	7.67	10.26	0.75	3.98	3.92	1.02
4	S2	16	41.00	0.39	6.235	7.00	0.89
5	S3	20	41.12	0.49	6.561	5.90	1.11
6	S4	14.01	36.96	0.38	3.803	4.60	0.83
7	S1-F1.2	9.12	18.00	0.51	3.10	4.49	0.69
8	S1F1.2#	8.93	3.6	2.48	2.39	2.15	1.11
9	S1F1.2	3.70	3.67	1.01	1.99	2.17	0.92
10	S2F1.2	10.04	10.09	0.99	3.43	3.77	0.91
11	S3F1.2	13.60	18.47	0.74	4.15	4.68	0.89
12	S4F1.2	7.40	11.19	0.66	3.16	3.51	0.90
13	S1F2.4	22.50	21.70	1.04	7.63	8.23	0.93
14	S2F2.4	63.00	57.00	1.11	21.63	15.00	1.44
15	S3F2.4	85.00	67.60	1.26	11.27	16.04	0.70
16	S4F2.4	29.00	35.10	0.83	9.03	10.20	0.88

* Service load = (2/3) ultimate load

Table (5-15) End-slip of composite beams

No.	Beams designation	End-slip at ultimate load (mm)		End-slip at service load (mm)	
		Experimental	Theoretical	Experimental	Theoretical
1	S1-F1.2	2.000	4.08	0.950	1.343
2	S1F1.2#	1.910	0.14	0.345	0.098
3	S1F1.2	0.012	0.041	0.004	0.020
4	S2F1.2	0.035	0.051	0.015	0.028
5	S3F1.2	0.055	0.042	0.021	0.025
6	S4F1.2	0.023	0.017	0.011	0.012
7	S1F2.4	0.0135	0.030	0.004	0.020
8	S2F2.4	0.044	0.020	0.012	0.014
9	S3F2.4	0.060	0.018	0.024	0.010
10	S4F2.4	0.032	0.013	0.009	0.009

Table (5-16) Comparison of experimental and theoretical strain for tested beams

No.	Beams designation	Compressive strain in Ferr. (top most fiber) at ultimate load ($x10^{-3}$)		Tensile strain in Al. (bottom most fiber) at ultimate load ($x10^{-3}$)	
		Experimental	Theoretical	Experimental	Theoretical
1	F1.2	-0.80	-1.00	6.50	8.60
2	F2.4	-3.90	-0.68	11.00	3.6
3	S1	-	-14.28	9.60	12.82
4	S2	-	-58.53	46.41	58.00
5	S3	-	-141.60	59.00	137.13
6	S4	-	-50.94	69.00	123.09
7	S1-F1.2	-3.30	-4.09	25.00	33.36
8	S1F1.2#	-3.10	-3.26	20.5	4.37
9	S1F1.2	-2.62	-3.90	3.55	4.48
10	S2F1.2	-4.09	-6.67	10.75	15.72
11	S3F1.2	-8.93	-12.48	32.02	38.18
12	S4F1.2	-9.68	-18.2	18.35	26.68
13	S1F2.4	-9.22	-8.53	16.68	15.89
14	S2F2.4	-12.90	-9.9	60.17	39.40
15	S3F2.4	-4.80	-9.34	27.00	49.43
16	S4F2.4	-8.60	-9.58	24.09	29.61

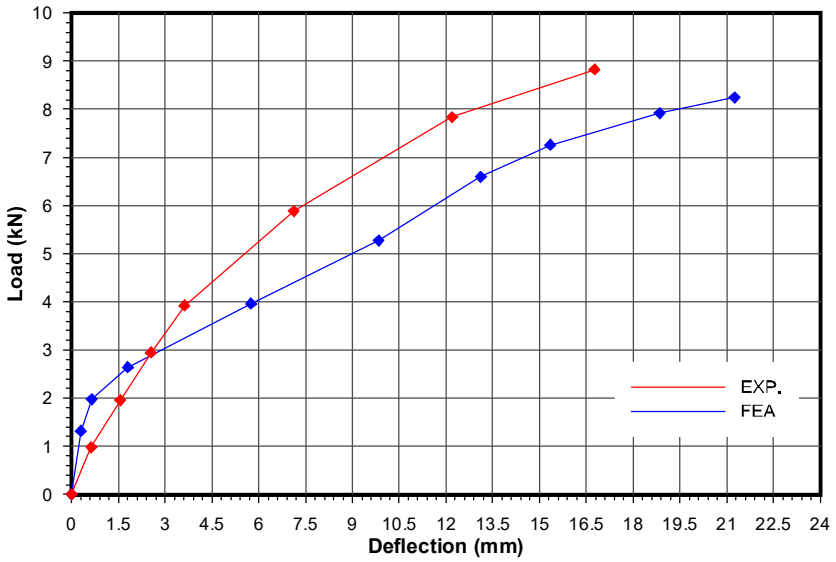

Figure (5-61) Variation of midspan deflection with load for ferrocement specimen (F1.2)

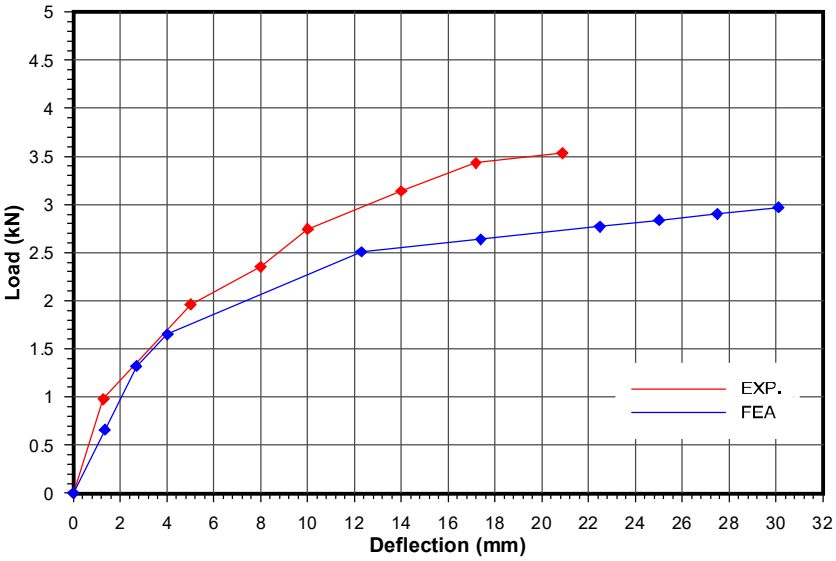

Figure (5-62) Variation of midspan deflection with load for ferrocement specimen (F2.4)

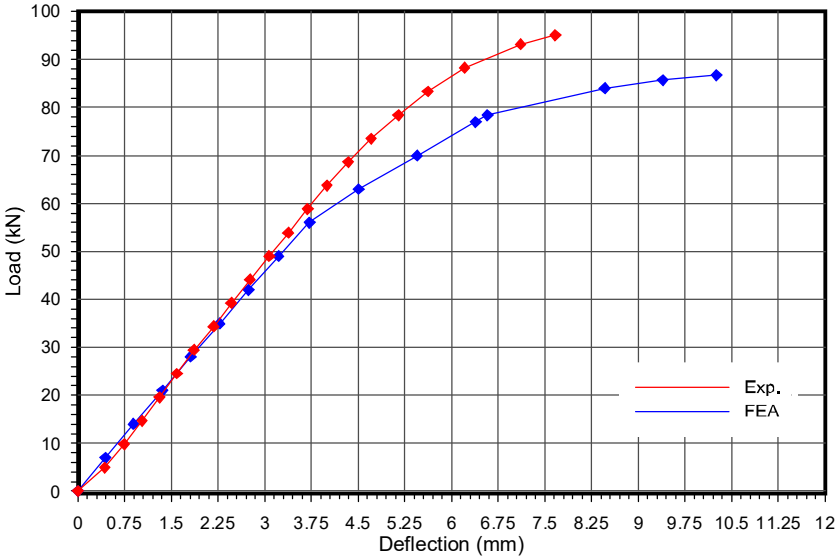

Figure (5-63) Variation of midspan deflection with load for aluminum beam (S1)

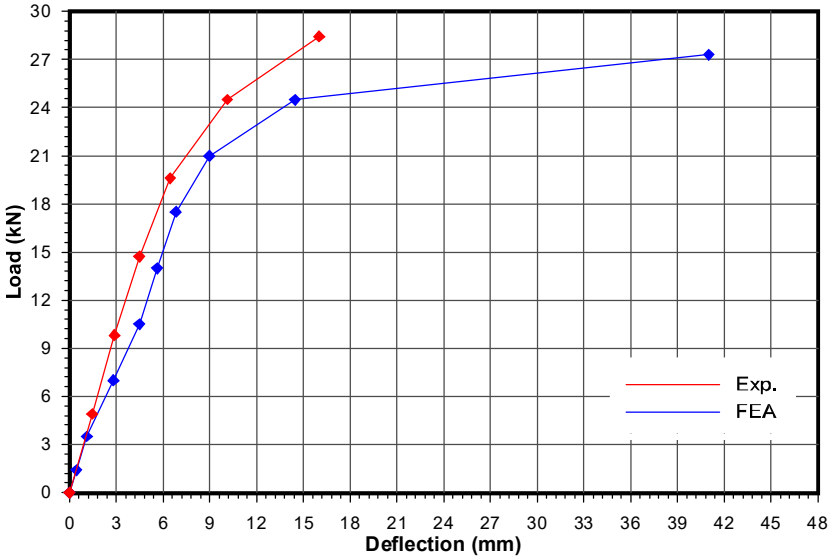

Figure (5-64) Variation of midspan deflection with load for aluminum beam (S2)

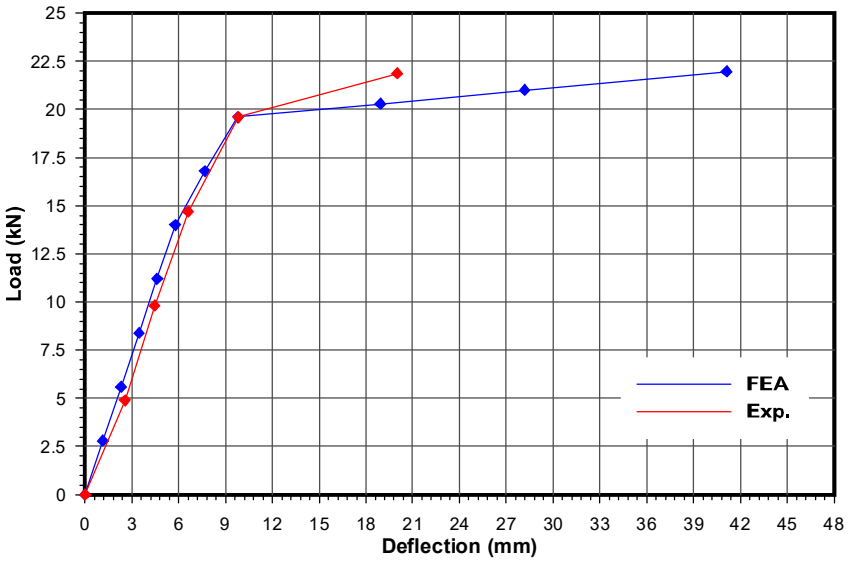

Figure (5-65) Variation of midspan deflection with load for aluminum beam (S3)

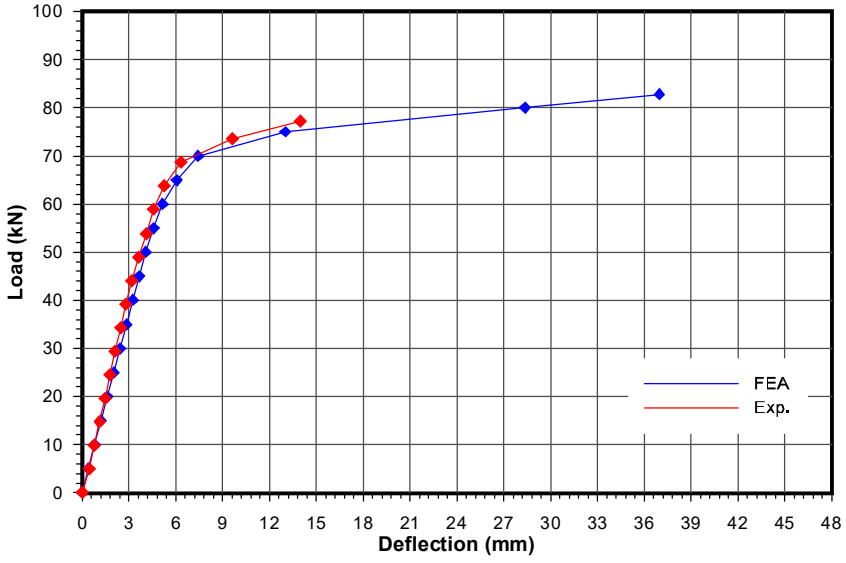

Figure (5-66) Variation of midspan deflection with load for aluminum beam (S4)

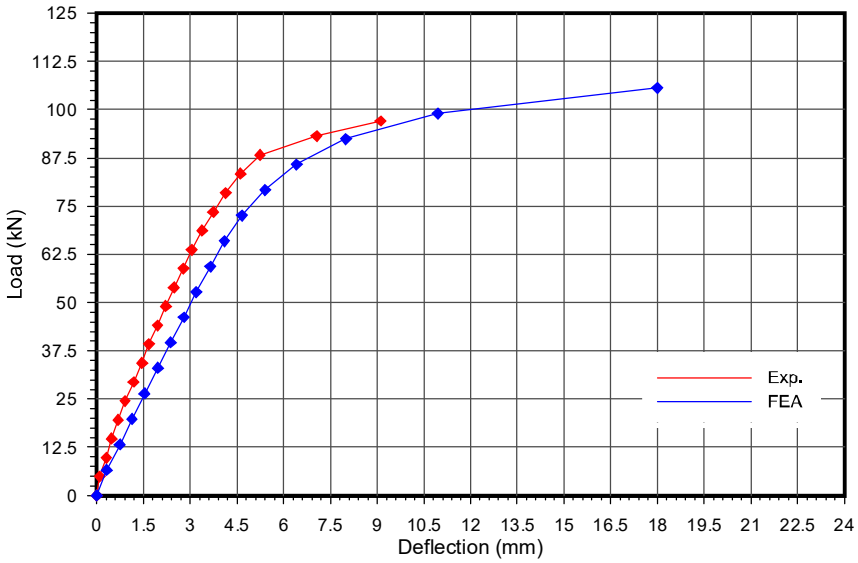

Figure (5-67) Variation of midspan deflection with load for composite beam without adhesive epoxy layer (S1-F1.2)

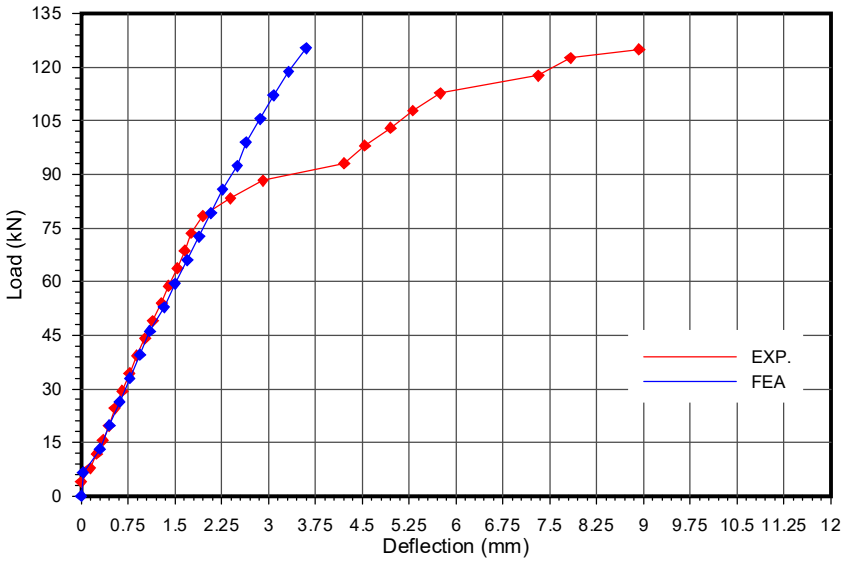

Figure (5-68) Variation of midspan deflection with load for composite beam (S1F1.2#)

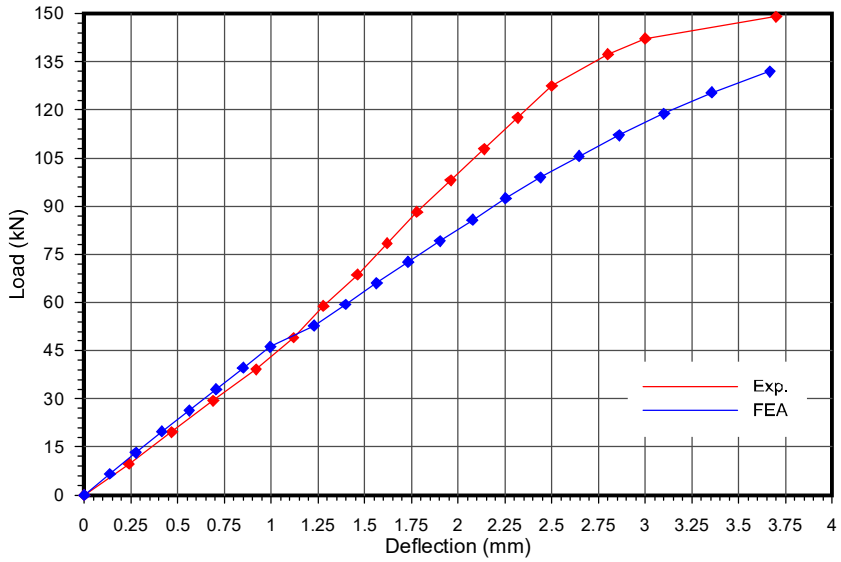

Figure (5-69) Variation of midspan deflection with load for composite beam (S1F1.2)

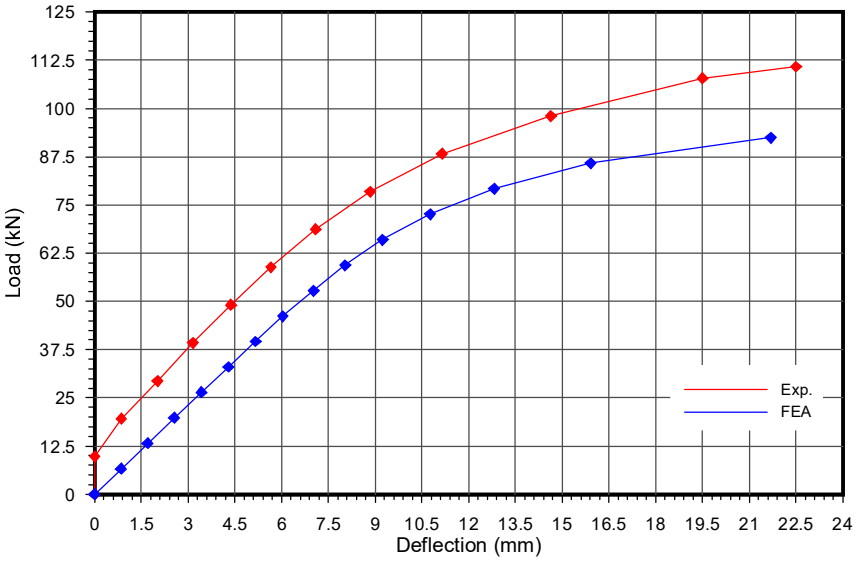

Figure (5-70) Variation of midspan deflection with load for composite beam (S1F2.4)

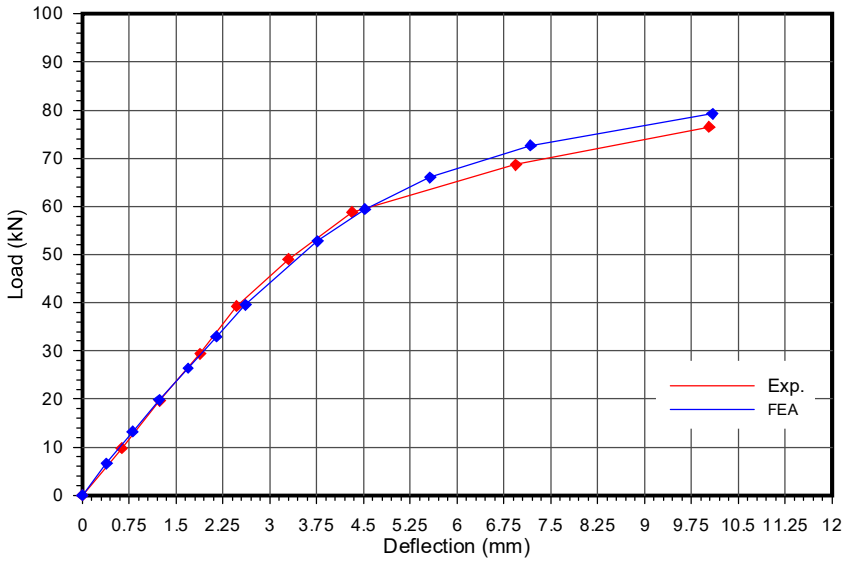

Figure (5-71) Variation of midspan deflection with load for composite beam (S2F1.2)

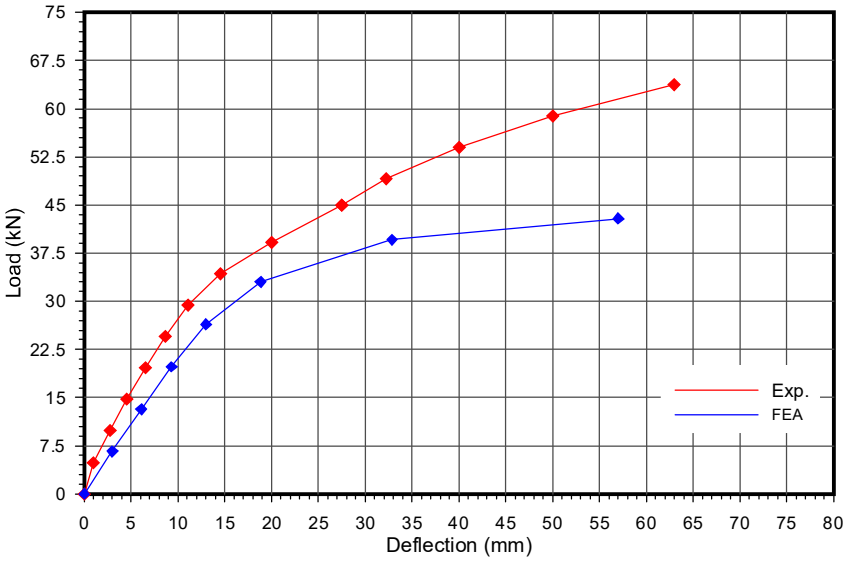

Figure (5-72) Variation of midspan deflection with load for composite beam (S2F2.4)

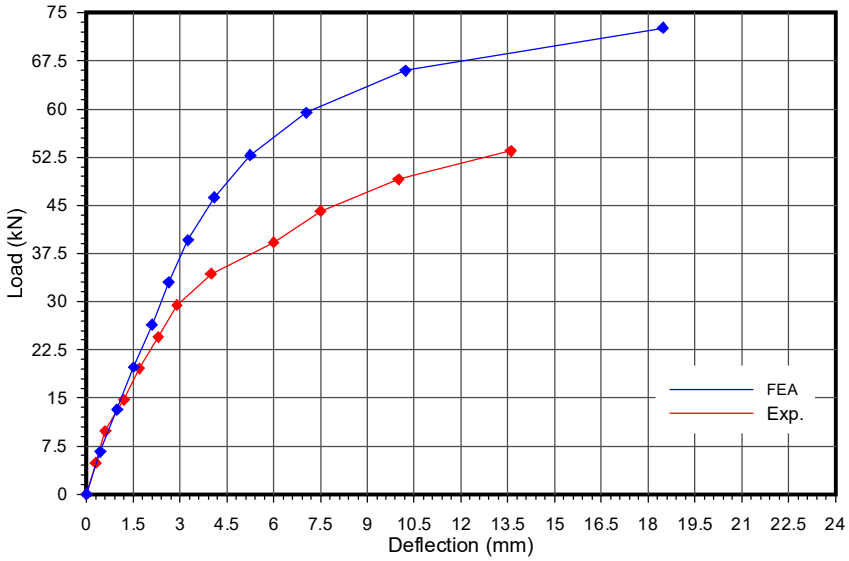

Figure (5-73) Variation of midspan deflection with load for composite beam (S3F1.2)

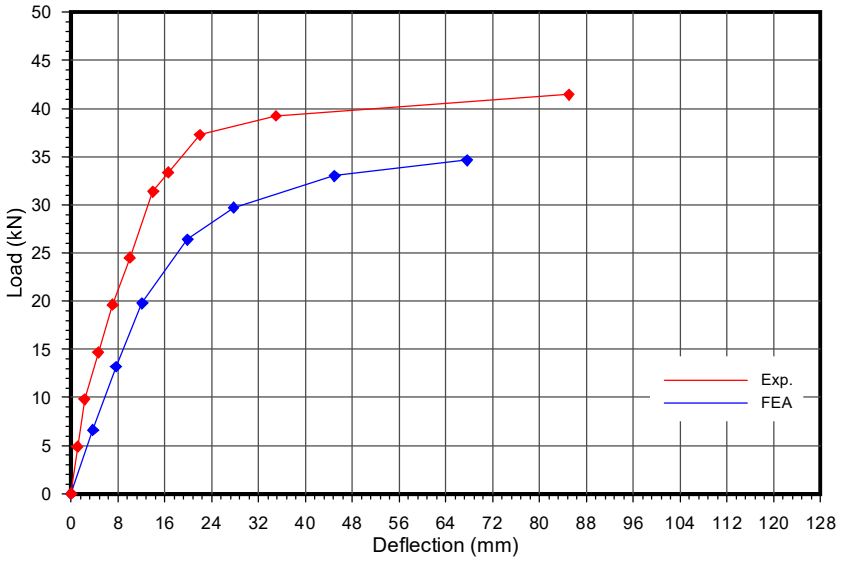

Figure (5-74) Variation of midspan deflection with load for composite beam (S3F2.4)

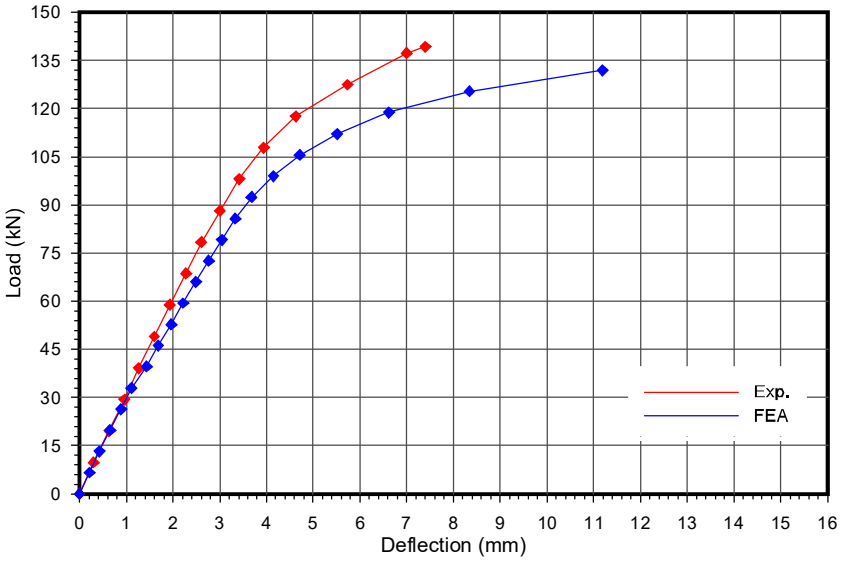

Figure (5-75) Variation of midspan deflection with load for composite beam (S4F1.2)

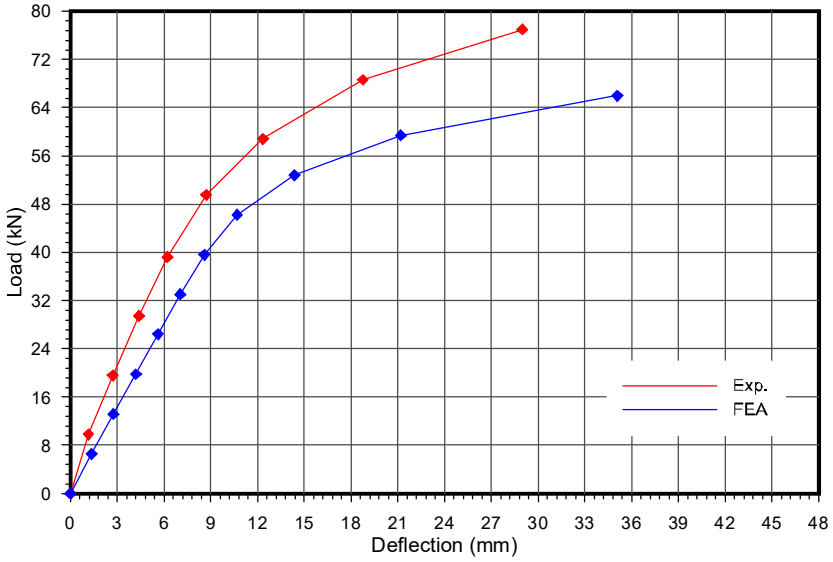

Figure (5-76) Variation of midspan deflection with load for composite beam (S4F2.4)

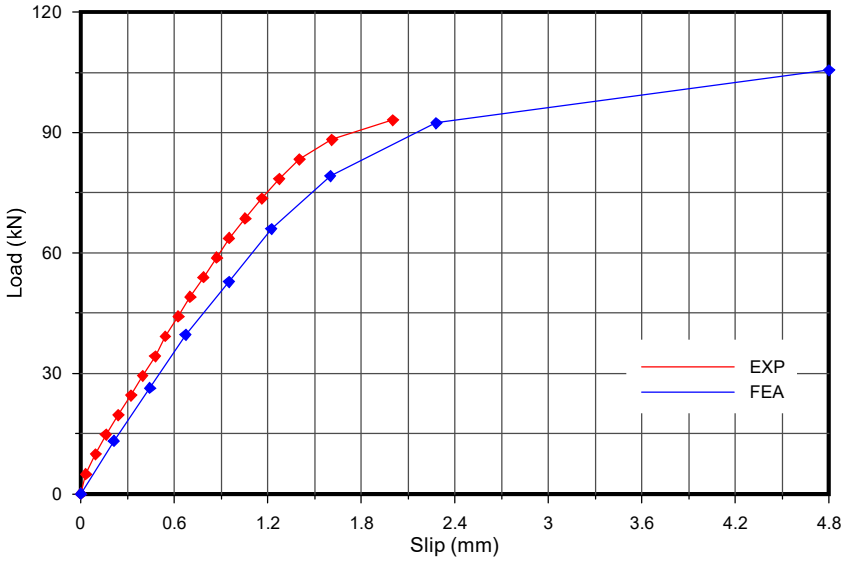

Figure (5-77) Variation of end slip with load for composite beam (S1-F1.2)

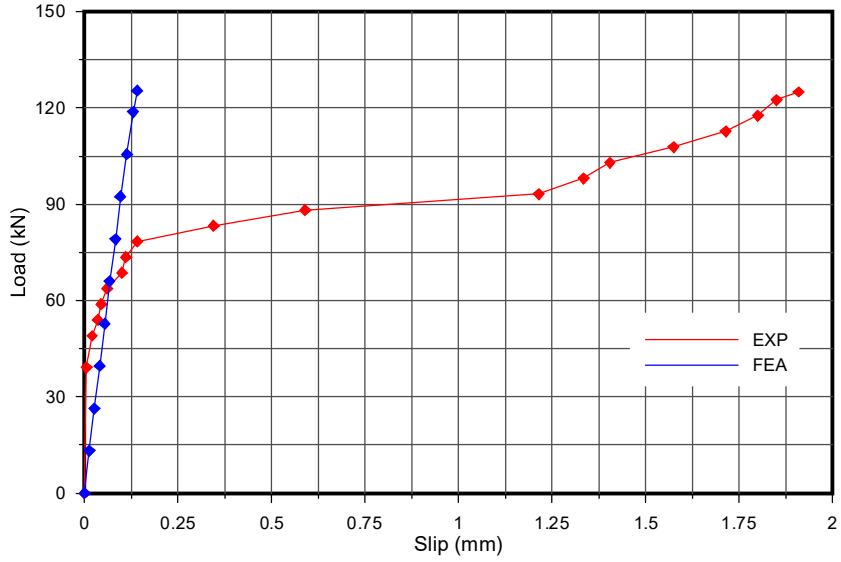

Figure (5-78) Variation of end slip with load for composite beam (S1F1.2#)

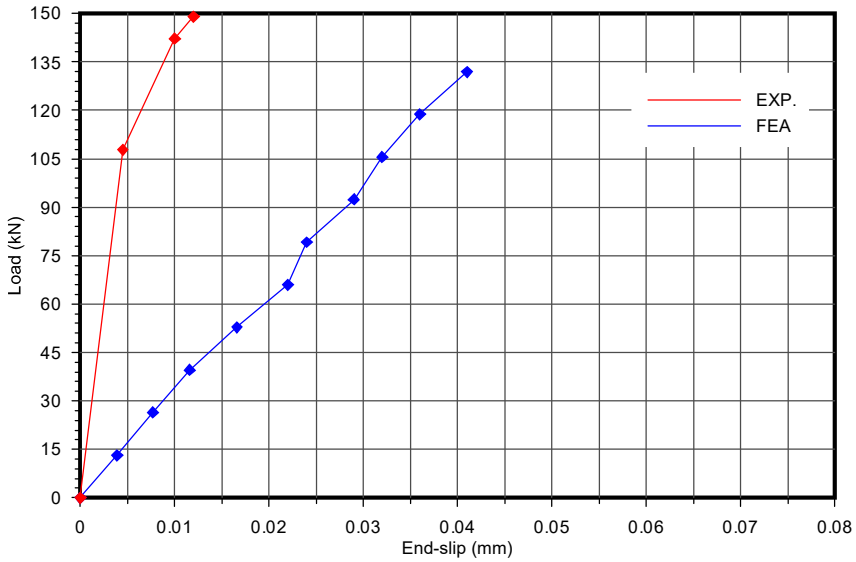

Figure (5-79) Variation of end slip with load for composite beam (S1F1.2)

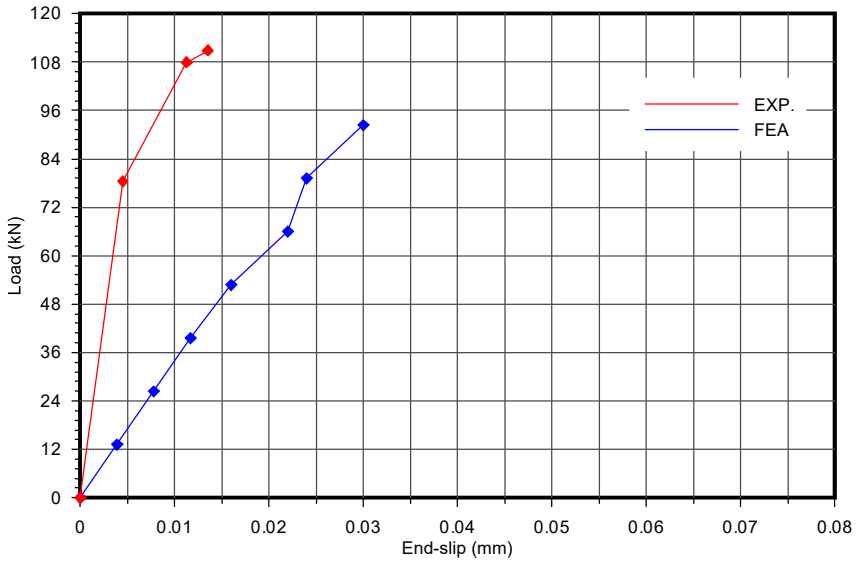

Figure (5-80) Variation of end slip with load for composite beam (S1F2.4)

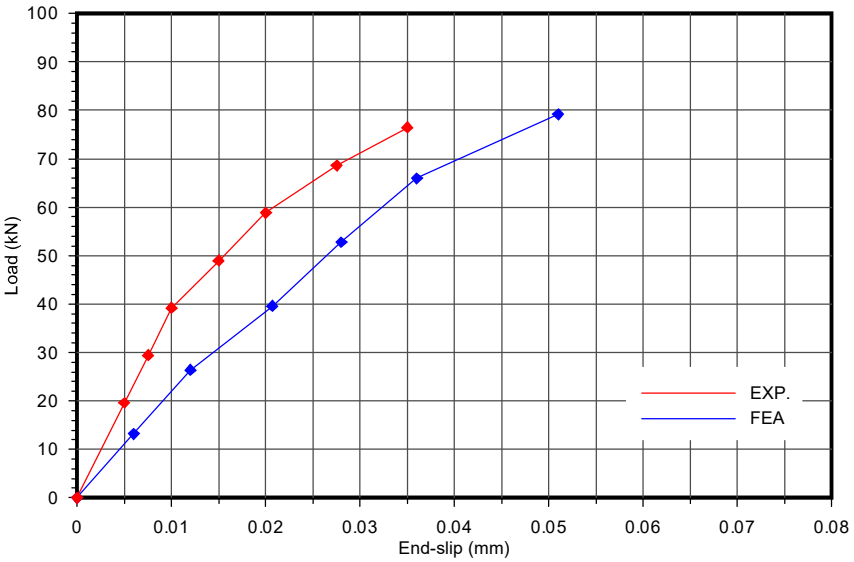

Figure (5-81) Variation of end slip with load for composite beam (S2F1.2)

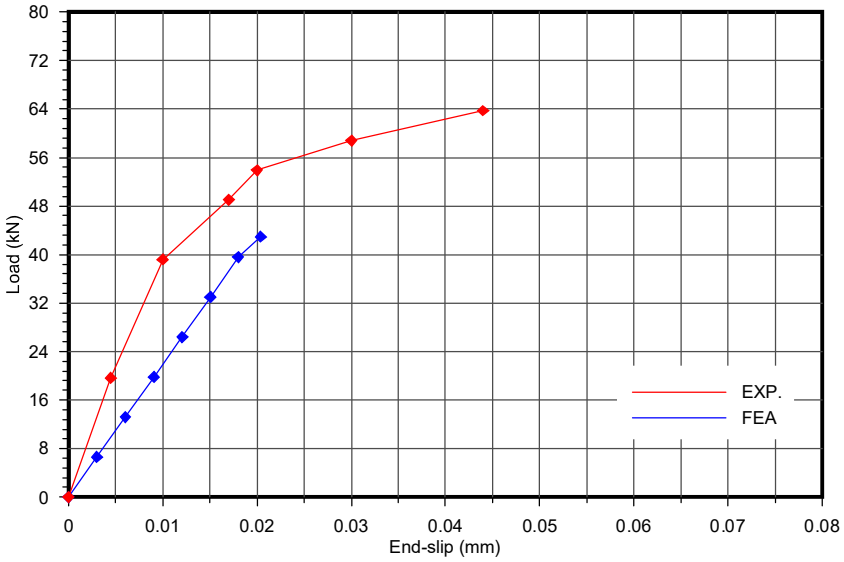

Figure (5-82) Variation of end slip with load for composite beam (S2F2.4)

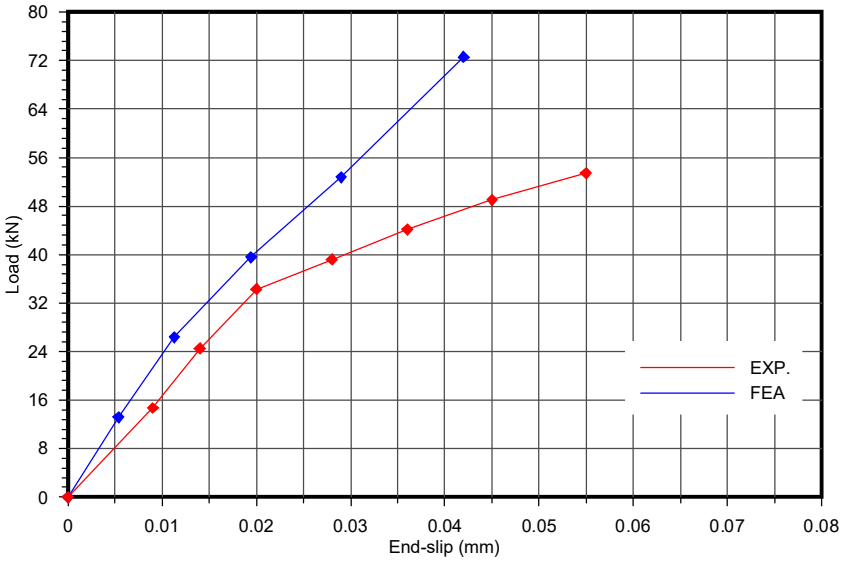

Figure (5-83) Variation of end slip with load for composite beam (S3F1.2)

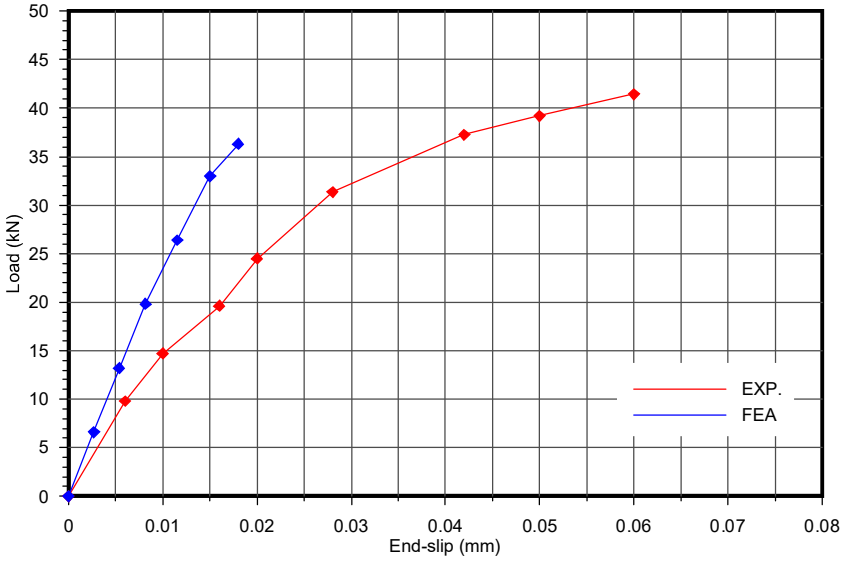

Figure (5-84) Variation of end slip with load for composite beam (S3F2.4)

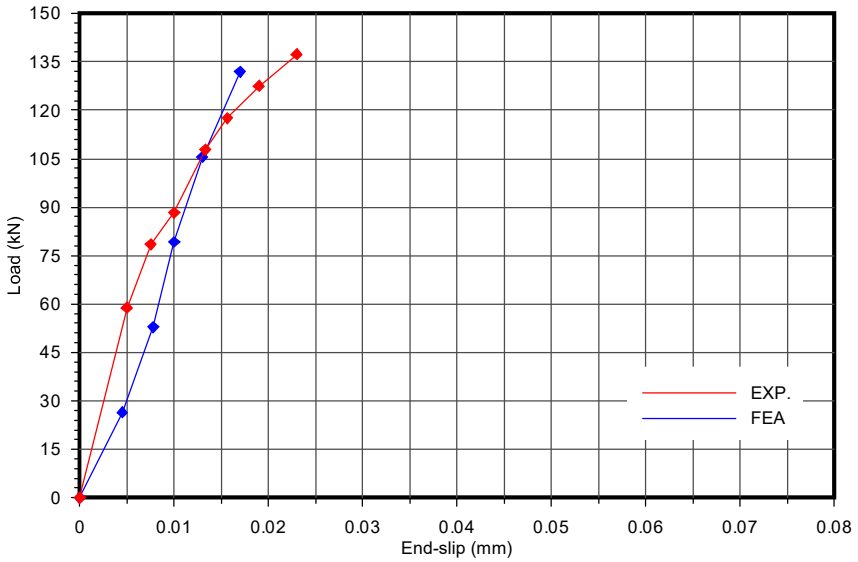

Figure (5-85) Variation of end slip with load for composite beam (S4F1.2)

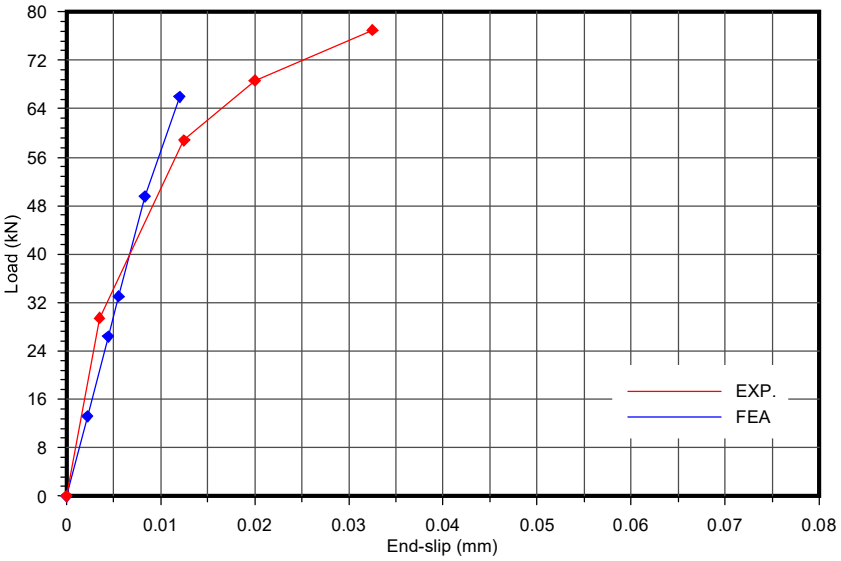

Figure (5-86) Variation of end slip with load for composite beam (S4F2.4)

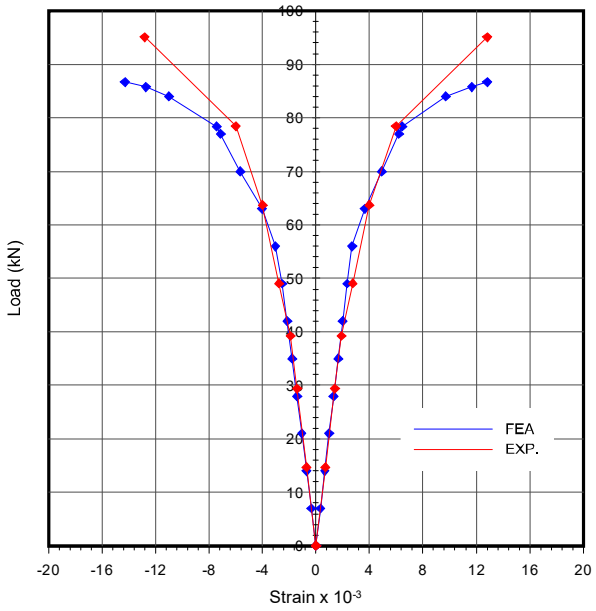

Figure (5-87) Variation of strain distribution with load at midspan for aluminum beam (S1)

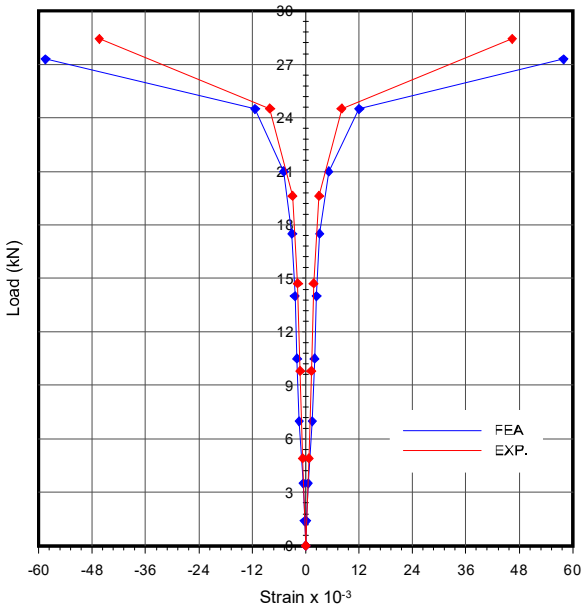

Figure (5-88) Variation of strain distribution with load at midspan for aluminum beam (S2)

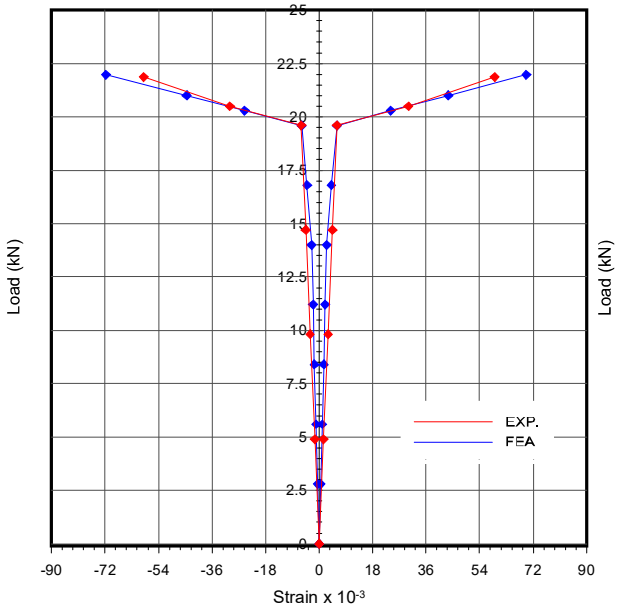

Figure (5-89) Variation of strain distribution with load at midspan for aluminum beam (S3)

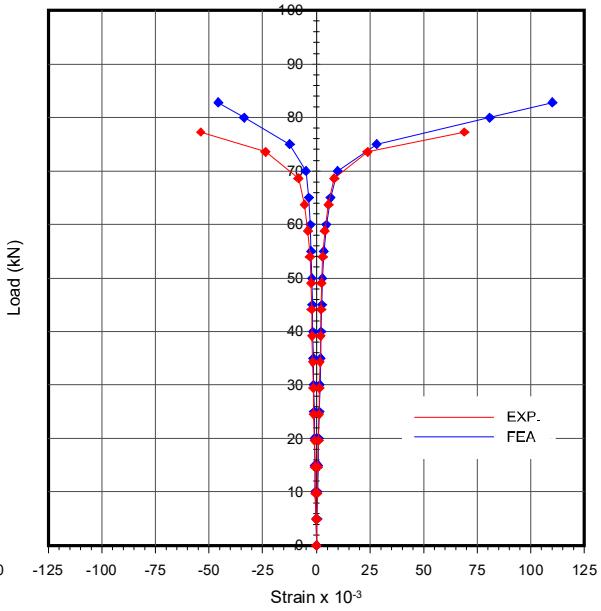

Figure (5-90) Variation of strain distribution with load at midspan for aluminum beam (S4)

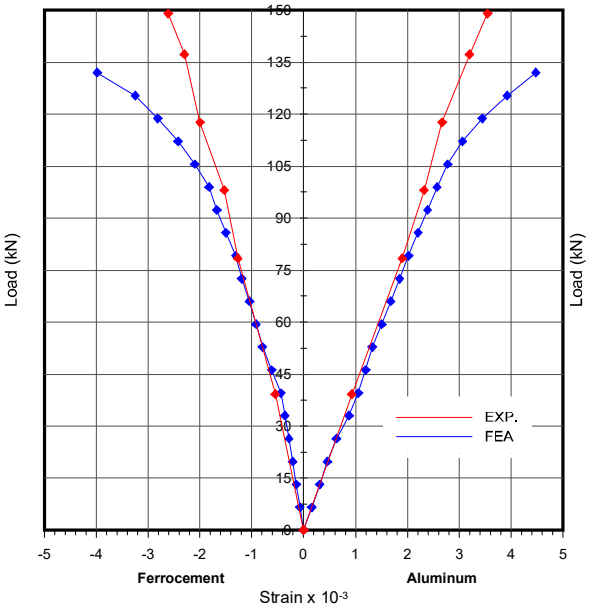

Figure (5-91) Variation of strain distribution with load at midspan for composite beam (S1F1.2)

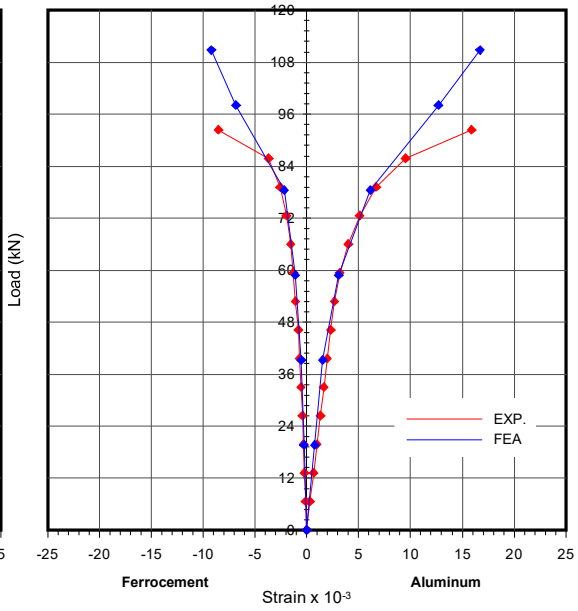

Figure (5-92) Variation of strain distribution with load at midspan for composite beam (S1F2.4)

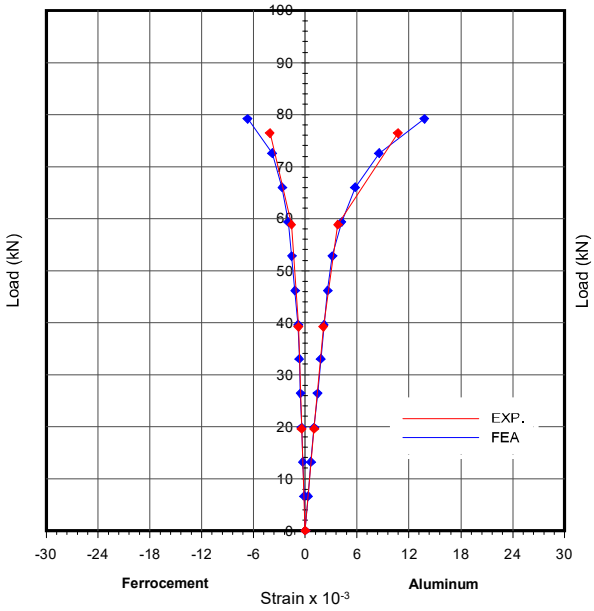

Figure (5-93) Variation of strain distribution with load at midspan for composite beam (S2F1.2)

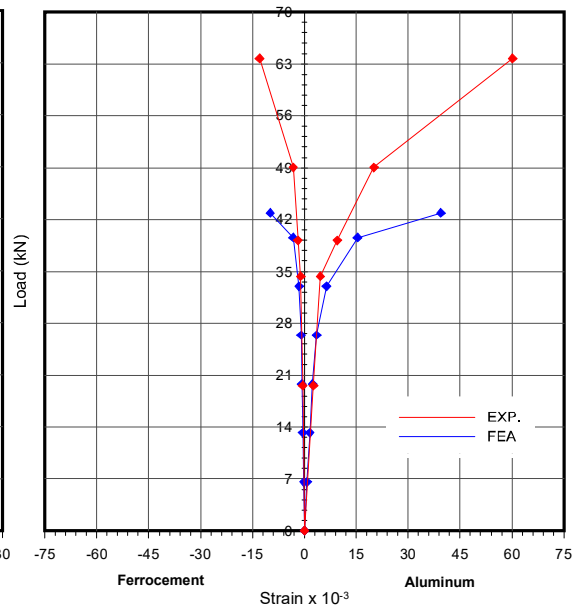

Figure (5-94) Variation of strain distribution with load at midspan for composite beam (S2F2.4)

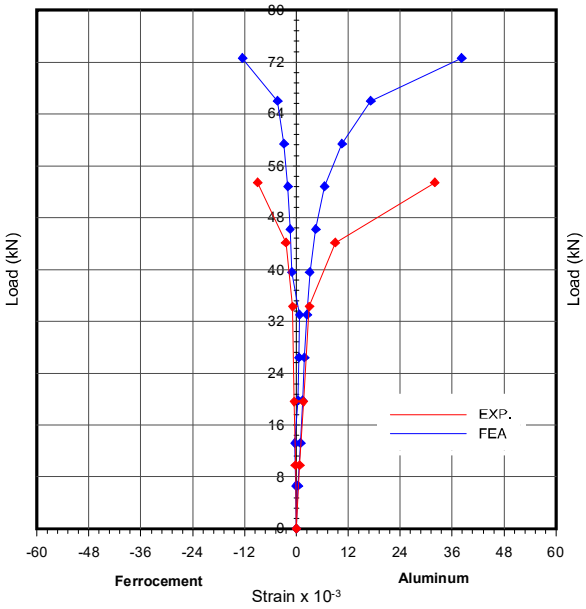

Figure (5-95) Variation of strain distribution with load at midspan for composite beam (S3F1.2)

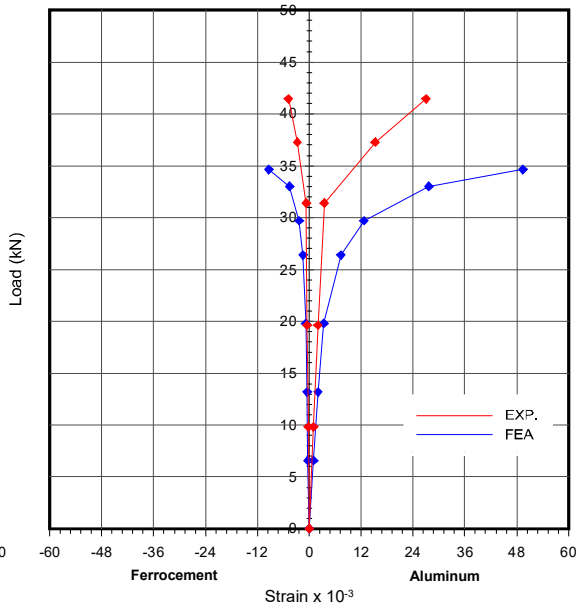

Figure (5-96) Variation of strain distribution with load at midspan for composite beam (S3F2.4)

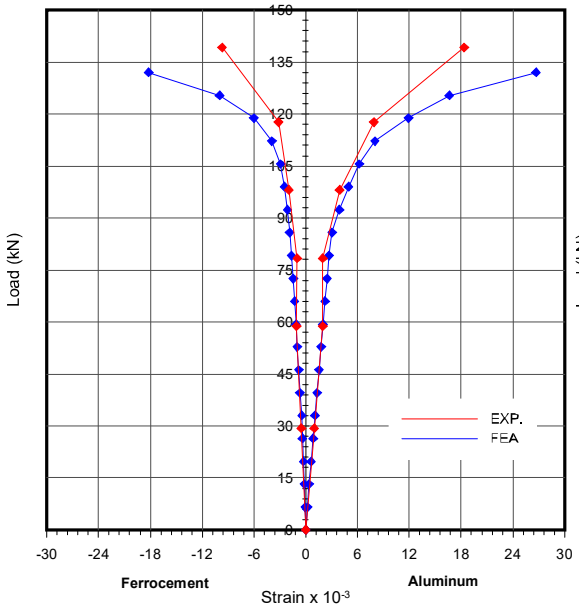

Figure (5-97) Variation of strain distribution with load at midspan for composite beam (S4F1.2)

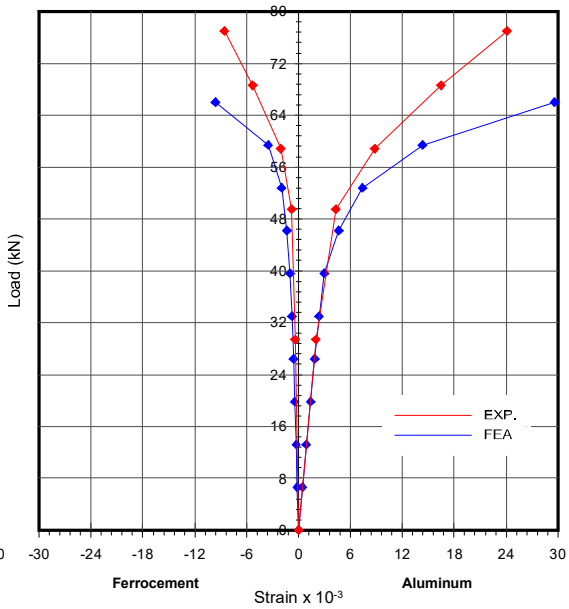

Figure (5-98) Variation of strain distribution with load at midspan for composite beam (S4F2.4)

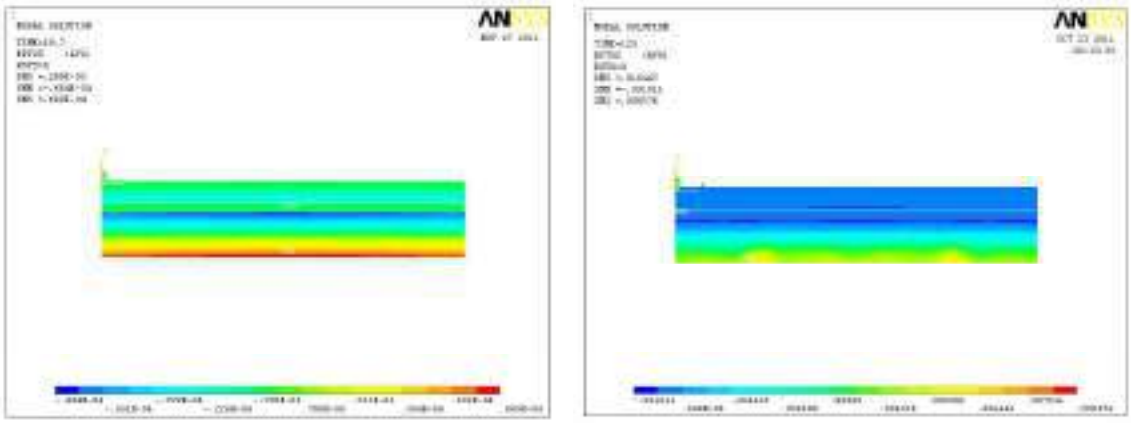

Front view

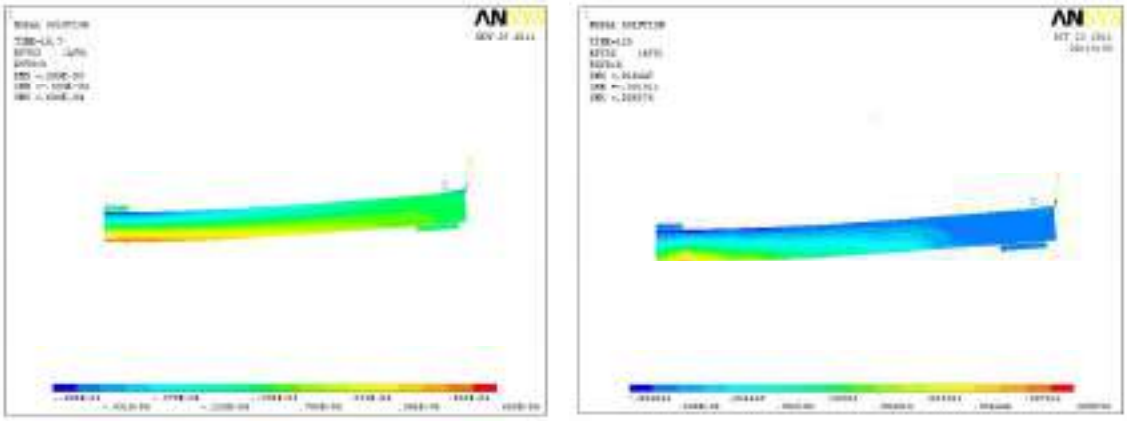

Side view

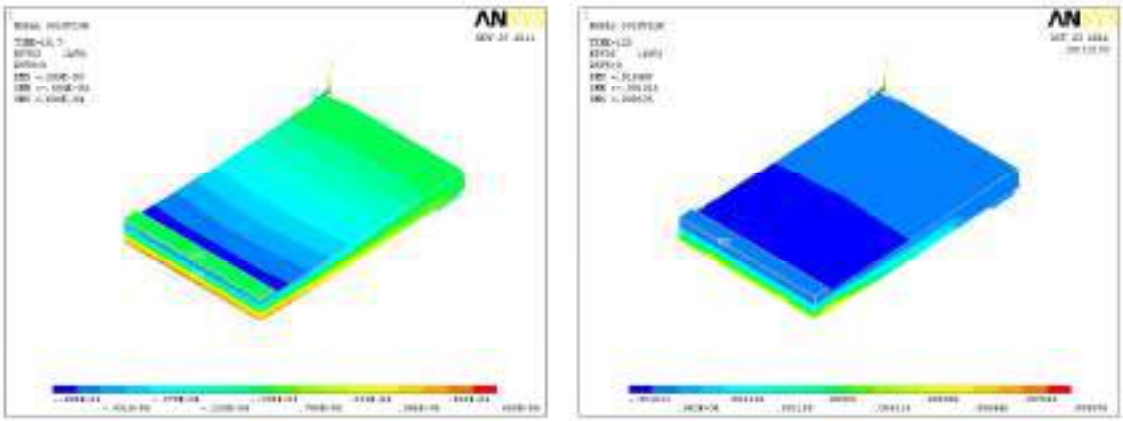

Isometric view

a-Intermediate load at linear stage (1.3 kN) **b-Ultimate load (8.25 kN)**

Figure (5-99) Deformed shapes and contour plots under intermediate load at linear stage and ultimate loads for longitudinal strain distribution of ferrocement slab (F1.2)

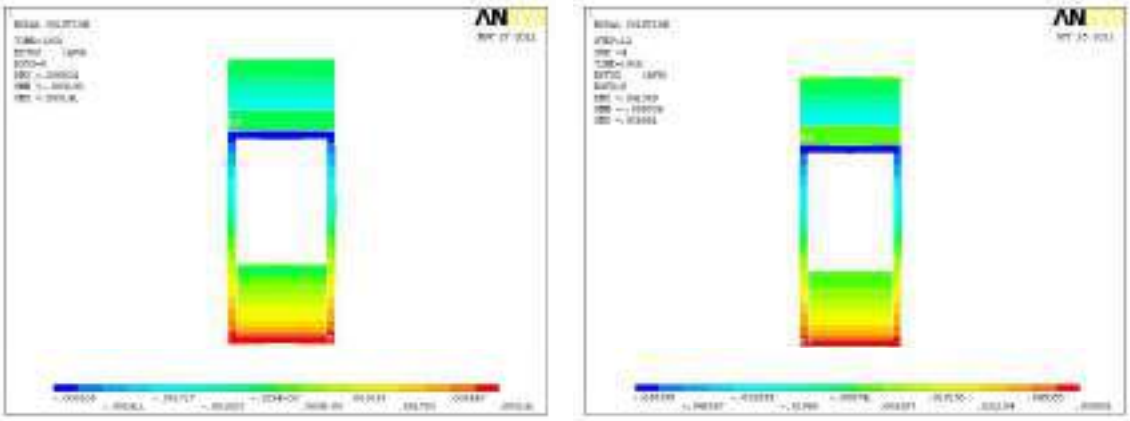

Front view

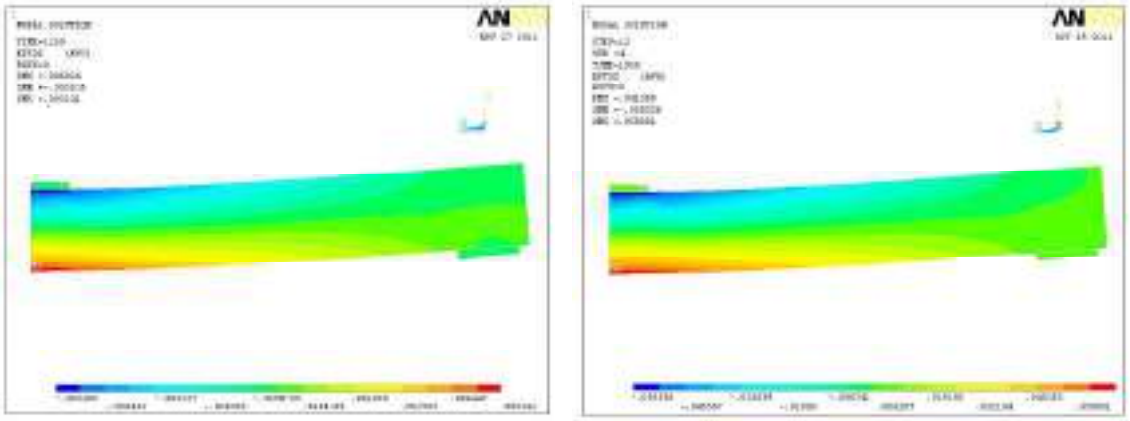

Side view

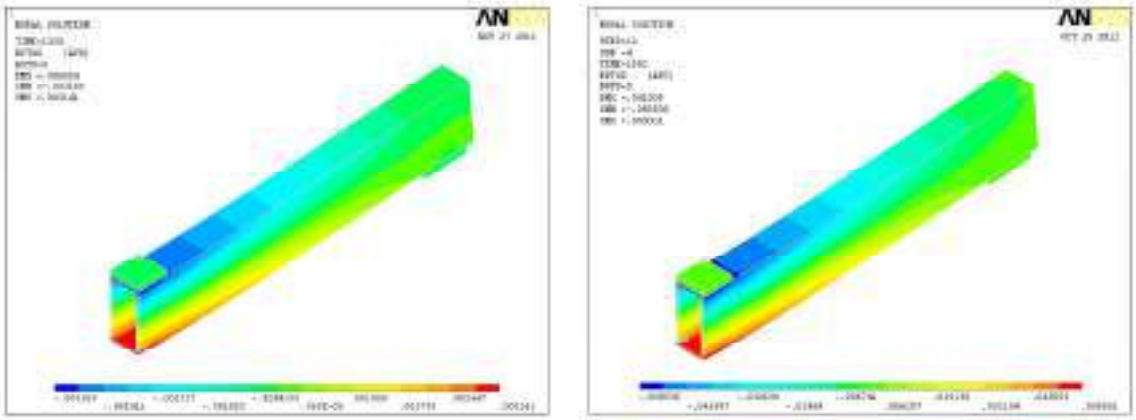

Isometric view

a-Intermediate load at linear stage (17.5 kN) **b-Ultimate load (27.3 kN)**

Figure (5-100) Deformed shapes and contour plots under intermediate load at linear stage and ultimate loads for longitudinal strain distribution of aluminum beam (S2)

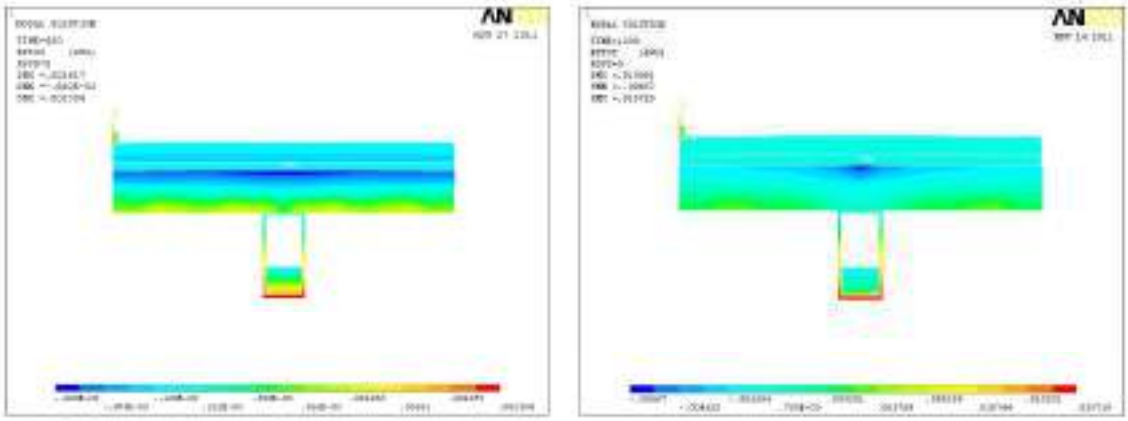

Front view

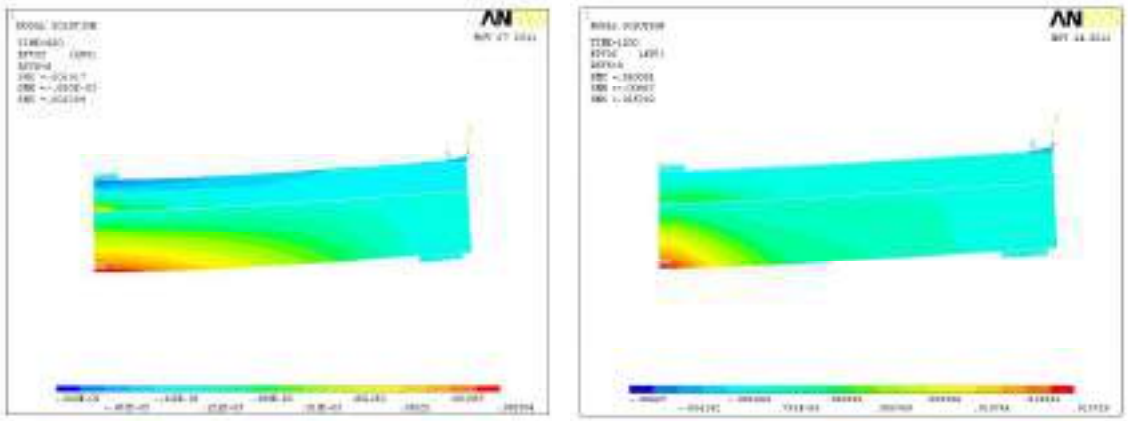

Side view

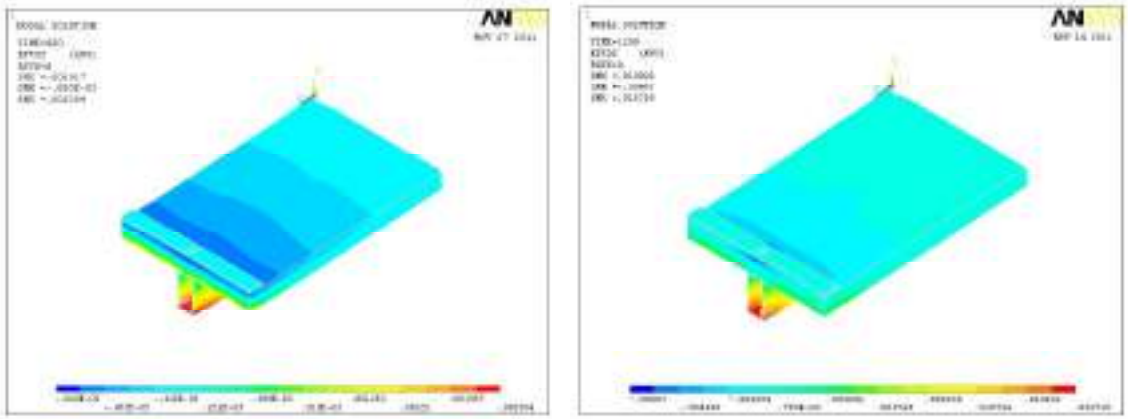

Isometric view

a-Intermediate load at linear stage (39.6kN) **b-Ultimate load (76.49kN)**

Figure (5-101) Deformed shapes and contour plots under intermediate load at linear stage and ultimate loads for longitudinal strain distribution of composite beam (S2F1.2)

5.4 Plastic Analysis

The resistance of studied sections is determined using plastic analysis principles. It is assumed that the strains across the section are sufficiently high that the aluminum stresses are at their yield values throughout the section and that the ferrocement has reached its compression strength. Plastic stress blocks are rectangular, unlike elastic stress blocks which are triangular.

Because a ferrocement section is reinforced with multiple layers of reinforcement, it shows a very ductile behavior and can be assumed to behave as a perfectly plastic material with different properties in compression and in tension. The properties in compression are assumed according to the ACI rectangular stress block [8].

So the compression resistance of the slab is:

$$R_f=0.85\, f'_c\, b_{eff}\, a \qquad (5\text{-}5)$$

where:

R_f is the compression force of ferrocement slab.

f'_c is ferrocement compression strength MPa.

b_{eff} is the effective breadth of the slab.

The behavior of aluminum cross sections and the corresponding idealization to be used in structural analysis shall be related to the capability to reach specified limit states, each of them corresponding to a particular assumption on the state of stress acting on the section referring to the global behavior of a cross section. The following limit states can be define [80]:

1. elastic buckling limit state
2. elastic limit state
3. plastic limit state
4. collapse limit state

Cross sections can be classified according to their capability to reach defined limit states and can be adopted when the section capabilities to get in to plastic range must be specified. Cross sections can be divided as follows:

1. Ductile sections (class1)

2. Compact sections (class 2)
3. Semi compact sections (class3)
4. Slender sections (class 4)

The load capacity of aluminum section can be evaluated with reference to the above mention limit states, The value of axial load for given limit state can be expressed by generalized formula which depends on practical rules.

The tensile resistance of the aluminum section is:

$R_a = \alpha f_{0.2} A_a$ (5-6)

where:

R_a is the tensile force in aluminum section, N.

α is a correction factor depending upon limit state.

$f_{0.2}$ is aluminum yield strength, MPa.

A_a is the net cross section area of aluminum beam, mm^2.

The classification of elements in cross section is linked to value of the slenderness parameter β (b/t) as follows:

1. $\beta \leq \beta_1$:class 1
2. $\beta_1 < \beta \leq \beta_2$:class 2
3. $\beta_2 < \beta \leq \beta_3$:class 3
4. $\beta_3 < \beta$:class4

The value of β_1 , β_2 and β_3 are clearly shown in Euro code 9.

The moment resistance of the cross-section can be evaluated by equating compression and tension across the section, the ferrocement is assumed to resist no tension.

Ferrocement is strong in compression and aluminum is susceptible to buckling in compression. Their respective advantage can be utilized to the fullest extent by making the neutral axis in top flange of aluminum beam or within the slab and avoiding the case of plastic neutral axis within beam web to be in safe side of local buckling of aluminum beam. So when plastic neutral axis in the ferrocement slab as is considered in the current study,

where $R_f \geq R_a$, The moment resistance is:

$M_p=R_a\, h/2+R_f\,[d - a/2]$ (5-7)

where: a is plastic neutral axis.

d is ferrocement slab thickness.

Table (5-17) shows the comparison of plastic analysis results with experimental and finite element results. The plastic analysis is found to give ultimate loads closer to the experimental and finite element analysis values and so it could be used for designing ferrocement aluminum composite beams.

The ratios of experimental to predicted plastic ultimate load are 0.92 to 2.07 with an average value of 1.37 while the ratios of the results of finite element analysis to predicted plastic ultimate loads are 0.82 to 1.19 with average value of 1.23. This finding confirms that the plastic analysis is more conservative to calculate ultimate load.

The plastic analysis results depicted that the ultimate strength capacity of ferrocement aluminum composite beams can be efficiently estimated by using conventional equilibrium procedures and the constitutive laws prescribed by Euro codes and standard tests for the materials.

Table (5-17) Comparison of plastic analysis results with experimental and FEA results for composite sections

No.	Beams designation	Ultimate load (kN)			P_{EXP}/P_P	P_{FEA}/P_P
		Experimental P_{EXP}	FEA P_{FEA}	Plastic analysis P_P		
1	S1F1.2	149.05	132.00	161.21	0.92	0.82
2	S2F1.2	76.49	79.20	64.53	1.19	1.23
3	S3F1.2	53.44	72.60	50.12	1.07	1.45
4	S4F1.2	139.25	132.00	115.58	1.20	1.14
5	S1F2.4	110.81	92.40	77.94	1.42	1.19
6	S2F2.4	63.74	42.90	30.86	2.07	1.39
7	S3F2.4	41.45	34.65	23.97	1.73	1.45
8	S4F2.4	76.98	66.00	55.28	1.39	1.19
Average					1.37	1.23

CHAPTER SIX

CONCLUSIONS AND RECOMMENDATIONS

6.1 Introduction

In this chapter, the conclusions drawn from the test results and theoretical analysis are described and some recommendations for future work are presented.

6.2 Conclusions

The main concluding remarks that have been achieved may be summarized as:

1. Composite ferrocement aluminum beams exhibited high increase of section capacity as compared with aluminum beams. Although the used ferrocement slab is thin (50 mm), and it adds (44 kg/m) for the aluminum beam weight, the overall stiffness and strength of the composite section increase with high ratio. The increase ratio in strength ranges between (1.57) and (2.69).
2. The ferrocement slab with full connection to aluminum beam provided sufficient constrain for the flange of aluminum beam and eliminate aluminum local buckling problem which is a characteristic problem for aluminum beam.
3. There are two signification mode of failure. In composite beams of 2.4 m length, failure is characterized by the crushing of ferrocement in compression zone. Composite beams of 1.2 m length, reveal a spalling mode of failure of ferrocement thin layer at the interface region without any indication of destruction of adhesive epoxy layer.
4. Under serviceability limit state conditions, no cracking is detected during the loading period. After the initiation of flexural cracks, the beams stiffness

reduces and the linear load – deflection behavior vanishes when the internal steel wire mesh begins to yield.

5. The suggested dimensions and properties for push - out tests may be considered as the standard test for adhesive epoxy layer as connectors in ferrocement - aluminum composite beams.
6. The behavior of load - slip relationship for adhesive epoxy layer may be represented by an exponential equation $P = a\ (e^{bS} - 1)$. This relationship different from that suggested for steel concrete composite beams.
7. The adhesive epoxy layer thickness is not effective parameter, as depicted by the push out test. The failure loads are changed from (55.7 kN) to (58.01 kN) as the thickness of the adhesive epoxy layer increased from 3 mm to 6 mm.
8. The hardening time for adhesive epoxy layer is very effective parameter. The full capacity of beams attained after 3 days of epoxy layering.
9. Strains larger than (0.003) are measured at topmost fibers of ferrocement slab. No crushing was observed at strain of (0.003).
10. It can be observed that using Sikadur 31 as adhesive epoxy layer provides adequate bond between the two layers. Measurements also show that the connection could be considered to be perfect as the slip remains very small during the test.
11. Nonlinear finite element solution by (ANSYS version 11.0) package program using three dimensional elements for modeling the ferrocement aluminum composite beam gives acceptable agreement with the experimental results for the load-deflection relationships.
12. Simulation of adhesive epoxy layer with linear spring COMPIN14 element is efficient and gives close results to experimental ones as well as less solution iterations and so less solution time.
13. Theoretical and experimental investigation gives small slip values for tested composite beams and it seems good to consider the used adhesive epoxy

layer as a stiff shear connection as compared with classical connectors used in composite beam.

14. The plastic analysis results depicted that the ultimate strength capacity of ferrocement aluminum composite beams can be conservatively estimated by using conventional equilibrium procedures and the constitutive laws prescribed by Euro codes and standard tests for the materials.

6.3 Recommendations for Future Work

Based on this work, the following suggestions are put forward:

1. Further testing is recommended to evaluate the effect of other parameters on the strength of ferrocement – aluminum composite beams, such as influence of other ferrocement matrix strengths, ferrocement slab depth, and volume fraction ratio of mesh reinforcement.
2. The effect of shear lag at interface region between ferrocement slab and aluminum beam may be included.
3. Experimental and theoretical studies for the fatigue problem in ferrocement - aluminum composite beam are required as aluminum is more prone to this problem than steel [5].
4. Other types of epoxy may be investigated.

References

1- Bouazaouia L., Jurkiewiezb B., Delmasa Y., and Lia A., "Static Behavior of A Full-Scale Steel - Concrete Beam with Epoxy-Bonding Connection", Journal of Engineering Structures, Vol. 30, February 2008, pp. 1981-1990.

2- Johnson, R. P., "Composite structures of steel and concrete, Vol. 1, Beams, Columns, Frames, Applications in Building", Crosby.

3- Davies and Roberts, "Resistance of Welded Aluminum alloy Plate Girders to Shear and Patch Loading", Journal of Structural Engineering, Vol. 125, No. 8, August 1999, pp. 930-931.

4- Paul, B.K., and Pama, R.P., "Ferrocement", International Ferrocement Information Center, IFC Pub., August 1978.

5- John Dwight, "Aluminum Design and Construction", First published, University of Cambridge, London, 1999.

6- Soetens, and Mennink "Aluminum Building and Civil Engineering Structure", Fourth International Conference on Steel and Aluminum Structures – Light Weight steel and aluminum structures, Department of Civil & Environmental Engineering, Helsinki University of Technology, Finland, June 1999, pp. 487-494.

7- Federico M. Mazzolani, "Aluminum Alloy Structures", Second edition, University of Naples, Italy, 1995.

8- Federico M. Mazzolani, "The Structural use of Aluminum: Design and Application", Fourth International Conference on Steel and Aluminum Structures – Light Weight steel and aluminum structures, pp. 475-486, Department of Civil & Environmental Engineering, Helsinki University of Technology, Finland, June 1999.

9- Antoine E. Naaman, "Ferrocement and laminated cementitious composites", Second edition, University of Michigan, Michigan, 2000.

10- Abdul Karim A.K. "Behavior of Ferrocement Beams under Pure Torsion", Ph.D. Thesis, University of Technology, Building and Construction Department, Baghdad, Iraq, June, 2005.

11- Brown and Evans, "Theoretical and Experimental Investigation of the Collapse Behavior of Transversely Stiffened Aluminum Alloy Plate Girders", Journal of Thin- Walled Structures, Vol.18 ,1994, pp. 225-246.

12- Landolfo and Mazzolani, "Different Approaches in the Design of Slender Aluminum Alloy Sections" , Journal of Thin- Walled Structures, Vol. 27, No. I, 1997, pp. 85-102.

13- Mazzolani and Piluso, "Prediction of the Rotation Capacity of Aluminum Alloy Beams", Journal of Thin- Walled Structures, Vol. 27, No. I, 1997, pp. 103-116.

14- Moen, Hopperstad, and Langseth, "Rotitional Capacity of Aluminum Beams under Moment Gradient, I:Experiments", ASCE, Journal of Structural Engineering, Vol. 125, No. 8, August, 1999.

15- Matteis, Moen, Langseth, Landolfo, Hopperstad, and Mazzolani, "Cross-Sectional Classification for Aluminum Beams - parametric Study", Journal of Structural Engineering, Vol. 127, No. 3, March, 2001, pp. 271-279.

16- Matteis, Landolfo, Manganiello, and Mazzolani, "Inelastic Behavior of I-Shaped Aluminum Beams: Numerical Analysis And Cross-Sectional Classification", Journal of Computers and Structures, Vol. 82 , August 2004, pp. 2157–2171.

17- Ji-Hua Zhu1 and Ben Young, "Experimental Investigation of Aluminum Alloy Thin-Walled Tubular Members in Combined Compression and Bending", Journal of Structural Engineering, Vol. 132, No. 12, December 2006, pp.1955-1966.

18- Manganielloa, Matteisb, and Landolfoa, "Inelastic Flexural Strength of Aluminum Alloys Structures", Journal of Engineering Structures, Vol. 28 , 2006, pp. 593–608.

19- Cheng Ming, Shi Yongjiu and Wang Yuanqing, "Inelastic Deformation Analysis of Aluminum Bending Members", Tsinghua Science and Technology , Vol. 11, No. 6, December 2006, pp648-656.

20- Koltsakis and Preftitsi, "Numerical Investigation of The Plastic Behavior of Short Welded Aluminum Double-T Beams", Journal of Engineering Structures, Vol. 30, 2008, pp.2022–2031.

21- Wanga, Hopperstada, Lademoa and Larsen, "Finite Element Modeling of Welded Aluminum Members Subjected to Four-Point Bending", Journal of Thin-Walled Structures, Vol. 45, 2007, pp. 307–320.

22- Ben Young, Feng Zhou, "Aluminum Tubular Sections Subjected to Web Crippling - Part II: Proposed Design Equations", Journal of Thin-Walled Structures, Vol. 46, 2008, pp. 352-361.

23- Bambach, "Behavior and Design of Aluminum Hollow Sections Subjected to Transverse Blast Loads", Journal of Thin-Walled Structures, Vol. 46, 2008, pp. 1370-1381.

24- Feng Zhou, Ben Young, and Xiao Ling Zhao, "Tests and Design of Aluminum Tubular Sections Subjected to Concentrated Bearing Load", Journal of Structural Engineering, Vol. 135, No. 7, July 2009, pp. 806-817.

25- Ji-Hua Zhu1 and Ben Young, "Design of Aluminum Alloy Flexural Members Using Direct Strength Method", ASCE, Journal of Structural Engineering, Vol. 135, No. 5, May 1, 2009. pp. 558-566.

26- Roa, A. K., and Gowder, C. K., " A Study of The Behavior of Ferrocement in Flexure", Indian Concrete Journal, April 1971, pp. 178-183.

27- Lee, S. L., Raisnghani, M., and Pama, R. P., "Mechanical Properties of Ferrocement", FAO Seminar on the Design and Construction of Ferrocement Vessels, October 1972.

28- Alwash, A. S., "Flexural Characteristics of Ferrocement", MS.C. Thesis, University of Baghdad, Iraq, June 1974.

29- Balaguru P. N., Naaman, A.E and Shah, S. P., "Analysis and Behavior of Ferrocement in Flexure", ASCE ,October 1977, pp. 1937-1951.

30- Fernandes. R., Goplaratnam. V. S., and Nimityongskul. p., "Evaluation of Ferrocement Folded-Plate Roofing Panels", Journal of Ferrocement, Vol. 10, No. 2, April 1980, pp. 69-88.

31- Paramasivam P., Mansur M.S., and Ong K.C., "Flexural Behavior of Light-Weight Ferrocement Slabs", Journal of Ferrocement, Vol.15, No.1, January 1985, pp. 25-33.

32- Mansur M.A., "Ultimate Strength Design of Ferrocement in Flexure", Journal of Ferrocement, Vol.18, No.4, October 1988, pp. 385-395.

33- Al Salihi M.Z., and Al-Rifaie W.N., "Design of Ferrocement in Flexure", Eng. and Technology, University of Technology, Baghdad, Vol. 18, No. 4, 1999.

34- Basunbul, Mohammed Saleem and A1-Sulaimani, "Flexural Behavior of Ferrocement Sandwich Panels", Journal of Cement &Concrete Composites, Vol. 13, January 1991, pp. 21-28

35- Shuxin Wang, Antoine E. Naaman and Victor C. Li, "Bending Response of Hybird Ferrocement Plates with Meshes and Fibers", Department of civil engineer, University of Michigan Ann Arbor, Michigan.

36- Nassif, H.H. and Najm, H., "Experimental and Analytical Investigation of Ferrocement-Concrete Composite Beams", Cement and Concrete Composites, Vol. 26, 2004, pp. 787-796.

37- Hago A.W. Al- Jabri, K.S., Alnuaimi, A.S., Al-Moqbali, H. and Al-Kubaisy, M.A., "Ultimate and Service Behavior of Ferrocement Roof Slab Panels", Construction and Building Materials, Vol. 19, 2005, pp.31-37.

38- Rao, T. C, Rao, T. D. G. and Rao, N. V. R., "An Experimental Study on Ferrocement Channel Units Under Flexural Loading", International Journal of Mechanics and Solids ISSN 0973-1881 Vol. 3, No. 2, 2008, pp. 195-203.

39- Boshra Aboul-Anen, Ahmed El-Shafey, and Mostafa El-Shami, "Experimental and Analytical Model of Ferrocement Slabs", International Journal of Recent Trends in Engineering, Vol. 1, No. 6, May 2009, pp. 25-29.

40- Ahmed Ibrahim Khalil Al-Hamada, "Fracture Resistance of Ferrocement Flexural Members", M.Sc. Thesis, University of Basrah, Iraq, 2010.

41- Chapman, J. C. and Balakrishnan, S., "Experiments on Composite Beams", The Structural Engineer, Vol. 42, No. 11, Nov. 1964, pp. 369-383.

42- Pincus, G., “Bonded Wood - Concrete T - Beams”, ASCE, Journal of Structural Division, Vol. 95, 1969, pp. 2265-2279.

43- Hirst, M. J. S. and Yeo, M. F., "The Analysis of Composite Beams Using Standard Finite Element Programs", Journal of Computers and Structures, Vol. 11, 1980, pp. 233-237.

44- Saadatmanesh, Hamid, Albrecht, Pedro, and Ayyub, Bilal M., "Experimental Study of Prestressed Composite Beams", Journal of Structural Engineering, Vol. 115, No. 9, September 1989, pp. 2348-2381.

45- Jasim, Nabeel Abdulrazzage and Mohamad Ali, A. A., "Deflections of Composite Beams with Partial Shear Connection", The Structural Engineer, Vol. 75, No.4, February 1997, pp. 58-161.

46- Jasim, Nabeel Abdulrazzage and Karim, Abdul Ameer Atalla, "A Simplified Method for Determining the Deflections of Partially Composite Beams", Fifth Basrah Engineering conference, March 10-11, 1999.

47- Baskar and Shanmugam, "Steel - Concrete Composite Plate Girders Subject to Combined Shear and Bending", Journal of Constructional Steel Research, Vol. 59, 2003, pp. 531–557.

48- Qing Quan Liang, Brian Uy, Mark A. Bradford and Hamid R. Ronagh, "Strength Analysis of Steel-Concrete Composite Beams in Combined Bending and Shear", Journal of Structural Engineering, Vol. 131, No. 10, October 2005, pp. 1593-1600.

49- Brunner, Romer, and Schnuriger, "Timber – Concrete Composite with An Adhesive Connector (Wet on Wet Process)", Journal of Materials and Structures, Vol. 40, 2007, pp.119–126.

50- Abdulnasser Mohammed Abbas, "Experimental and Numerical Investigation of Simply Supported Concrete - Steel Composite Beams", Ph. D. Thesis, University of Basrah, Iraq, 2007.

51- Ihab Sabri Salih, "Experimental and Theoretical Investigation in to The Structural Behavior of Timber - Concrete Composite Beams", Ph. D. Thesis, University of Basrah, Iraq, 2010.

52- Triantafillou, Kim and Meier, "Optimization of Hybrid Aluminum / CFRP Box Beams ", Int. J. Mech. Vol, 33, No. 9, 1991, pp. 729-739.

53- Taylor, Macadonald and Rhodes, "The Design Analysis of Light Structures with Combined Aluminum - Steel Sections", Journal of Thin- Walled Structures, Vol. 30, Nos. 1-4, 1998, pp. 111-133.

54- Randolph K. and Robert L. Ferry, "Aluminum structures; A Guide to Their Specifications and Design", Second edition, New York, 2002.

55- American Society of Testing and Material (ASTM) (2003). " Standard: Test Methods of Tension Testing Wrought and Cast Aluminum- and Magnesium-Alloy Products". ASTM B557M, West Conshohocken, PA.

56- American Society of Testing and Material (ASTM) (2003). " Standard Test Methods for Chemical Analysis of Aluminum and Aluminum-Base Alloys ". ASTM E-34, West Conshohocken, PA.

57- Paul, B.K., and Pama, R.P., "Ferrocement", International Ferrocement Information Center, IFIC Pub., August 1978.

58- American Society of Testing and Material (ASTM) (2003). "Standard Test Method for Time of Setting of Hydraulic Cement by Vicat Needle". ASTM C-191, West Conshohocken, PA.

59- American Society of Testing and Material (ASTM) (2003). "Standard Test Method for Compressive Strength of Hydraulic Cement Mortars". ASTM C - 109, West Conshohocken, PA.

60- Iraqi Standard (I.O.S. 5/1984).

61- American Society of Testing and Material (ASTM) (2003). "Standard Test Method for Sieve Analysis of Fine and Coarse Aggregates". ASTM C-136, West Conshohocken, PA.

62- Iraqi Standard (I.O.S. 45/1984).

63- ACI Committee 549, "Guide for the Design, Construction, and Repair of Ferrocement", ACI 549.1R-93.

64- American Society of Testing and Material (ASTM) (2003). " Standard Practice for Mechanical Mixing of Hydraulic Cement Pastes and Mortars of Plastic Consistency ". ASTM C-305, West Conshohocken, PA.

65- British Standard Institute, "Method of Testing Concrete", Part 118, BS - 1881, 1983.

66- American Society of Testing and Material (ASTM) (2003). "Standard Specification for Epoxy-Resin-Base Bonding Systems for Concrete". ASTM C - 881, West Conshohocken, PA.

67- Product Data Sheet 2003-07 "Sikadur 31" Thixotropic Epoxy Resin Adhesive.

68- Hinton, E. and Owen, D. R. J., "Finite element Programming", Academic Press Inc. Ltd., London, 1977.

69- Hinton, E. and Owen, D. R. J., "An introduction to finite element computations", Pine ridge Press limited, Swansea, U. K., 1979.

70- Zienkiewicz, O. C., "The Finite Element Method", Third edition, McGraw-Hill Book Company, New York, 1977.

71- Desayi, P., and Krishnan, S., "Equation for the Stress-Strain Curve of Concrete", Journal of the American Concrete Institute, 61, March 1964, pp.345-350.

72- Cervera and Hinton, "Non-Linear Analysis of Reinforced Concrete Plates and Shells Using a Three Dimensional Model", In the Computational Modelling of Reinforced Concrete Structures,Eds. Hinton, E. and Owen, R., Pineridge Press, Swansea, U. K., 1986, PP. 327-370.

73- ANSYS, 2011, "ANSYS Help", Release 11.0.

74- Willam, K. J. and Warnke, E. P., "Constitutive Model for the Triaxial Behavior of Concrete", Proceedings, International Association for Bridge and Structural Engineering, Vol. 19, ISMES, Bergamo, Italy, 1975, pp.174.

75- Al-Shaarbaf, I. A. S., "Three-Dimensional Non-Linear Finite Element Analysis of Reinforced Concrete Beams in Torsion", Ph.D. Thesis University of Bradford, U.K., 1990. 316^{pp}..

76- ANSYS, "Analysis Guide", Version 11, Swanson Analysis System, Inc., 2007.

77- Yam, L. C. P. and Chapman, J. C., "The inelastic behaviour of simply supported composite beams of steel and concrete", Proc. Instn. Civ. Engrs, Vol. 41, 1968, pp. 651-683.

78- Gelfi and Giuriani, "Influence of Slab - Beam Slip on the Deflection of Composite Beams", International Journal for Restoration of Buildings and Monuments, Vol. 9, No. 5, p.p. 475-490 (2003).

79- Aussi A. N., "Presstressed Fiber Reinforced Polymer (FRP) for Strengthening of Concrete Members", Ph.D thesis, University of Baghdad, College of Engineering, Civil Engineering department,2009.

80- Eurocode 9. "Design of aluminium structures", Part 1-1: General structural rules. European Committee for Standardisation; 1999.

Appendix A

The Aluminum Association's designation system for aluminum alloys was introduced in 1954. Under this system, a four-digit number is assigned to each alloy registered with the Association. The first number of the alloy designates the primary alloying element, which produces a group of alloys with similar properties. The Association sequentially assigns the last two digits.

The second digit denotes a modification of an alloy. For example, 6463 is a modification of 6063 with slightly more restrictive limits on certain alloying elements, such as iron, manganese, and chromium, to obtain better finishing characteristics. The primary alloying elements and the properties of the resulting alloys are listed below and summarized in Table (A1):

1xxx: This series is for *commercially pure aluminum,* defined in the industry as being at least 99% aluminum. Alloy numbers are assigned within the 1xxx series for variations in purity and which elements compose the impurities; the main ones are iron and silicon. The primary uses for alloys of this series are electrical conductors and chemical storage or processing because the best properties of the alloys of this series are electrical conductivity and corrosion resistance. The last two digits of the alloy number denote the two digits to the right of the decimal point of the percentage of the material that is aluminum. For example, 1060 denotes an alloy that is 99.60% aluminum.

2xxx: The primary alloying element for this group is *copper*, which produces high strength but reduced corrosion resistance. These alloys were among the first aluminum alloys developed and were originally called *duralumin.*

Alloy 2024 is, perhaps, the best known and most widely used alloy in aircraft. Most aluminum-copper alloys fell out of favor, though, because they

demonstrated inadequate corrosion resistance when exposed to the weather without protective coatings and are difficult to weld.

3xxx: *Manganese* is the main alloying element for the 3xxx series, increasing the strength of unalloyed aluminum by about 20%. The corrosion resistance and workability of alloys in this group, which primarily consists of alloys 3003, 3004, and 3105, are good. The 3xxx series alloys are well suited to architectural products, such as rain-carrying goods and roofing and siding.

Table A1 Wrought alloy designation system and characteristics

Series Number	Primary Alloying Element	Relative Corrosion Resistance	Relative Strength	Heat Treatment
1xxx	none	excellent	fair	non-heat-treatable
2xxx	copper	fair	excellent	heat-treatable
3xxx	manganese	good	fair	non-heat treatable
4xxx	silicon	—	—	varies by alloy
5xxx	magnesium	good	good	non-heat-treatable
6xxx	magnesium and silicon	good	good	heat-treatable
7xxx	zinc	fair	excellent	heat-treatable

4xxx: *Silicon* is added to alloys of the 4xxx series to reduce the melting point for welding and brazing applications. Silicon also provides good flow characteristics, which in the case of forgings provide more complete filling of complex die shapes. Alloy 4043 is commonly used for weld filler wire.

5xxx: The 5xxx series is produced by adding *magnesium*, resulting in strong, corrosion resistant, high welded strength alloys. Alloys of this group are used in ship hulls and other marine applications, weld wire, and welded storage vessels. The strength of alloys in this series is directly proportional to the magnesium content, which ranges up to about 6%.

6xxx: Alloys in this group contain *magnesium* and *silicon* in proportions that form magnesium silicide (Mg*2*Si). These alloys have a good balance of corrosion resistance and strength. 6061 is one of the most popular of all aluminum alloys and has a yield strength comparable to mild carbon steel. The

6xxx series alloys are also very readily extruded, so they constitute the majority of extrusions produced and are used extensively in building, construction, and other structural applications.

7xxx: The primary alloying element of this series is *zinc*. The 7xxx series includes two types of alloys: the aluminum-zinc-magnesium alloys, such as 7005, and the aluminum-zinc-magnesium-copper alloys, such as 7075 and 7178. The alloys of this group include the strongest aluminum alloy, 7178, which has a minimum tensile ultimate strength of 84 ksi [580 MPa] in the T6 temper, and are used in aircraft frames and structural components. The corrosion resistance of those 7xxx series alloys alloyed with copper is less, however, than the 1xxx, 3xxx, 5xxx, and 6xxx series, while the corrosion resistance of the 7xxx alloys alloyed without copper is fairly good. Some 7xxx alloys without copper, such as 7008 and 7072, are used as cladding to cathodically protect less corrosion resistant alloys.

8xxx: The 8xxx series is reserved for alloying elements other than those used for series 2xxx through 7xxx. *Iron* and *nickel* are used to increase strength without significant loss in electrical conductivity, and so are useful in such conductor alloys as 8017. Aluminum-lithium alloy 8090, which has exceptionally high strength and stiffness, was developed for aerospace applications.

9xxx: This series is not currently used.

Appendix B

Samples of finite element programs edited by Ansys version 11.0:

- Ferrocement slab, F1.2

```
Finish
/clear
/com                                    Ferrocement slab F1.2
/FILNAM,F1.2
/PREP7
/unit,si
ET,1,solid65                            !Ferrocement
KEYOPT,1,1,0
KEYOPT,1,3,2
KEYOPT,1,5,0
KEYOPT,1,6,0
KEYOPT,1,7,1
KEYOPT,1,8,0
ET,2,solid45
ET,4,inter205
R,1,2,0.00651,90,90,2,0.00651,
RMORE,0,90, , , , ,
R,2
R,3   !for epoxy
Mp,EX,1,28.975E9
MP,DENS,1,2200
MP,PRXY,1,0.15
!TBDE,CONC,1,,,
TB,CONC,1,1,9,
TBTEMP,0
TBDATA,,0.2,0.7,4e6,-1,,
TBDATA,,,,,,,
TB,mela,1,1,12,
TBPT,,0,0
TBPT,,0.0002,5795000
TBPT,,0.00041,11878930
TBPT,,0.0005,13983000
TBPT,,0.00075,20083000
TBPT,,0.001,25282000
TBPT,,0.00125,29516000
TBPT,,0.0015,32725000
TBPT,,0.00175,35064000
TBPT,,0.002,36606000
TBPT,,0.00225,37529000
TBPT,,0.0025,37923000
TBPT,,0.003,38000000
TBPLOT,mela,1
Mp,EX,2,88E9
MP,DENS,2,7800
MP,PRXY,2,0.3
Mp,EX,3,88E9
MP,DENS,3,7800
MP,PRXY,3,0.3
TB,BISO,2,1,2,
TBTEMP,0
TBDATA,,400e6,0,,,,
TBPLOT,BISO,2
GMAX = 0.001
TNMAX = 38e6
TB,CZM,8,,,EXPO
TBDATA,1,TNMAX,GMAX,0.1
MP,EX,6,200E12                          !Loading plate
MP,DENS,6,100
MP,PRXY,6,0.35
n,1
ngen,33,1,1,,,0.0125
ngen,5,100,1,33,,,-0.0125
ngen,2,1000,1,433,,,,0.015
ngen,3,1000,1001,1433,,,,0.035
```

```
ngen,20,1000,3001,3433,,,,0.025
ngen,3,1000,22001,22433,,,,0.020
type,1
Real,1
Mat,1
e,102,2,1,101,1102,1002,1001,1101
egen,32,1,1,,,,,,,,0.0125
egen,4,100,1,32,,,,,,,,-0.0125
egen,24,1000,1,128              !generation all elem. from all type in z direction
!Rigid supporting plate
n,60000,0,-0.06,0.015
ngen,33,1,60000,,,0.0125
ngen,3,1000,60000,60032,,,,0.035
type,2
Real,2
Mat,6
e,60001,61001,61000,60000,1402,2402,2401,1401
egen,32,1,3073,,,,,,,,0.0125
egen,2,1000,3073,3104,,,,,,,,0.035
!Rigid loading plate
n,70000,0,0,0.56
ngen,33,1,70000,,,0.0125
ngen,3,1000,70000,70033,,,,0.02
type,4
Real,2
Mat,8
e,22002,23002,23001,22001,70001,71001,71000,70000
egen,32,1,3137,,,,,,,,0.0125
egen,2,1000,3137,3168,,,,,,,,0.02
n,80000,0,0.01,0.56
ngen,33,1,80000,,,0.0125
ngen,3,1000,80000,80033,,,,0.02
type,2
Real,2
Mat,6
e,70001,80001,80000,70000,71001,81001,81000,71000
egen,32,1,3201,,,,,,,,0.0125
egen,2,1000,3201,3232
ANTYPE,STATIC
NROPT,full,,OFF            ! USE FULL NEWTON-RAPHSON WITHOUT ADAPTIVE DESCENT
D,61000,UX,0,,61032,1,UY
nsel,s,loc,z,0.6
Dsym,SYMM,Z
D,24001,Uz,0,,24033,1
D,24101,Uz,0,,24133,1
D,24201,Uz,0,,24233,1
D,24301,Uz,0,,24333,1
D,24401,Uz,0,,24433,1
nsel,all
!SFE,553,3,PRES, ,1481482
/SOLU
NROPT,full,,OFF
CNVTOL,F,,0.005,1,-1
LSWRITE,1,
Time,50
NEQIT,100
AUTOTS,1
OUTRES,,1                    ! WRITE SOLUTION ON RESULTS FILE FOR EVERY SUBSTEP
F,82000,FY,-10,,82032,1
F,81000,FY,-20,,81032,1
F,80000,FY,-20,,80032,1
NSUBST,5,10,2
solve
save
Finish
/FILNAM,F1.2
                                  ! CONTINUE WITH FILES NAMED F1.2
/SOLU
ANTYPE,,REST
LSWRITE,2,
Time,100
NEQIT,100
```

```
AUTOTS,1
OUTRES,,2
F,82000,FY,-20,,82032,1
F,81000,FY,-40,,81032,1
F,80000,FY,-40,,80032,1
NSUBST,5,10,2
solve
save
Finish
/FILNAM,F1.2
/SOLU
ANTYPE,,REST
LSWRITE,3,
AUTOTS,1
Time,125
NEQIT,100
OUTRES,,3
F,82000,FY,-25,,82032,1
F,81000,FY,-50,,81032,1
F,80000,FY,-50,,80032,1
NSUBST,5,10,2
solve
save
Finish
/FILNAM,F1.2
/SOLU
ANTYPE,,REST
LSWRITE,4,
Time,150
NEQIT,100
AUTOTS,1
OUTRES,,4
F,82000,FY,-30,,82032,1
F,81000,FY,-60,,81032,1
F,80000,FY,-60,,80032,1
NSUBST,5,10,2
solve
save
```

- Aluminum Beam, S2

```
Finish
/clear
/com                                    ! Aluminum beam S2
/FILNAM,s2h
/PREP7
/unit,si
ET,2,solid45   !for Aluminum
ET,3,inter205  !for Epoxy
R,1,2,0.0651,0,0,2,0.0651,
RMORE,0,1.57, , , , ,
RMORE,
R,2
R,3
MP,EX,4,64.516129E9                     !Aluminum
MP,DENS,4,2700
MP,PRXY,4,0.25
TB,MISO,4,1,11,
TBPT,,0,0
TBPT,,0.00031,20000000
TBPT,,0.0006,38000000
TBPT,,0.00158,100000000
TBPT,,0.00222,140000000
TBPT,,0.00256,160000000
TBPT,,0.00272,170000000
TBPT,,0.0032,180000000
TBPT,,0.00753,200000000
TBPT,,0.0185,210000000
TBPT,,0.039,215000000
TBPT,,0.0734,224000000
TBPLOT,MISO,4
GMAX = 0.001
```

```
TNMAX = 38e6
TB,CZM,7,,,EXPO
TBDATA,1,TNMAX,GMAX,0.1
MP,EX,6,200E12
MP,DENS,6,100
MP,PRXY,6,0.35
N,500,0.175,-0.053
N,501,0.179,-0.053
N,502,0.1875,-0.053
N,503,0.20,-0.053
N,504,0.2125,-0.053
N,505,0.221,-0.053
N,506,0.225,-0.053
Ngen,2,7,500,506,,,-0.004
ngen,2,50,500,513,,,-0.096
N,514,0.175,-0.063
N,515,0.179,-0.063
N,516,0.221,-0.063
N,517,0.225,-0.063
ngen,9,4,514,517,,,-0.01
ngen,49,1000,500,563,,,,0.0125
type,2
Real,2
Mat,4
!e,503,504,417,416,1503,1504,1417,1416
e,507,508,501,500,1507,1508,1501,1500
e,508,509,502,501,1508,1509,1502,1501
e,509,510,503,502,1509,1510,1503,1502
e,510,511,504,503,1510,1511,1504,1503
e,511,512,505,504,1511,1512,1505,1504
e,512,513,506,505,1512,1513,1506,1505
egen,2,50,1,6,,,,,,,,-0.097
e,514,515,508,507,1514,1515,1508,1507
e,519,515,514,518,1519,1515,1514,1518
egen,8,4,14,,,,,,,,,-0.01
e,550,551,547,546,1550,1551,1547,1546
egen,2,2,14,21,,,,,,,0.046
e,516,517,513,512,1516,1517,1513,1512
e,556,549,548,555,1556,1549,1548,1555
egen,48,1000,1,32,,,,,,,,,0.0125  !generation all elem. from all type in z direction
!Rigid supporting plate
N,60000,0.175,-0.163,0.0125
N,60001,0.179,-0.163,0.0125
N,60002,0.1875,-0.163,0.0125
N,60003,0.20,-0.163,0.0125
N,60004,0.2125,-0.163,0.0125
N,60005,0.221,-0.163,0.0125
N,60006,0.225,-0.163,0.0125
ngen,7,1000,60000,60006,,,,0.0125
type,2
Real,2
Mat,6
e,60001,1558,1557,60000,61001,2558,2557,61000
e,60002,1559,1558,60001,61002,2559,2558,61001
e,60003,1560,1559,60002,61003,2560,2559,61002
e,60004,1561,1560,60003,61004,2561,2560,61003
e,60005,1562,1561,60004,61005,2562,2561,61004
e,60006,1563,1562,60005,61006,2563,2562,61005
egen,6,1000,1537,1542,,,,,,,,,0.0125
!Rigid loading plate
N,70000,0.175,-0.053,0.55
N,70001,0.179,-0.053,0.55
N,70002,0.1875,-0.053,0.55
N,70003,0.20,-0.053,0.55
N,70004,0.2125,-0.053,0.55
N,70005,0.221,-0.053,0.55
N,70006,0.225,-0.053,0.55
ngen,5,1000,70000,70006,,,,0.0125
type,3
Real,2
Mat,7
e,44501,45501,45500,44500,70001,71001,71000,70000
```

```
e,44502,45502,45501,44501,70002,71002,71001,70001
e,44503,45503,45502,44502,70003,71003,71002,70002
e,44504,45504,45503,44503,70004,71004,71003,70003
e,44505,45505,45504,44504,70005,71005,71004,70004
e,44506,45506,45505,44505,70006,71006,71005,70005
egen,4,1000,1573,1578,,,,,,,,0.0125
N,80000,0.175,-0.043,0.55
N,80001,0.179,-0.043,0.55
N,80002,0.1875,-0.043,0.55
N,80003,0.20,-0.043,0.55
N,80004,0.2125,-0.043,0.55
N,80005,0.221,-0.043,0.55
N,80006,0.225,-0.043,0.55
ngen,5,1000,80000,80006,,,,0.0125
type,2
Real,2
Mat,6
e,70001,80001,80000,70000,71001,81001,81000,71000
e,70002,80002,80001,70001,71002,81002,81001,71001
e,70003,80003,80002,70002,71003,81003,81002,71002
e,70004,80004,80003,70003,71004,81004,81003,71003
e,70005,80005,80004,70004,71005,81005,81004,71004
e,70006,80006,80005,70005,71006,81006,81005,71005
egen,4,1000,1597,1602,,,,,,,,0.0125
ANTYPE,STATIC
NROPT,full,,OFF            ! USE FULL NEWTON-RAPHSON WITHOUT ADAPTIVE DESCENT
D,63000,UX,0,,63006,1,UY
nsel,s,loc,z,0.6
Dsym,SYMM,Z
D,48500,Uz,0,,48563,1
nsel,all
/SOLU
NROPT,full,,OFF
CNVTOL,F,,0.005,1,-1
LSWRITE,1,
Time,250
NEQIT,100
AUTOTS,1
OUTRES,,1              ! WRITE SOLUTION ON RESULTS FILE FOR EVERY SUBSTEP
F,81000,FY,-250,,81006,1
NSUBST,5,10,2
solve
save
Finish
/FILNAM,s2h
/SOLU
ANTYPE,,REST
LSWRITE,2,
Time,500
NEQIT,100
AUTOTS,1
OUTRES,,2
F,84000,FY,-500,,84006,1
NSUBST,5,10,2
solve
save
Finish
/FILNAM,s2h
/SOLU
ANTYPE,,REST
LSWRITE,3,
AUTOTS,1
Time,750
NEQIT,100
OUTRES,,3
F,84000,FY,-750,,84006,1
NSUBST,5,10,2
solve
save
Finish
/FILNAM,s2h
/SOLU
```

```
ANTYPE,,REST
LSWRITE,4,
Time,1000
NEQIT,100
AUTOTS,1
OUTRES,,4
F,84000,FY,-1000,,84006,1
NSUBST,5,10,2
solve
save
Finish
/FILNAM,s2h
/SOLU
ANTYPE,,REST
LSWRITE,5,
Time,1250
NEQIT,100
AUTOTS,1
OUTRES,,5
F,84000,FY,-1250,,84006,1
NSUBST,5,10,2
solve
save
Finish
/FILNAM,s2h
/SOLU
ANTYPE,,REST
LSWRITE,6,
Time,1400
NEQIT,100
AUTOTS,1
OUTRES,,6
F,84000,FY,-1400,,84006,1
NSUBST,5,2,2
solve
save
Finish
/FILNAM,s2h
/SOLU
ANTYPE,,REST
LSWRITE,7,
Time,1450
NEQIT,100
AUTOTS,1
OUTRES,,7
F,84000,FY,-1450,,84006,1
NSUBST,5,2,2
solve
save
Finish
/FILNAM,s2h
/SOLU
ANTYPE,,REST
LSWRITE,8,
Time,1500
NEQIT,100
AUTOTS,1
OUTRES,,8
F,84000,FY,-1500,,84006,1
NSUBST,5,2,2
solve
save
Finish
/FILNAM,s2h
/SOLU
ANTYPE,,REST
LSWRITE,9,
Time,1750
NEQIT,100
AUTOTS,1
OUTRES,,9
F,84000,FY,-1750,,84006,1
```

```
NSUBST,5,2,2
solve
save
Finish
/FILNAM,s2h
/SOLU
ANTYPE,,REST
LSWRITE,10,
Time,1900
NEQIT,100
AUTOTS,1
OUTRES,,10
F,84000,FY,-1900,,84006,1
NSUBST,5,2,2
solve
save
Finish
/FILNAM,s2h
/SOLU
ANTYPE,,REST
LSWRITE,11,
Time,1925
NEQIT,100
AUTOTS,1
OUTRES,,11
F,84000,FY,-1925,,84006,1
NSUBST,5,2,2
solve
save
Finish
/FILNAM,s2h
/SOLU
ANTYPE,,REST
LSWRITE,12,
Time,1950
NEQIT,100
AUTOTS,1
OUTRES,,8
F,84000,FY,-1950,,84006,1
NSUBST,5,2,2
solve
save
Finish
```

- Composite Beam, S2F1.2

```
Finish
/clear
/com                                ! Composite beam S2F1.2
/FILNAM,S2F1.2
/PREP7
/unit,si
ET,1,solid65                        !Ferrocement
KEYOPT,1,1,0
KEYOPT,1,3,2
KEYOPT,1,5,0
KEYOPT,1,6,0
KEYOPT,1,7,1
KEYOPT,1,8,0
ET,2,solid45                        !Aluminum
ET,3,combin14                       !Epoxy
KEYOPT,3,2,2
ET,4,combin14
KEYOPT,4,2,3
ET,5,combin14
KEYOPT,5,2,1
ET,6,inter205
R,1,2,0.00651,90,90,2,0.00651,
RMORE,0,90, , , , ,
R,2
R,3,1416e6  !y
R,4,1875e4  !z
```

```
R,5,1875e4  !x
Mp,EX,1,28.975E9
MP,DENS,1,2200
MP,PRXY,1,0.15
TBDE,CONC,1,,,
TB,CONC,1,1,9,
TBTEMP,0
TBDATA,,0.2,0.7,3.8e6,-1,,
TBDATA,,,,,,,
TB,Mela,1,1,12,
TBPT,,0,0
TBPT,,0.0002,5795000
TBPT,,0.00041,11878930
TBPT,,0.0005,13983000
TBPT,,0.00075,20083000
TBPT,,0.001,25282000
TBPT,,0.00125,29516000
TBPT,,0.0015,32725000
TBPT,,0.00175,35064000
TBPT,,0.002,36606000
TBPT,,0.00225,37529000
TBPT,,0.0025,37923000
TBPT,,0.003,38000000
TBPLOT,Mela,1
Mp,EX,2,90E9
MP,DENS,2,7800
MP,PRXY,2,0.3
Mp,EX,3,90E9
MP,DENS,3,7800
MP,PRXY,3,0.3
TB,BISO,2,1,2,
TBTEMP,0
TBDATA,,404e6,17e9,,,,
TBPLOT,BISO,2
MP,EX,4,64.516129E9
MP,DENS,4,2700
MP,PRXY,4,0.25
TB,Mela,4,1,11,
TBPT,,0,0
TBPT,,0.00031,20000000
TBPT,,0.0006,38000000
TBPT,,0.00158,100000000
TBPT,,0.00222,140000000
TBPT,,0.00256,160000000
TBPT,,0.00272,170000000
TBPT,,0.0032,180000000
TBPT,,0.00753,200000000
TBPT,,0.0185,210000000
TBPT,,0.039,215000000
TBPT,,0.0734,224000000
TBPLOT,Mela,4
MP,EX,5,4.3E9
MP,DENS,5,1500
MP,PRXY,5,0.15
GMAX = 0.001
TNMAX = 38e6              !* TENSILE STRENGTH
TB,CZM,7,,,EXPO           !* COHESIVE ZONE MATERIAL
TBDATA,1,TNMAX,GMAX,0.1
MP,EX,6,200E12              !rigid plate
MP,DENS,6,100
MP,PRXY,6,0.35
n,1
ngen,33,1,1,,,0.0125
ngen,5,100,1,33,,,-0.0125
N,500,0.175,-0.05
N,501,0.179,-0.05
N,502,0.1875,-0.05
N,503,0.20,-0.05
N,504,0.2125,-0.05
N,505,0.221,-0.05
N,506,0.225,-0.05
Ngen,2,7,500,506,,,-0.004
```

```
ngen,2,50,500,513,,,-0.096
N,514,0.175,-0.06
N,515,0.179,-0.06
N,516,0.221,-0.06
N,517,0.225,-0.06
ngen,9,4,514,517,,,-0.01
ngen,2,1000,1,563,,,,0.015
ngen,3,1000,1001,1563,,,,0.035
ngen,20,1000,3001,3563,,,,0.025
ngen,3,1000,22001,22563,,,,0.02
type,1
Real,1
Mat,1
e,102,2,1,101,1102,1002,1001,1101
egen,32,1,1,,,,,,,0.0125
egen,4,100,1,32,,,,,,,-0.0125
type,2
Real,2
Mat,4
e,507,508,501,500,1507,1508,1501,1500
e,508,509,502,501,1508,1509,1502,1501
e,509,510,503,502,1509,1510,1503,1502
e,510,511,504,503,1510,1511,1504,1503
e,511,512,505,504,1511,1512,1505,1504
e,512,513,506,505,1512,1513,1506,1505
egen,2,50,129,134,,,,,,,-0.096
e,514,515,508,507,1514,1515,1508,1507
e,519,515,514,518,1519,1515,1514,1518
egen,8,4,142,,,,,,,,-0.01
e,550,551,547,546,1550,1551,1547,1546
egen,2,2,142,149,,,,,,,0.046
e,516,517,513,512,1516,1517,1513,1512
e,556,549,548,555,1556,1549,1548,1555
type,3
Real,3
E,500,415
E,502,416
E,503,417
E,504,418
E,506,419
type,4
Real,4
E,500,415
E,502,416
E,503,417
E,504,418
E,506,419
type,5
Real,5
!Mat,5
E,500,415
E,502,416
E,503,417
E,504,418
E,506,419
egen,24,1000,1,175  !generation all ele from all type in z direction
!Rigid supporting plate
N,60000,0.175,-0.16,0.015
N,60001,0.179,-0.16,0.015
N,60002,0.1875,-0.16,0.015
N,60003,0.20,-0.16,0.015
N,60004,0.2125,-0.16,0.015
N,60005,0.221,-0.16,0.015
N,60006,0.225,-0.16,0.015
ngen,3,1000,60000,60006,,,,0.035
type,2
Real,2
Mat,6
e,60001,1558,1557,60000,61001,2558,2557,61000
e,60002,1559,1558,60001,61002,2559,2558,61001
e,60003,1560,1559,60002,61003,2560,2559,61002
e,60004,1561,1560,60003,61004,2561,2560,61003
```

```
e,60005,1562,1561,60004,61005,2562,2561,61004
e,60006,1563,1562,60005,61006,2563,2562,61005
egen,2,1000,4201,4206,,,,,,,,0.025
!Rigid loading plate
n,70000,0,0,0.56
ngen,33,1,70000,,,0.0125
ngen,3,1000,70000,70033,,,,0.02
type,6
Real,2
Mat,7
e,22002,23002,23001,22001,70001,71001,71000,70000
egen,32,1,4213,,,,,,,,0.0125
egen,2,1000,4213,4244,,,,,,,,0.02
n,80000,0,0.01,0.56
ngen,33,1,80000,,,0.0125
ngen,3,1000,80000,80033,,,,0.02
type,2
Real,2
Mat,6
e,70001,80001,80000,70000,71001,81001,81000,71000
egen,32,1,4277,,,,,,,,0.0125
egen,2,1000,4277,4308,,,,,,,,0.02
ANTYPE,STATIC
NROPT,full,,OFF            ! USE FULL NEWTON-RAPHSON WITHOUT ADAPTIVE DESCENT
D,61000,UX,0,,61006,1,UY
nsel,s,loc,z,0.6
Dsym,SYMM,Z
D,24001,Uz,0,,24033,1
D,24101,Uz,0,,24133,1
D,24201,Uz,0,,24233,1
D,24301,Uz,0,,24333,1
D,24401,Uz,0,,24433,1
D,24500,Uz,0,,24563,1
nsel,all
/SOLU
NROPT,full,,OFF
CNVTOL,F,,0.005,1,-1
LSWRITE,1,
Time,100
NEQIT,100
AUTOTS,1
OUTRES,,1              ! WRITE SOLUTION ON RESULTS FILE FOR EVERY SUBSTEP
F,82000,FY,-20,,82032,1
F,81000,FY,-40,,81032,1
F,80000,FY,-40,,80032,1
NSUBST,5,10,2
solve
save
Finish
/FILNAM,S2F1.2-h-s3.8
/SOLU
ANTYPE,,REST
LSWRITE,2,
Time,200
NEQIT,100
AUTOTS,1
OUTRES,,2
F,82000,FY,-40,,82032,1
F,81000,FY,-80,,81032,1
F,80000,FY,-80,,80032,1
NSUBST,5,10,2
solve
save
Finish
/FILNAM,S2F1.2-h-s3.8
/SOLU
ANTYPE,,REST
LSWRITE,3,
AUTOTS,1
Time,300
NEQIT,100
OUTRES,,3
```

```
F,82000,FY,-60,,82032,1
F,81000,FY,-120,,81032,1
F,80000,FY,-120,,80032,1
NSUBST,5,10,2
solve
save
Finish
/FILNAM,S2F1.2-h-s3.8
/SOLU
ANTYPE,,REST
LSWRITE,4,
Time,400
NEQIT,100
AUTOTS,1
OUTRES,,4
F,82000,FY,-80,,82032,1
F,81000,FY,-160,,81032,1
F,80000,FY,-160,,80032,1
NSUBST,5,10,2
solve
save
Finish
/FILNAM,S2F1.2-h-s3.8
/SOLU
ANTYPE,,REST
LSWRITE,5,
Time,500
NEQIT,100
AUTOTS,1
OUTRES,,5
F,82000,FY,-100,,82032,1
F,81000,FY,-200,,81032,1
F,80000,FY,-200,,80032,1
NSUBST,5,10,2
solve
save
Finish
/FILNAM,S2F1.2-h-s3.8
/SOLU
ANTYPE,,REST
LSWRITE,6,
Time,600
NEQIT,100
AUTOTS,1
OUTRES,,6
F,82000,FY,-120,,82032,1
F,81000,FY,-240,,81032,1
F,80000,FY,-240,,80032,1
NSUBST,5,2,2
solve
save
Finish
/FILNAM,S2F1.2-h-s3.8
/SOLU
ANTYPE,,REST
LSWRITE,7,
Time,700
NEQIT,100
AUTOTS,1
OUTRES,,7
F,82000,FY,-140,,82032,1
F,81000,FY,-280,,81032,1
F,80000,FY,-280,,80032,1
NSUBST,5,10,2
solve
save
Finish
/FILNAM,S2F1.2-h-s3.8
/SOLU
ANTYPE,,REST
LSWRITE,8,
Time,800
```

```
NEQIT,100
AUTOTS,1
OUTRES,,8
F,82000,FY,-160,,82032,1
F,81000,FY,-320,,81032,1
F,80000,FY,-320,,80032,1
NSUBST,5,10,2
solve
save
Finish
/FILNAM,S2F1.2-h-s3.8
/SOLU
ANTYPE,,REST
LSWRITE,9,
Time,900
NEQIT,100
AUTOTS,1
OUTRES,,9
F,82000,FY,-180,,82032,1
F,81000,FY,-360,,81032,1
F,80000,FY,-360,,80032,1
NSUBST,5,10,2
solve
save
Finish
/FILNAM,S2F1.2-h-s3.8
/SOLU
ANTYPE,,REST
LSWRITE,10,
Time,1000
NEQIT,100
AUTOTS,1
OUTRES,,10
F,82000,FY,-200,,82032,1
F,81000,FY,-400,,81032,1
F,80000,FY,-400,,80032,1
NSUBST,5,10,2
solve
save
Finish
/FILNAM,S2F1.2-h-s3.8
/SOLU
ANTYPE,,REST
LSWRITE,11,
Time,1100
NEQIT,100
AUTOTS,1
OUTRES,,11
F,82000,FY,-220,,82032,1
F,81000,FY,-440,,81032,1
F,80000,FY,-440,,80032,1
NSUBST,5,10,2
solve
save
Finish
/FILNAM,S2F1.2-h-s3.8
/SOLU
ANTYPE,,REST
LSWRITE,12,
Time,1200
NEQIT,100
AUTOTS,1
OUTRES,,12
F,82000,FY,-240,,82032,1
F,81000,FY,-480,,81032,1
F,80000,FY,-480,,80032,1
NSUBST,5,10,2
solve
save
Finish
```

Appendices

الـخـلاصـة

تهدف الدراسة الحالية إلى بحث السلوك الإنشائي للعتبات المركبة ذات الإسناد البسيط، والتي يربط فيها بلاط من الفيروسمنت مع عتبة من الألمنيوم. مقاطع إنشائية من الألمنيوم (I ، صندوق) أردنية الصنع تم استخدامها في الدراسة. سيكادور 31 و هو مادة ايبوكسي لاصق استخدم كرابط قص، يتكون من مركبين و يخضع للمواصفة ASTM C881-78.

تشتمل الدراسة على جزئين، الجزء الأول يتضمن العمل المختبري والذي تم من خلاله فحص ثلاث نماذج لفحص الرابط المقترح وعشرة نماذج لعتبات مركبة مصممة للفشل بالانحناء و أربعة نماذج لعتبات من الألمنيوم بالإضافة إلى نموذجين من بلاطات الفيروسمنت. تم إجراء سلسلة من الفحوصات على النماذج المختلفة من العتبات لبيان مدى تأثير أبعاد مقطع الألمنيوم على التصرف الإنشائي و المقاومة القصوى لهذه العتبات. جميع النماذج تعرضت لفحص الانحناء باستخدام حمل واحد مركز في منتصف العتبة. العلاقة بين الحمل و الانحناء، الحمل و الانزلاق النسبي، و الحمل و الفصل العمودي مثلت في الدراسة. بينت الدراسة إن المقاطع المقترحة (مقاطع مركبة من الفيروسمنت و الألمنيوم) تملك مقاومة جيدة للأحمال بالنسبة إلى وزنها، حيث إن زيادة المقاومة تراوحت بين 1,57 و 2,69 ، كذلك لوحظ إن آلية التركيب تلغي ظاهرة الانبعاج المحلى في مقاطع الألمنيوم. يمكن أن يلاحظ إن استخدام المادة الرابطة بين طبقات العتبة المركبة توفر ربط كافي و يمكن اعتبار الارتباط تام كون الانزلاق النسبي صغير جدا كما يمكن اعتبار استخدام المادة الرابطة بديل لآلية الربط التقليدية المستخدمة في العتبات المركبة.

في الجزء الثاني من الدراسة تم استخدام طريقة العناصر المحددة لتحليل العتبات المفحوصة باستخدام نمذجة ثلاثية الأبعاد. النماذج التركيبية للسلوك اللاخطي للفيروسمنت والألمنيوم و شبكة التسليح أخذة بنظر الاعتبار العلاقات اللاخطية للإجهاد-الانفعال، في طريقة الحل. تم اعتماد برنامج ANSYS version 11.0 لتحليل النموذج الثلاثي البعد، و جرت نمذجة الفيروسمنت باستخدام عناصر من نوع SOLID65 بثمانية عقد ونمذجة عتب الألمنيوم

بعناصر SOLID45 أيضا بثمانية عقد. استخدمت نمذجات مختلفة لتمثيل طبقة الايبوكسي كمرابط قص وتم تعميم استخدام عنصر CONBIN14 لنمذجة مرابط القص كون النتائج المستحصلة من استخدامها قريبة للنتائج العملية، النسبة هي 1.03، بالإضافة لقلة وقت الحل. أما شبكة التسليح فقد تمت نمذجتها كنسبة من الحجم ضمن عناصر الفيروسمنت.و تم افتراض ترابط تام بين الفيروسمت وشبكة التسليح. وجد بان نماذج العناصر المحددة تعطي قيم للأحمال القصوى و للإزاحات والانفعالات والانزلاق ذات اتفاق جيد مع النتائج المختبرية.

كذلك تم حساب كفاءة المقاطع المركبة باستخدام مبادئ التحليل اللدن، و أوضحت نتائج التحليل اللدن إن المقاومة القصوى للعتبات المركبة من الفيروسمنت و الألمنيوم يمكن أن تهن باستخدام معادلات التوازن التقليدية بالاعتماد على Euro code ونتائج الفحوص القياسية.

التصرف الإنشائي للعتبات المركبة من الفيروسمنت والألمنيوم ذات الإسناد البسيط

رسالة مقدمة إلى

كلية الهندسة – جامعة البصرة

كجزء من متطلبات نيل درجة دكتوراه فلسفة في

الهندسة المدنية (إنشاءات)

من قبل

سعد فهد رسن

شباط ٢٠١٢